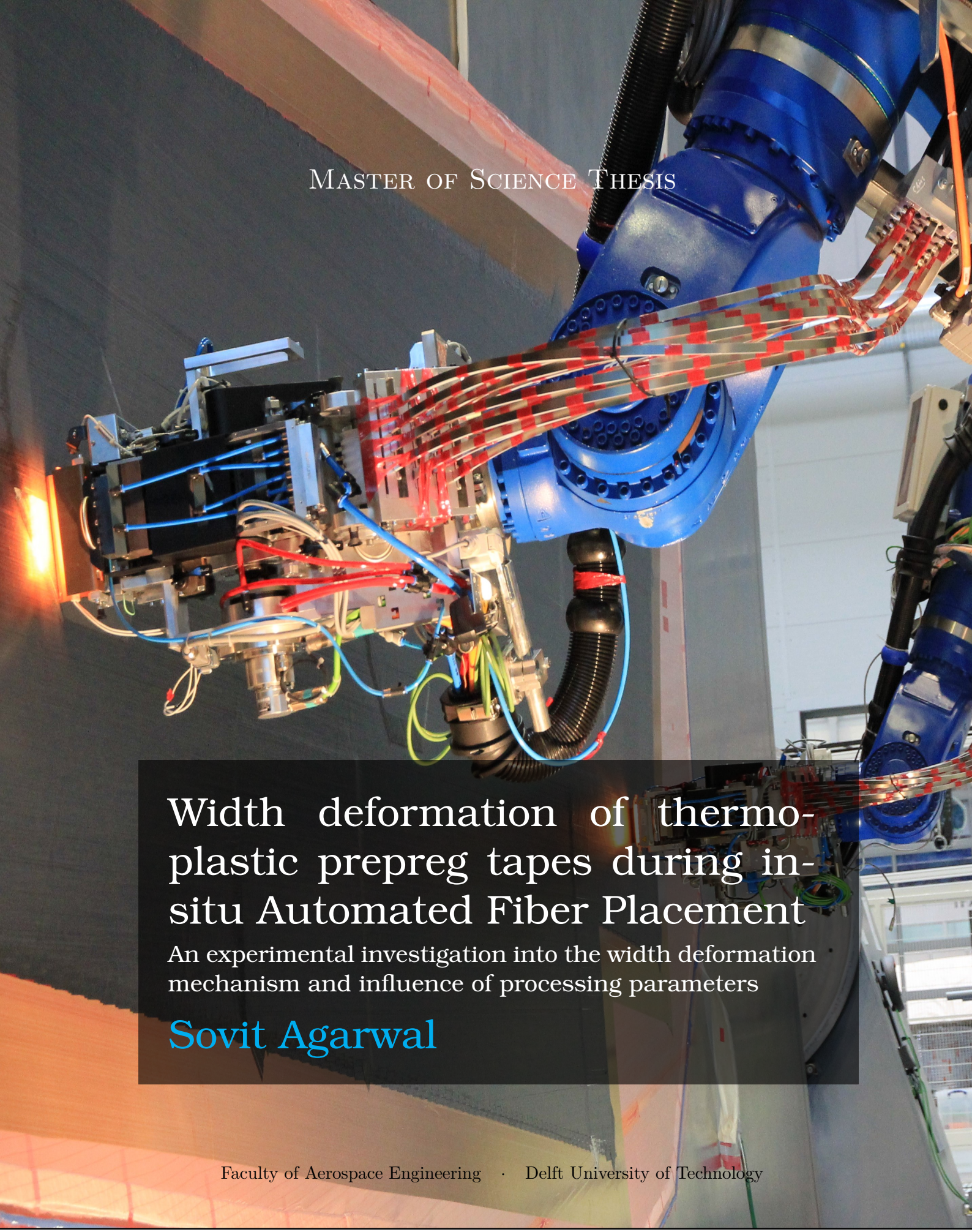

Master of Science Thesis

# Width deformation of thermoplastic prepreg tapes during in-situ Automated Fiber Placement

An experimental investigation into the width deformation mechanism and influence of processing parameters

Sovit Agarwal

Faculty of Aerospace Engineering · Delft University of Technology

TU Delft Delft University of Technology

# Width deformation of thermoplastic prepreg tapes during in-situ Automated Fiber Placement

## An experimental investigation into the width deformation mechanism and influence of processing parameters

Master of Science Thesis

For obtaining the degree of Master of Science in Aerospace Engineering
at Delft University of Technology

Sovit Agarwal

14 September, 2023

Faculty of Aerospace Engineering · Delft University of Technology

The work in this thesis was in collaboration with Center for lighweight production technology, German Aerospace Center (DLR), Stade. Their cooperation is gratefully acknowledged.


Delft University of Technology
Faculty of Aerospace Engineering
Department of Aerospace Structures and Materials

**GRADUATION COMMITTEE & SUPERVISORS**

Dated: 14 September, 2023

Chair person:

Dr.ir. J.J.E. Teuwen

Supervisor:

Dr.ir. D.M.J. Peeters

Committee members:

Dr.ir. O.K. Bergsma

Ir. Andreas Kolbe

External Supervisors:

Ir. Dominik Delisle

Dr.ir. Daniel Stefaniak

# Acknowledgments

Firstly, I would like to thank my daily supervisor from TU Delft, Daniel Peeters, for his constant support, guidance and feedback throughout this journey of completing my master thesis. I am very grateful to him for giving me the opportunity to work on this topic that I was very interested in. His critical questions during the update meetings challenged me to dive further into the topic and pushed me to think beyond the usual.

I would also like to thank my daily supervisor from DLR during my three months spent there, Dominik Delisle, for his support and ensuring that I get all the resources from DLR to carry out my experimental work. During my time at DLR, his constant guidance made the work look very easy and I would like to thank him for his help with any problems that I faced and for always thinking along with me to try to find a solution. While working in the production plant at DLR, I also had the pleasure to meet other DLR staff and I would like to especially thank Sebastian Renge for providing support for the manufacturing.

Additionally, I would like to thank Daniel Stefaniak from DLR and Andreas Kolbe from Airbus for joining some of the update meetings and providing valuable feedback.

I would also like to thank the assessment committee, Julie Teuwen and Otto Bergsma from TU Delft, for taking the time to read and review my thesis and taking interest in the work I performed.

A special thanks to my friends and colleagues who inspired me to work hard and made the time at the university a very pleasant one. Their companionship and support during the stressful moments are invaluable and I am grateful to have made such good friends during my time here.

Finally, a big thank you to my family for always supporting me through thick and thin and always believing in me. I am grateful for their constant love and encouragement.

Delft University of Technology — Sovit Agarwal
14 September, 2023

# Summary

Increasing demands for composite structures and sustainability goals have resulted in the growth of thermoplastic polymer matrix composites and automated manufacturing technologies. The in-situ Automated Fiber Placement (AFP) manufacturing of thermoplastic prepreg tapes has the potential to provide a fast and cost-effective manufacturing solution for large composite structures. However, it is still under development because of the complex mechanisms and short processing times involved which leads to several defect formations, especially gaps and overlaps. One of the primary reasons for the formation of these gaps and overlaps is the tape width deformation during placement.

Current literature on tape width deformation shows that the resulting tape width is influenced by several processing parameters such as temperature, pressure and placement speed. However, results from different studies do not agree with each other, indicating that the tape temperature distribution might be at play. Additionally, the conventionally considered tape width deformation mechanism i.e., transverse squeeze flow has been suggested to be incorrect for the AFP process as the experimental deformations do not agree with the results of the transverse squeeze flow model. Therefore, the research objective for this study was to experimentally investigate the width deformation mechanism and the influence of processing parameters for thermoplastic prepreg tapes using in-situ AFP manufacturing and humm3® (from Heraeus) as the heating device.

The specimens were manufactured according to a full-factorial Design of Experiments (DoE) with two settings (high and low) for the following processing parameters: heated length, nip-point temperature and compaction force. The tape width was measured for all the specimens to investigate the influence of the different processing parameters and some post-processing analyses were carried out to understand the tape width deformation mechanism. This included width measurement in the heating phase of the process, surface roughness analysis, tape cross-section profile inspection and fiber-resin content analysis.

From the post-processing analyses and investigations, it was found that the tape width deforms in the heating as well as the consolidation phase of the process. Additionally, the cross-section images show that the conformable roller led the tape edge profile to have a gradual decrease in thickness with a clear slope and the tape edges show a clear indication of

spreading of the fiber-resin mixture due to the presence of both fibers and resin. Moreover, the surface roughness data show an indication of the role of temperature distribution because the as-received tape surface roughness was achieved for the higher temperature and longer heated length settings which are assumed to promote better heat distribution in the material.

The influence of the processing parameters on the tape width deformation did not show clear trends for all specimen configurations. However, the exceptions pointed towards the role of temperature distribution in the tape that led to the overshadowing of the effect of other processing parameters. Considering this, it was observed that the change in heated length did not have a significant effect on the tape width except for one configuration i.e., 300 N, 370 °C, wherein a clear increase with no overlap in data was seen. For the effect of temperature and compaction force, it was found that they have an influence on the tape width for temperatures lower than the melting temperature of the polymer resin ($T_m$). Additionally, the fiber straining effect on the tape width deformation with compaction force was suggested for the higher temperature specimens.

# Nomenclature

## Abbreviations

| Abbreviation | Definition |
|---|---|
| AFP | Automated Fiber Placement |
| ATL | Automated Tape Layup |
| ATP | Automated Tape Placement |
| CAD | Computer-Aided Design |
| CCD | Charged-Coupled Device |
| CF-PA6 | Carbon Fiber-Polyamide 6 (Nylon 6) |
| CF-PEEK | Carbon Fiber-Poly Ether Ether Ketone |
| DoE | Design of Experiments |
| FRP | Fiber Reinforced Polymer |
| HGT | Hot Gas Torch |
| HL | Heated Length |
| LAFP | Laser Assisted Fiber Placement |
| LM-PAEK | Low-Melt Poly Aryl Ether Ketone |
| LSCM | Laser Scanning Confocal Microscope |
| PEEK | Poly Ether Ether Ketone |
| PEKK | Poly Ether Ketone Ketone |
| PMC | Polymer Matrix Composite |
| PPS | Poly Phenylene Sulphide |
| RGB | Red, Green and Blue |
| RQ | Research Question |
| SD | Standard Deviation |
| SMC | Sheet Moulding Compound |
| SQ | Sub Question |
| UD | Uni-Directional |

# Symbols

| Symbol | Definition |
|---|---|
| $\epsilon$ | Emissivity |
| $h_f$ | Final height |
| $h_i$ | Initial height |
| $\lambda$ | Wavelength |
| $L_c$ | Contact length under roller |
| $L_h$ | Heated length |
| $R_a$ | Arithmetical mean roughness |
| $R_q$ | Root mean square roughness |
| $T_g$ | Glass transition temperature |
| $T_m$ | Melting temperature |
| $T_p$ | Processing temperature |
| $W_f$ | Final tape width |
| $W_i$ | Initial tape width |

# Table of Contents

# List of Figures

# List of Tables

# Chapter 1

# Introduction

Polymer Matrix Composites (PMC) or Fiber Reinforced Polymers (FRP) have become an integral part of several industries such as aerospace, automotive, wind energy, etc. in the past few decades. This is because of their superior properties like high weight-specific strength and stiffness that is crucial in applications that aim to optimize performance by minimizing weight such as the aerospace industry.

For high-performance aerospace applications, thermoset polymer matrices have been a traditional choice [1] and its use in aircraft primary structures and large composite structures has grown significantly over the past few years, for example in the Airbus A350 XWB and Boeing B787 where FRP constitutes half of the total aircraft's weight [2]. However, looking into the growing demands of the aerospace industry [3][4] and sustainability & environmental requirements [5], these thermoset polymer matrix composite structures are not a viable option for the future as it requires a very slow, cost-expensive & high energy autoclave processing [6] and are not recyclable directly [1].

Therefore, thermoplastic polymer matrix composites are of growing interest and are emerging at a very fast pace because of their faster processing times, new manufacturing methods and recyclability benefits when compared to thermoset polymer composites [6]. Their ability to be reprocessed (soften on application of heat and consolidate again after cool-down) and the absence of chemical cross-linking of molecules (as in thermoset polymers) allows for new out-of-autoclave processing such as forming, welding and in-situ Automated Fiber Placement (AFP) manufacturing which have the benefits of high production rates, faster assembly and one-step manufacturing (layup and consolidation) respectively. Other benefits of thermoplastic polymer matrix composites include infinite shelf life at room temperatures, high impact resistance and high temperature performance [7].

In-situ AFP manufacturing is an emerging and promising processing technique for thermoplastic composites as it has the potential to meet the growing demands of composite structures. However, it is still prone to several defect formations during manufacturing, especially gaps and overlaps which is a major one and leads to several other defects [8] [9]. One of the primary causes for these gaps and overlaps is the tape width deformation during placement

and it becomes very crucial for in-situ AFP manufacturing as there is no secondary autoclave processing step that might alleviate it by the flow of the fiber-resin mixture under a uniform heat and pressure applied to the part. Currently, the knowledge on this topic is lacking and additional research is required to mitigate the formation of gaps and overlaps due to tape width deformation. Therefore, the research objective for this study is to understand the governing mechanism behind tape width deformation of thermoplastic prepreg tapes for in-situ AFP manufacturing and to gain insight into the influence of various processing parameters on it. The humm3® xenon flashlamp was used as the heating device for this study.

A detailed literature review is first presented in chapter 2 that forms the knowledge base for this study followed by the research definition presented in chapter 3, where the research gaps are identified and the research objective and questions are introduced. chapter 4 then presents the methodology used for the study based on the research questions formulated. chapter 5 explains the experimental setup used for the specimen manufacturing and post-process experiments in detail. This is followed by chapter 6 where all the results are presented, analysed and discussed. Finally, the conclusions based on the obtained results are drawn in chapter 7 and some recommendation for future work are listed in chapter 8.

# Chapter 2

# Literature review

This chapter describes the state-of-the-art and background literature about the Automated Fiber Placement (AFP) process in general and with humm3® as the heating device in section 2.1. Further, section 2.2 and section 2.3 dives deep into the defect formation during AFP processing and currently available knowledge on tape width deformation which was used to draw motivation, identify gaps and form a base for this study.

## 2.1 Automated Fiber Placement

Automated Fiber Placement (AFP) is a commonly used automated manufacturing technique consisting of a robotic arm/gantry on which the fiber placement head is mounted. The fiber placement head consists of a series of rollers as shown in Figure 2.1 to direct and control the restarting of individual composite tows/tapes and a heating device is used to heat the incoming tape before it is placed on the tool. Compaction rollers are used to apply pressure and conform the placed tapes to the tool or the previously placed laminate called the substrate and adhesion is achieved by controlling the various process parameters such as temperature, pressure and tension depending on the tape material [10]. The commonly used tape width ranges from 1/8" to 1/2" (3.175 mm to 12.7 mm) and up to 32 tapes can be placed simultaneously to improve productivity of the process.

Three types of tape materials are placed using AFP technique i.e., thermoset prepregs, dry fibers and thermoplastic prepregs.

Thermoset prepregs have been used commonly with AFP processing as the required processing temperature is quite low (about 70 °C) to avoid progression of the cure reaction of the resin. This heat is required to increase the tackiness of the prepreg tapes to adhere to complex tool shapes and geometries. The laminate is then processed in a secondary step in an autoclave or oven where heat and pressure is applied to completely cure the resin and consolidate the laminate. This secondary step also helps in removing AFP induced defects such as voids, gaps and overlaps by helping in the flow of the fiber-resin mixture under a uniform heat and pressure applied to the whole part.

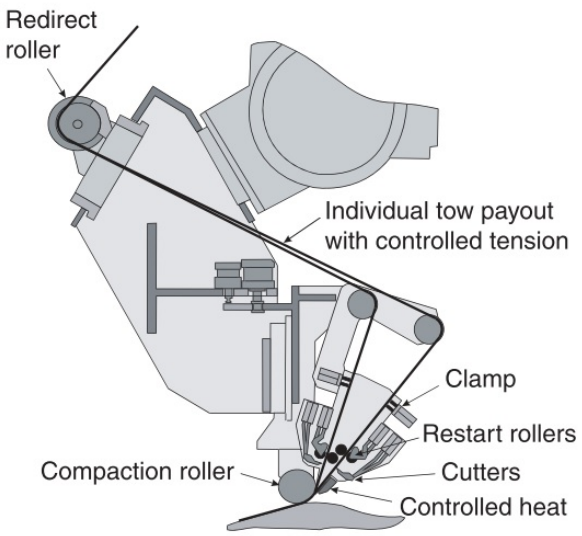


**Figure 2.1:** AFP head [11]

Dry fibers are not pre-impregnated with any type of resin but usually contain small amounts (5-17 %) of thermoplastic veil or binders to increase the tackiness and stabilize the tapes during placement [12]. Again, a secondary step of resin infusion is required after the AFP processing of the laminate.

Thermoplastic prepregs require higher temperature (about 150 °C) as it does not have a natural tackiness at room temperature and must be above the glass transition temperature ($T_g$) to be able to conform and stick to the tool surface. Processing at the material $T_g$ would require a secondary consolidation step in the autoclave/oven to ensure full consolidation and maintain consistent part quality. However, the time required in the autoclave/oven is usually much less than for thermoset laminates [6]. Additionally, the absence of chemical cross-linking for consolidation allows for the possibility to consolidate the laminate in-situ i.e., without requiring any additional processing steps by applying a temperature higher than the material's melting temperature ($T_m$, about 300 - 350 °C) and pressure during placement that is enough for in-situ fusion bonding.

However, in-situ AFP manufacturing of thermoplastic composites still lacks maturity in terms of process control and part quality and therefore is an interesting topic of research as it combines the benefits of thermoplastics with that of a one-step manufacturing process, preventing the need to use a time and energy consuming, expensive and size-limiting autoclave processing. Thus, it has the potential to meet the growing demands of the aerospace and other composite structure industries. The in-situ AFP process is described further in the following sub-sections.

### 2.1.1 Bonding mechanism

In-situ AFP thermoplastic composite processing is based on fusion bonding that consists of three basic mechanisms i.e., intimate contact development, autohesion and consolidation. For successful bonding between the incoming tape and the substrate, the two surfaces need to

be in good intimate contact. This is achieved by application of heat and pressure to enable viscous deformations of the fiber-resin mix i.e., squeeze flow and through-thickness percolation flow of the resin to flatten the asperities on the bonding surfaces. Once the surfaces are in contact, the polymer chains can diffuse across the two surfaces (polymer reptation theory) in order to "heal", also known as autohesion. The polymer healing or autohesion is a temperature dependant process as the polymer chains need to move relative to each other [13]. Amorphous polymers need to be above their $T_g$ and semi-crystalline polmers above their $T_m$ for autohesion [14]. Finally, after the boundary between the two surfaces has been "erased" by autohesion, the bond needs to be consolidated. This occurs during cooling down to temperatures below the $T_g$ after which the polymer chains can no longer move and hence regain their initial stiffness. Pressure plays an important role in this step to prevent disbonding or delaminations to occur at the bonding interface and deconsolidation or porosity to occur in the top layer. Figure 2.2 illustrates the fusion bonding mechanism.

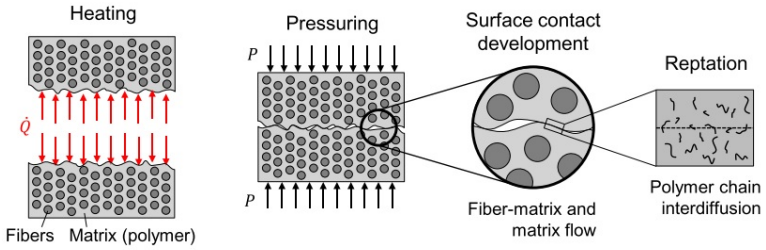


**Figure 2.2:** Fusion bonding mechanism [15]

### 2.1.2 Processing phases

In-situ AFP processing can be divided into three phases i.e., heating, consolidation and solidification [16] as illustrated in Figure 2.3. Each phase consists of several complex phenomena that have an effect on the tape property and the final part quality. These are further discussed here.

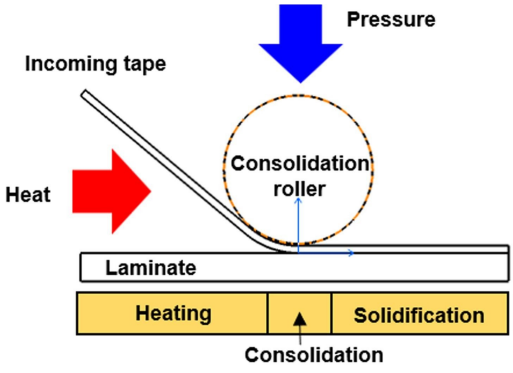


**Figure 2.3:** In-situ AFP processing phases of thermoplastic prepregs [16]

#### Heating phase

This is the phase where the incoming tape and the substrate/tool is heated to the processing temperature which is slightly above the $T_m$ for semi-crystalline thermoplastic prepregs.

Therefore, prior to the nip-point (point where compaction from the roller starts), the temperature should be above the $T_m$ in order to form a good intimate contact and hence good bond development in the next phase. Several mechanisms play a role in the deconsolidation of the tape during this phase due to application of heat without any pressure. These include fiber decompaction, void growth, specific volume change and release of residual stresses from tape manufacturing which ultimately leads to an increased thickness, surface roughness, final void content and waviness of the tape [17].

The heating device plays an important role as several parameters are directly controlled by it. Available heating devices for thermoplastic AFP are Hot Gas Torches (HGT), Lasers and Pulsed light flashlamps. The parameters that are common to all these heating devices include heating temperature, rate, area, distribution and angle. These are controlled by the nozzle, laser optics and light guide for HGT, laser and flashlamp systems respectively. However, the heating mechanism differs. For the HGT, the surface of the tape is heated via convective heat transfer by the gas [18]; for the laser, only the fibers are heated via radiation of infrared light which in turn heats up the surrounding resin via conduction [10]; and for the pulsed light flashlamp, the tape surface and bulk is heated via radiation of broadband visible light [19].

A pulsed light flashlamp system such as the humm3® from Heraeus is a relatively new addition to the list of heating devices that can be used for processing thermoplastic prepreg tapes and uses broadband radiation from a xenon flashlamp to deliver high energy pulses for heating the material to high temperatures at a heating rate and temperature equivalent to the laser system [20], while at the same time being safer than using a laser heating system, and more controllable than a hot gas torch system. The pulsed energy is delivered to the desired location by a transparent light guide that collects all the energy and directs it towards the end of the guide. Therefore, the shape of the light guide end can be optimized to provide the desired heat zone or profile [21]. The flashlamp system can transfer the heat energy into the material differently based on its three programmable parameters i.e., pulse energy, duration and frequency [21] [22]. These three parameters i.e., the energy put into a pulse, the length of the pulse (in milliseconds) and the number of pulses emitted in a given amount of time (typically 60 Hz or higher) determines the heat profile and provide an additional control over the surface and bulk temperatures [23] [19]. Hence, this heating system has advantages compared to laser heating systems commonly used.

**Consolidation phase**

The bonding of the tape to the substrate as described in subsection 2.1.1 takes place in this phase under the compaction roller. The consolidation phase consists of three processes i.e., intimate contact development, polymer healing and recompaction; all of which occurs in a span of few milliseconds while under the roller.

Intimate contact development itself involves several complex mechanisms. The heated material and pressure from the compaction roller helps in flattening the surface asperities through squeeze flow of the fiber-resin mixture, which has been considered to be the sole mechanism for intimate contact conventionally. However, recent studies on both thermoset [24] and thermoplastic [25] AFP indicate that resin percolation flow also plays a role in gap filling and intimate contact development. Therefore, the degree of intimate contact depends on several AFP process parameters such as placement speed, compaction pressure and temperature [25]. The compaction pressure distribution on the tape is directly controlled by the roller.

Once intimate contact is achieved, the polymer chains can diffuse across the interface and ultimately erase the interface, forming a uniform bond between the tape and the substrate. The movement of the polymer chains is temperature dependant and a recent study [26] shows that bonding occurs at sub-melt temperatures also, for both amorphous and semi-crystalline polymers, since the chain movement can occur above the polymer $T_g$. Further, as the tape cools down (ideally below the $T_g$) under the roller, the tape is fully consolidated and no more decompaction can occur after the roller has passed. Additionally, the deconsolidation effects on the tape as described in the heating phase such as thickness increase, surface roughness, void growth and waviness were reported to have vanished in this phase in a study by Çelik et al. [27]. However, the authors do note that the processing time used i.e., heating rate of 60 °C/min, dwell time of 20 seconds and cool down at 60 °C/min was significantly longer than in an actual AFP setting, which might have a larger effect on consolidation of the tape than in reality.

A typical temperature profile for Laser AFP process in reality is shown in Figure 2.4. It can be seen that the tape is only heated up to a specific point called the "visible" nip-point (see Figure 2.5) before the "actual" nip-point after which the temperature in the shadow region (the region between the "visible" and "actual" nip-point where the laser beam is blocked by the geometry of the roller) starts to drop. This cooling down depends on several factors such as material properties, tool & roller geometry, placement speed, surrounding temperatures and laser properties [28]. Therefore, the temperature of the incoming tape is usually above the $T_m$ in the consolidation phase for a very short time (less than a second) depending on the process parameters. As the incoming tape and the tool/substrate make contact, the temperatures merge and then start reducing as no more heat is applied, thereby quickly dropping below the $T_m$ under the compaction roller [26].

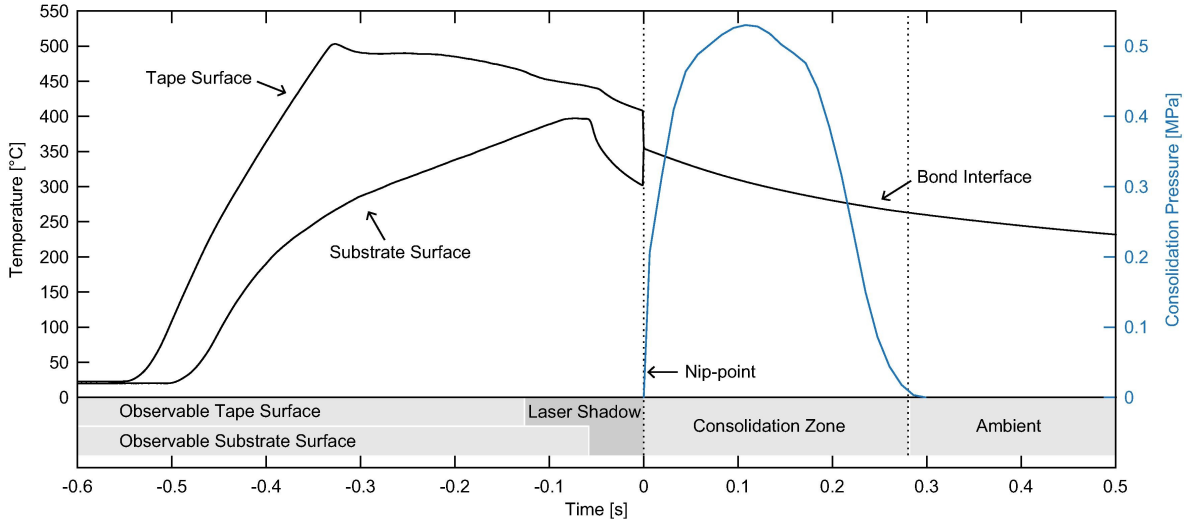


**Figure 2.4:** Typical temperature profile for Laser AFP process [29].

### Solidification phase

This is the final phase after the roller where the tape and the substrate is cooled below the $T_g$ to room temperature. Sufficient consolidation and cool-down under the roller prevents any further decompaction or void growth in the material and therefore leads to a perfect

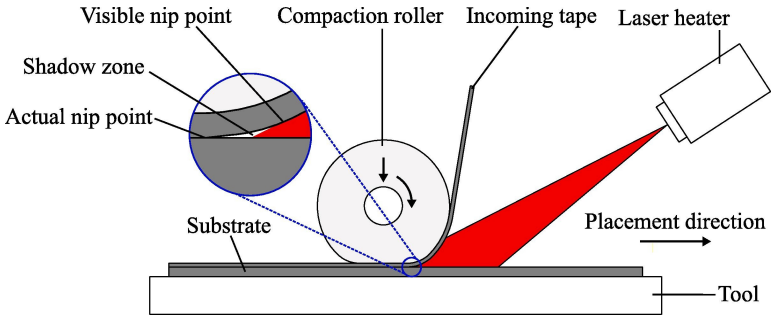


**Figure 2.5:** Schematic diagram illustrating the shadow region for Laser AFP [25].

bond. However, crystallization and thermal stresses can still continue to form in this phase depending on the cool-down rate determined by the release temperature of the tape, tool temperature and room temperature, thereby changing the material properties.

## 2.2 Defect formation - Gaps and overlaps

Although the AFP process has been used since many years, it is still prone to several defect formations during manufacturing [8] [9]. Currently, the time spent on quality assurance and rework is more than the AFP deposition time because of the manual inspections performed [30]. This negates the benefits of AFP manufacturing of being a fast and cost-effective process. Gaps and overlaps are the most predominant defect in AFP manufacturing and has a significant effect on the manufactured part quality [8]. This is further discussed in-detail here and hence the focus of this literature review is introduced.

AFP manufacturing involves building each ply of a laminate tape-by-tape by placing each tape next to each other. If these tapes are not perfectly adjacent to each other, defects such as gaps and overlaps i.e., tapes too close or far from each other, occur. These gaps and overlaps then become the starting point for several other defects such as tape wrinkling, insufficient intimate contact and bonding between subsequent plies, interlaminar voids, resin-rich areas within the laminate and thickness variations which ultimately becomes a failure initiation point and reduces the mechanical properties of the AFP manufactured parts [9].

Formation of gaps and overlaps are not yet predictable. In industrial manufacturing using AFP, the parameters of the machine are therefore set to form only gaps or only overlaps [31]. For example, thermoset AFP processing usually involves leaving small gaps only as the post curing step in the autoclave can help reduce these gaps by squeeze flow of the resin into the gaps [32]. However, for in-situ consolidation of thermoplastic composites, gaps and overlaps is a huge challenge as there is no secondary consolidation process that might give the resin another chance to fill these gaps.

### 2.2.1 Cause

Gaps and overlaps can be formed within a course [1] in a multi-tow placement head or between the courses due to several factors. These include machine & material related and process related factors. Machine & material related factors can be considered to be the primary cause as it is independent of any specific part geometries, placement strategies or fiber steering and is valid for all AFP processing. These are:

**Machine accuracy**

The placement of the tows is directly affected by the accuracy of the AFP machine. Errors in positioning the tows perfectly adjacent to each other will result in the formation of gaps and overlaps. This factor, however, can be disregarded due to the development of the enhanced robotic systems and control softwares over the years. Accurate robots are capable of placing the tows with an accuracy of $\pm 0.03$ to $\pm 0.08$ mm.

**Tape width inconsistency of the as-received tape**

Gaps and overlaps can be formed if the raw material i.e., the as-received tows/tapes are not consistent in their width. This factor is dependant on the supplier and the manufacturing quality of the tows. In a research done by Kollenburg [33], the width of the as-received tow from two different suppliers i.e., Toray and Suprem was measured using a dedicated set-up with a laser-line scanner as the measuring device. It was found that the standard deviation for the two materials was just 0.4 % and 0.5 % for a 0.25" wide tape after smoothing of the data as opposed to the 4-12 % indicated by various literature. Another study by Yadav and Schledjewski [34] on tape material from SGL Carbon found the standard deviation to be 0.004 % for a 1" wide tape. This negligible width variation in as-received tape from Suprem was also shown by Khan in his study [35]. Therefore, looking at the manufacturing developments by the suppliers and accuracy of the supplied tows/tapes, this factor can also be disregarded.

**Tape width deformation during placement**

One of the primary reasons for the formation of gaps and overlaps is the tape width deformation during placement. Since the tape is processed entirely in-situ, several mechanisms as described in subsection 2.1.2 and process settings change the tape width during placement. Although it is an important factor in the formation of gaps and overlaps, only few research has been focused entirely on this. These are discussed in detail in section 2.3 and is the main focus of this literature review.

Processing related factors that play a role in the formation of gaps and overlaps is majorly due to the complex part geometries, placement strategies and fiber steering [8] [9] [33]. Complex part geometries that require variable tape width such as tapered or double-curved surfaces (Figure 2.6a); tow placement strategies such as the conventionally used shifted method in which the adjacent tows do not fit exactly next to each other due to radius variation along the tow course (Figure 2.6b); and fiber steering induced defects such as fiber wrinkling and buckling (Figure 2.6c) lead to the formation of gaps and overlaps.

[1] A course is defined as a single run of the AFP head along a programmed path. Several courses are programmed adjacent to each other to form a complete layer in a laminate.

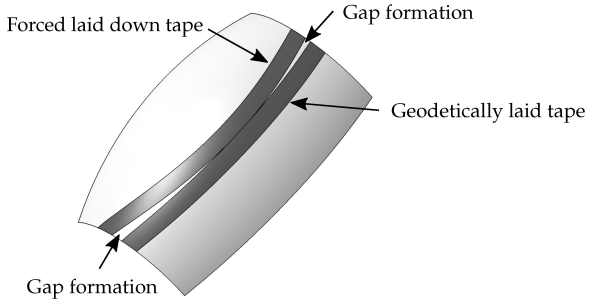


**(a)** Gap formation through forced paths on a curved surface [36].

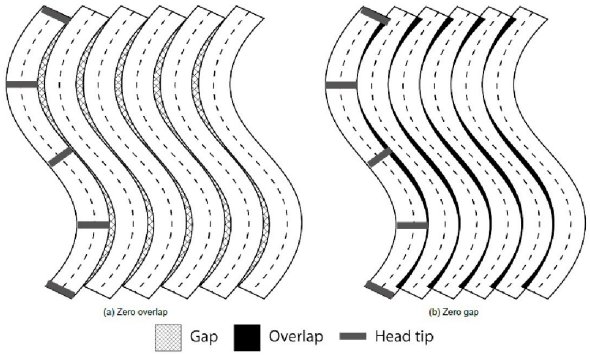


**(b)** Gaps and overlaps due to the shifted method [33].

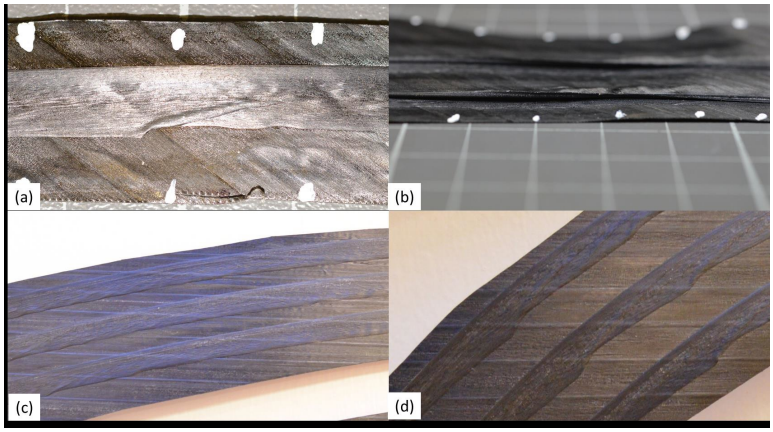


**(c)** Width variations leading to gaps and overlaps while steering due to fiber wrinkling, buckling and pull-up [37].

**Figure 2.6:** Processing related factors that lead to the formation of gaps and overlaps.

### 2.2.2 Effects

Gaps and overlaps have major effects on the final quality of the manufactured laminate. Some of the related literature and their findings are summarized below.

In a study by Sawicki and Minguet [38], it was concluded that the primary cause of strength reduction due to gaps and overlaps is out-of-plane waviness in adjacent plies. A compression strength reduction of $5 - 27\%$ was reported for a single gap or overlap of 0.03" and it was found that this reduction in strength did not increase with increasing size of the gap/overlap and increasing number of defects. However, a recent study by Nguyen et al. [39] found that both the tensile and compressive strengths and stiffness decreased with increasing size of the gaps due to more prominent localization of the failure strain in the gaps. Tensile stiffness reduction upto 60% and strength reduction upto 45% for the gap size of 0.5"; and compressive stiffness and strength reduction upto 45% for the gap size of 0.25" was reported. For small gaps of size 0.0625" and 0.03125", the tensile stiffness did not have any effect while the tensile strength reduction reported was about 0-20 %. Additionally, the effect of small gaps on the compressive strength was found to be significantly large (30-35 %) due to bending of the specimen caused by asymmetry of the laminate. On the other hand, the influence of

increasing overlap size was found to be marginal on the tensile properties; and compressive properties did not show any significant influence of overlaps.

Experimental study by Marouene et al. [40] on the effects of gaps and overlaps on the buckling behaviour of variable stiffness laminates showed that the laminates with 100% overlaps had higher buckling resistance than laminates with 100% gaps. Pre-buckling stiffness and buckling load were reported to be 40% and 69% higher respectively. However, these results were reported without normalizing with respect to either thickness or weight.

Another study by Ghayour et al. [41] on the effect of tow gaps on the low velocity impact strength of thin laminates showed that the maximum impact force reduced by 17% for impact energies less than 15 J on a composite plate with 8% gaps. The delamination area was also observed to increase by 50%, where the gaps served to be the delamination initiation sites.

Guin et al. [42] studied the effects of inter-tow gaps in notched and unnotched specimens. Two different configurations were used for the gaps i.e., one with a 0.050" gaps in all the plies and the other with these gaps in only the 90°plies in a laminate with the stacking sequence: $[+45/-45/90/0]_{2s}$. These were compared with a baseline specimen with no intended gaps. Several interesting conclusions were drawn from the experimental results: 1) The fiber waviness was significant throughout the laminate in which the gaps were present in all the plies while for the laminates in which the gaps were only in the 90°plies, the waviness was limited only to the adjacent plies (0°plies). 2) For unnotched tension and compression tests, it was found that except the tensile modulus, the tensile and compressive properties i.e., strength and modulus reduced when compared to the baseline specimen. This is due to the fact that tensile loading leads to the reduction in fiber waviness and therefore does not have any significant effect on the modulus whereas, the compressive loading leads to an increase in fiber waviness. 3) For notched compression testing, the strength reduced again but the reduction was relatively lower when compared to unnotched compression testing. 4) The tensile and compressive properties (both notched and unnotched) for the specimens with gaps only in the 90°plies was unaffected. This is an interesting result as systematic defects such as the one where all the plies have gaps are highly unlikely in an industrial setting. Therefore, it is suggested that the mechanical properties of AFP manufactured laminates with incidental gaps in random locations will not be significantly affected as in the case of systematic defects in all plies.

All the above literature is based on large and systematic defects in AFP manufacturing with thermoset matrix having a secondary curing step in the autoclave. For in-situ AFP manufacturing, both increase and reduction of the effect of gaps and overlaps on the mechanical properties is expected. Increased effect due to the absence of a secondary processing step in the autoclave which might have reduced the amount of gaps and overlaps. And, reduced effect due to randomly occurring gaps and overlaps which might compensate for one another. Therefore, more research needs to be done on the mechanical characterization of in-situ AFP manufactured thermoplastic composite laminates and the effects of randomly placed defects such as long, narrow gaps and overlaps that is usually caused by the tow width variations.

### 2.2.3 Mitigation

Several studies have proposed different mitigation techniques to counter gaps and overlaps in AFP manufacturing. These are listed below.

1. Staggering [43]: In this approach, the plies of same orientation are shifted with respect to each other in order to distribute the thickness variations caused by gaps and overlaps. However, this approach is questionable as it introduces certain constraints on the stacking sequence and does not provide enough improvement in mechanical properties [44].

2. Rakhshbahar and Sinapius [45] proposed a technique to mitigate the effects of gaps by scanning them with profile sensors, filling it with externally 3D printed carbon continuous-fiber reinforced plastics and consolidating in a press. This secondary processing step, however, is a drawback for industrialization even though the mechanical properties were found comparable to the laminates with no gaps.

3. Two different ply construction methods i.e, parallel and continuous tow shearing methods can be used instead of the conventionally used shifted method that is prone to gaps and overlaps [33] [46]. Figure 2.7 illustrates these methods. However, these methods result in accumulation of curvatures to a point where the steering radius becomes too high for the tape and may lead to defects such as fiber wrinkling, buckling and pull-up [7].

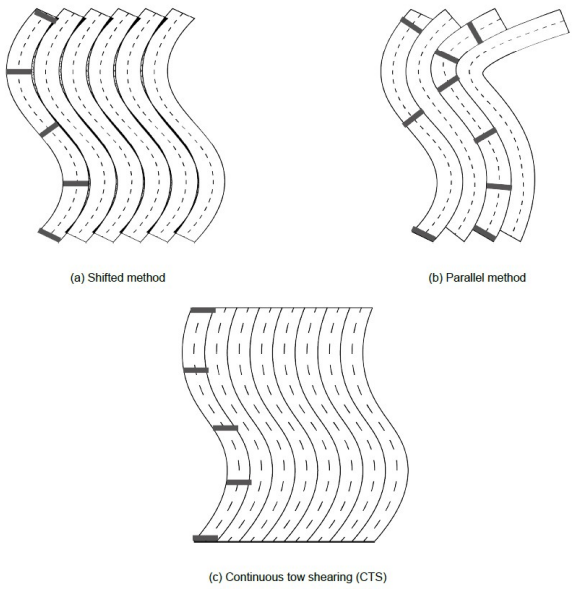


**Figure 2.7:** Different ply construction techniques [33]

4. Kollenburg [33] investigated the feasibility of eliminating gaps and overlaps by local fiber steering and concluded that it can be used to reduce it but not completely eliminate it.

5. In-line tape width control or spreading is another approach where the tape width is purposefully varied in-line as the tapes are being placed. This was initially studied by Wang and Gutowski [47] but as a separate consolidation step. Two different techniques for in-line spreading have been proposed i.e., by controlling the compaction force by the AFP roller [34] and a dedicated device that can control various process parameters like temperature, pressure and pulling rate to spread the tape to the desired dimension [48]. These techniques can also be applied for fiber steering in variable stiffness composites

and complex double-curved surfaces. The concept of in-line tape width control looks promising but is still in its preliminary design stage.

## 2.3 Tape width deformation

Tape width deformation during placement as described in subsection 2.2.1 is one of the primary causes for gaps and overlaps in AFP manufacturing. Several studies have been done previously investigating dry fiber tow spreading using a system of rollers. Some of the findings from these studies include dependence of dry tow spreading on the angle and lateral distance between the rollers [49] and applied tension on the tow [50]. However, very limited study has been performed on the tape width variation of prepreg tapes during placement in AFP manufacturing. Currently available knowledge on this and related literature based on the parametric studies performed are discussed in this section.

### 2.3.1 Tape width deformation mechanism

Transverse squeeze flow is often considered to be the main tape width deformation mechanism. At processing temperatures, the resin becomes highly viscous and the squeeze flow is described as the shear deformation of the fiber-resin mixture as it is being compressed. This results in the deformation of the material only in the thickness and width directions i.e., perpendicular to the fiber direction because of low stiffness when compared to that along the fibers [51] [52] [53].

Previous studies on transverse squeeze flow have also investigated the influence of various parameters like pressure, temperature, fiber content, orientation and number of plies on the width and thickness changes and have found that the fiber content, orientation and number of plies also plays a role in the transverse squeeze flow. Higher fiber content [51] and larger angle between the adjacent plies [52] prevents squeeze flow because of the higher stiffness of the fibers and more restricted movement of the resin respectively. This was, however, contrasted with a study by Brulotte [54], where it was found that higher angle difference between the substrate and the deposited ply increased the width deformation. Friction effect between the plies was suggested to be the cause i.e., higher surface irregularity along the fibers creates more friction between same angled plies and thus prevents it from sliding and deforming. It was also found that the tested temperatures above the material $T_m$ did not have any effect on the tape width deformation because of negligible change in material viscosity above the $T_m$. Another study showed that increase in the number of plies in the laminate leads to an increased width deformation [53]. It was also found that the unconsolidated plies did not cause any transverse squeeze flow at lower nominal applied pressure because of consolidation effects [53]. Wang and Gutowski [47] concluded from their study on elimination of gaps and overlaps that the squeeze flow is a time-dependant phenomenon i.e., it increases rapidly initially and then slows down as the time progresses, indicating that slower AFP processing time would cause more width deformations when compared to faster processing as the time available for squeeze flow increases. These studies, however, have been performed under static conditions where the tape is heated and compressed between two platens.

This transverse squeeze flow mechanism has been adapted to model tape width deformation for AFP process by Kok [32]. However, experimental validation of the transverse squeeze flow

model performed by Khan [35] and Kok [32] shows that the experimental results do not represent the results obtained by the model. Additionally, it was observed that the experimental width change required a strain well above the strain at break of the fiber if the width change occurred only in a short length under the roller as shown in Figure 2.8; suggesting that the conventionally accepted tape width deformation mechanism i.e., transverse squeeze flow does not hold for AFP processing.

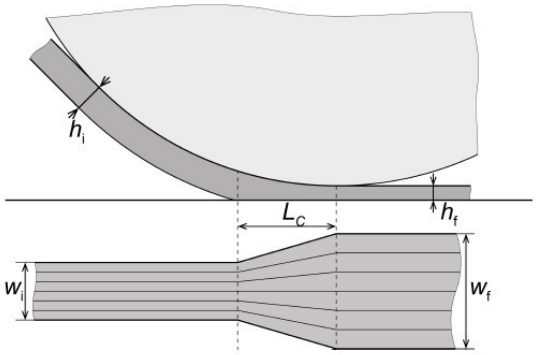


**Figure 2.8:** Tape width deformation based on transverse squeeze flow model [32]

### 2.3.2 Tape width deformation profile

Tape width deformation profile under static conditions was analysed both numerically and experimentally by Wang and Gutowski [47]. The tape width deformation was modelled based on transverse flow of a power law fluid and aramid tracers were used through the thickness of the laminate to determine the displacement at several points experimentally. The results indicated that transverse shear deformation takes place but not on the top and bottom surfaces as shown in Figure 2.9. It was also concluded that Sheet Moulding Compound (SMC) with randomly oriented fibers do not deform in the same way and therefore, continuous fiber reinforced material with misalignment or entanglements could also deviate from the observed deformation profile.

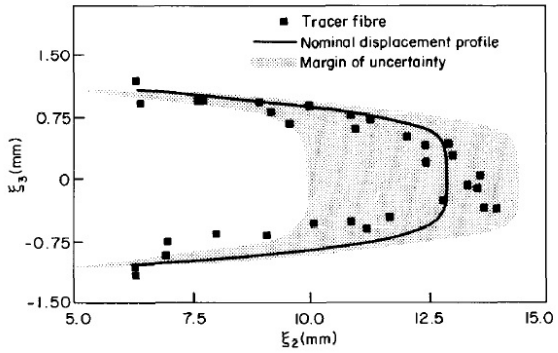


**Figure 2.9:** Numerical and experimental transverse deformation profile [47]

Edge deformation profile for AFP processed CF-PEEK prepreg tape was analysed under the microscope by Khan [35]. It was found that the tapes deformed in three different profiles

as shown in Figure 2.10 and were categorized as types II, III and IV (considering that type I is the rectangular profile of the as-received unprocessed tape) based on the radial velocity profiles for squeeze flow of viscoplastic fluids between two disks. The different profiles were then correlated to the energy input during the AFP processing and it was concluded that low energy input i.e., low gas volume flow & high process velocity caused type II deformation and high energy i.e., high gas volume flow & low process velocity caused type IV deformation. Type III deformation was caused by intermediate energy input and can be considered to be the transition type between type II and IV.

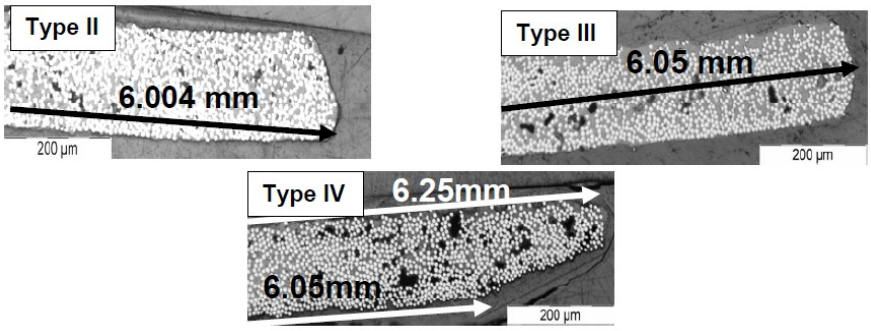


**Figure 2.10:** Tape edge profile analysis with half width measurement indicated [35]

### 2.3.3 Influence of processing parameters

Currently available studies have shown that the tape width is a function of various processing parameters of AFP manufacturing. These are discussed below.

Experimental characterization of the tape width deformation for AFP processing was performed by Khan [35]. The study was performed on CF-PEEK prepreg material with a mean initial width of 11.88 mm and hot gas torch as the heating device. Width change was determined by measuring the width of the consolidated tape using a CCD camera installed behind the roller and compared with the initial width of the tape scanned by the same camera without any consolidation first. Parametric studies on layup velocity and hot gas flow volumes were performed by laying up tapes on a heated tool and the graphs obtained is shown in Figure 2.11.

For hot gas torch as the heating device, the temperature is directly related to the gas volume. Therefore, the graph can be seen as a function of temperature. It is clear from the graph that the temperature does not have a distinct influence on the tape width as the trend changes with the layup velocity. Additionally, the effect of varying layup velocities cannot be deduced from this study as it is not isolated from other parameters like temperature. The tape temperature is directly related to the gas volume flow in a hot gas torch and the placement speed. Therefore, large change in width at low velocity is most likely due to higher temperature of the tape.

Predictive modelling of width variation based on the squeeze flow model with a semi-slip boundary condition was attempted by Brulotte [54]. Input parameters from both steady state deformation tests and ATP processed tapes were used to feed the width variation model.

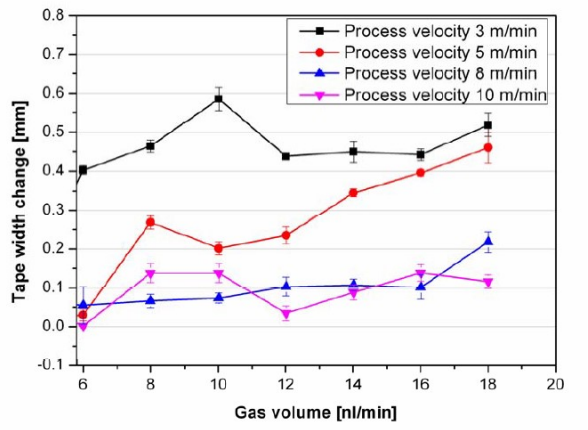


**Figure 2.11:** Experimental results of tape width change as a function of gas volume at different layup velocities [35]

However, the modelling results did not match with the experimental results and the cause of the error was suggested to be due to underestimation of the compaction pressure and temperature related material viscosity. Therefore, a correction factor of 500 was used in the model to fit the results according to the experimental results. After a good fit was established, the model was used to predict the influence of compaction force, orientation between the plies and placement speed on width deformation. It was concluded that the tape width deformation increases with increasing compaction force and orientation between the plies and decreases with increasing placement speed. This is illustrated in Figure 2.12 as a surface plot, where strain represents the change in width.

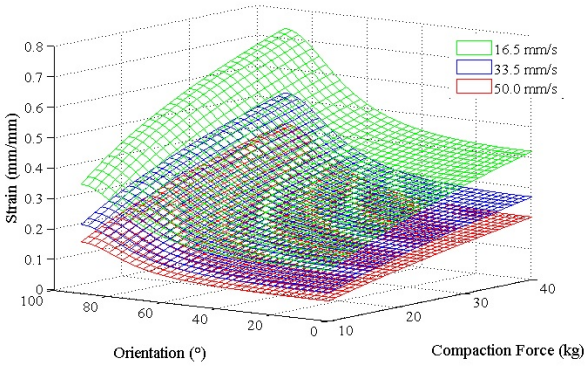


**Figure 2.12:** Width deformation prediction surface plots [54]

An experimental analysis on width variation in LAFP by Kok [32] showed that the tape width deformation is a function of temperature only and not compaction pressure as shown in Figure 2.13. This study was also performed on CF-PEEK prepreg material except that quarter inch tapes were laid on press-consolidated substrate made of the same material with a stacking sequence of $[0/90]_{2s}$. The tapes were placed perpendicular to the base ply at a placement speed of 100 mm/s for all specimens and width change was determined using microscopy images of the as-received and the processed tapes.

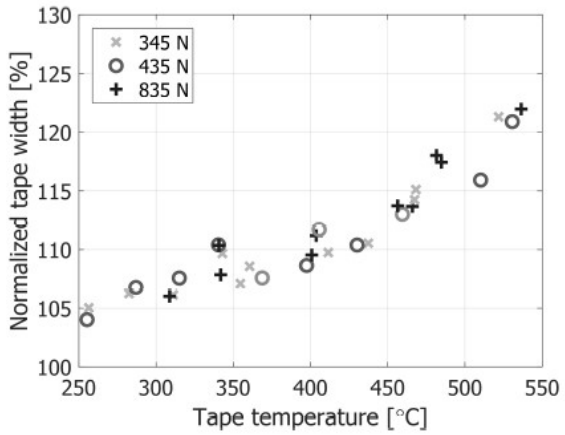


**Figure 2.13:** Experimental results of tape width as a function of tape temperature at different compaction pressures [32]

However, a recent study on in-line tape width control for CF-PA6 ATL by Yadav and Schledjewski [34] showed that the tape width increased non-linearly with increasing compaction force as shown in Figure 2.14 (left). The experiment was performed with humm3® flashlamp as the heating device and tape widths before and after consolidation were scanned using two integrated laser profile scanners on the ATL head. Tapes with a mean initial width of 25.4 mm were laid on a heated tool at 30 °C at a layup velocity of 50 mm/s for all the specimens. It was also found that increasing the heat input power of the humm3® by 10% did not have any effect on the width change (Figure 2.14 (right)). However, it was not mentioned which parameter of the flashlamp i.e., pulse energy, duration or frequency, was changed for increasing the heat input power.

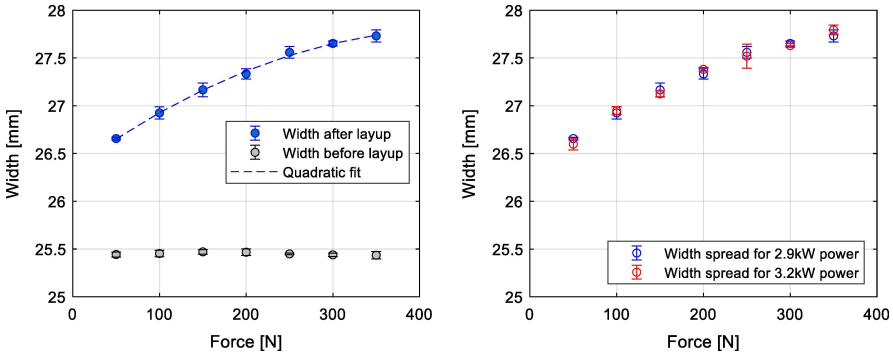


**Figure 2.14:** Width variation as a function of compaction force (left) and width variation for two different heat input powers (right) [34]

Therefore, based on these results, it was observed that a minimal force of 50 N was enough for the majority of the tape width deformation and increasing the tape temperature by increasing the input power did not have any effect as the melt viscosity of the material does not change significantly after the material $T_m$.

These observations are in contrast to that of Kok's [32] where the tape width variation was found to be a function of the temperature instead of the compaction pressure. The influence

of compaction pressure was also shown by Clancy et al. [48] in their study where only the pressure was varied to achieve 45% tape spread. This, however, was done in a spreading device with two hot platens but under dynamic conditions.

Tape width variations were also checked by Oromiehie et al. [55]. CF-PEEK prepreg material with an initial width of 6.35 mm was used in an HGT-assisted AFP machine to manufacture samples with 24 different processing conditions by varying the temperature, force, and placement speed. The results obtained are shown in Figure 2.15. General observation from these graphs indicate increase in width with increasing temperature. The influence of consolidation force and placement speed is not clear as it does not follow a common trend between varying temperatures. These results, however, cannot be used as a reference for further studies on tape width deformation as the samples manufactured consist of 21 plies laid on top of each other to create a laminate. This approach does not isolate the effects of processing parameters to study its direct influence and may cause other factors such as machine inaccuracy, width variation of the as-received tape and substrate thickness influence to also have an effect on the final width.

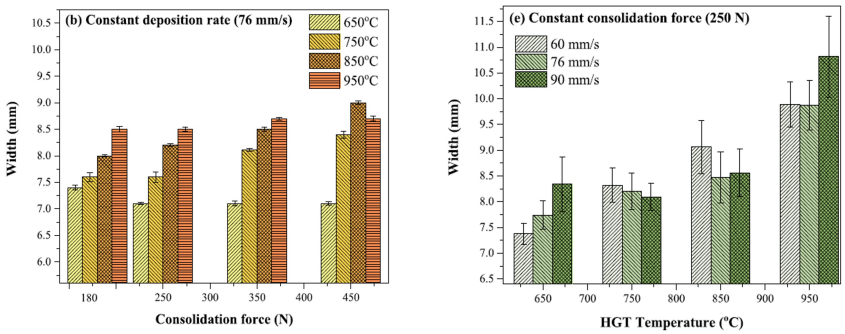


**Figure 2.15:** Width variation with different processing parameters [55]

The effect of tape tension during the heating phase of LAFP process on the width variation has also been researched by Blommert [56] and the experimental results show no correlation betweeen the two. However, the research only studied the effect due to deconsolidation of the tape during heating and did not study the effects when combined with consolidation too. Therefore, the result cannot be related to in-situ AFP processing.

A width shrinkage of about 12-22% was reported by Valverde et al. [57] for carbon/epoxy material in the release phase of the AFP process. This is because of the volumetric shrinkage of polymers as it cools down. This effect can be even larger if the tape is released above the glass transition temperature $T_g$. Other mechanisms that could influence the tape width after the release phase are waviness and void expansion as reported in literature [27] [58] for release temperatures above the $T_g$.

# Chapter 3

# Research definition

Based on the literature review on tape width deformation during in-situ AFP manufacturing, research gaps have been identified. This is presented in this chapter along with the introduction of the research objective and some research questions with possible hypothesis for it. The answers to these questions will help in filling the knowledge gaps identified.

## 3.1 Research gap

As discussed in the previous chapter, tape width deformation during placement is one of the primary cause of gaps and overlaps defect in AFP manufacturing. And, this becomes more important for in-situ AFP manufacturing as there is no secondary step that might alleviate it. Therefore, it is very important to minimize the occurrence of these gaps and overlaps for in-situ AFP manufacturing of thermoplastic composites in order for it to be realized as a viable manufacturing technique for aerospace applications with high quality standards.

The first step towards mitigation of this defect is understanding the mechanism behind the tape width deformation and how it is influenced as it is placed during AFP processing. Clearly, the current knowledge on this topic is lacking and therefore, tape width deformation during placement in AFP can be considered as a general research gap. Specific research gap addressing the width deformation mechanism and influence of tape temperature distribution is discussed below.

**Tape width deformation mechanism**

As discussed in subsection 2.3.1, the transverse squeeze flow model did not represent the width deformation in AFP processing conditions when checked experimentally. Kok [32] incorporated fiber spreading into the transverse squeeze flow model of Ranganathan et al. [59] as it was observed that the experimental width change required a strain well above the strain at break of the fiber if the width change occurred only in a short length under the roller as shown in Figure 2.8. Therefore, models incorporating fiber spreading and practical changes such as fiber continuity and longer contact length under a deformable roller in the

transverse squeeze flow model were checked. It was found that neither of them represented the experimental results. Therefore, it was suggested that the width deformation is based on quasi-static deformation i.e., spreading of the fibers before the nip-point instead of under the roller as illustrated in Figure 3.1. This should, however, be experimentally checked.

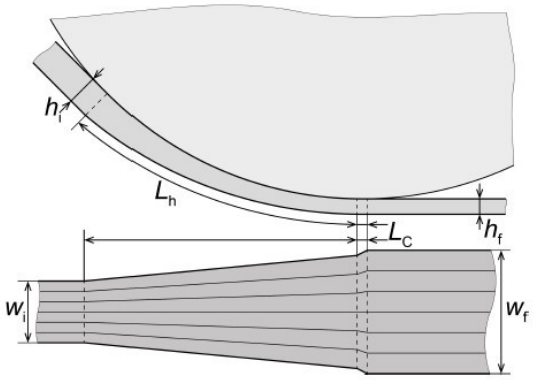


**Figure 3.1:** Tape width deformation based on spreading before the nip-point [32]

#### Influence of tape temperature distribution

Based on the literature found on influence of processing parameters in subsection 2.3.3, it is clear that the temperature and pressure play a major role in the tape width deformation. However, results from different studies do not agree with each other, indicating that the tape temperature distribution might be at play. This is also suggested by Kok [32] in the quasi-static deformation model, where the heated length instead of the temperature might influence the tape width deformations as spreading occurs before the nip-point. Here, the heated length is defined as the length of the tape above the melt temperature. Hence, a research gap is identified and a parametric study on heated length of the tape with other processing parameters i.e., temperature and pressure should be performed since the heating mechanism for the humm3® xenon flashlamp differs from the other heating devices commonly used.

## 3.2 Research objective

The research objective is to investigate the tape width deformation mechanism for in-situ AFP processing of thermoplastic prepreg tapes using humm3® as the heating device and understand the influence of process parameters on the width deformation.

## 3.3 Research questions

Based on the research objective and gaps identified, the main research questions are formulated below along with certain sub-questions to answer these questions:

**RQ1.** ***What is the governing mechanism behind tape width deformation during in-situ AFP processing of thermoplastic prepregs?***

SQ1.1 In which phase of the process does the width deformation take place?

SQ1.2 What are the geometrical changes on the tape after the process?

SQ1.3 How does the tape deform in the micro scale?

**RQ2.** ***How does the process parameters influence the width deformation?***

SQ2.1 How does the heated tape length influence the tape width deformation?

SQ2.2 How does the processing temperature influence the tape width deformation?

SQ2.3 How does the compaction pressure influence the tape width deformation?

The answer to these questions will help in achieving the research objective set for this study and better understand the mechanism at play during AFP.

Furthermore, the result of this study will lead to accurate prediction of approximate tape width after placement based on the manufacturing parameters of AFP, which will ultimately add value to the final goal of eliminating gaps and overlaps in AFP manufactured parts. It will contribute to having a predictive model with close resemblance to the actual manufactured structure.

## 3.4 Hypotheses

Based on the gathered literature and knowledge on this topic, hypotheses are proposed for the above formulated research questions. These hypotheses should be checked experimentally to answer the main research question.

1. The width deformation is expected to take place in the heating phase rather than the consolidation phase of the process.
2. Transverse spreading of the fiber-resin mixture is expected. Resin percolation flow is not expected in the transverse (width) direction due to lower permeability in the transverse direction and high melt viscosity of thermoplastic polymer matrix.
3. It is expected that when a longer heated length is available, more tape width deformation will occur. This is expected for two reasons.

   One, the fibers are in molten, low-viscosity, resin for a longer length. This will allow the fibers to start spreading at a larger length. Therefore, the fiber straining in the transverse direction is reduced and more spreading is possible.

   Two, the heat will have more time to propagate through the thickness, leading to a larger part of the tape (in thickness direction) being in molten state. Therefore, better heat distribution through the thickness should promote spreading.

4. Once the temperature is above the $T_m$, the temperature will not play a role in the width deformation but only the heated length due to negligible change in melt viscosity. At sub-melt temperatures, some width deformation is still expected as spreading is possible due to the movement of the polymer (resin) chains.

5. Once the temperature is above the $T_m$, the spreading is only restricted by the maximum strain i.e., strain at break of the fibres. Therefore, increasing the pressure will not have any effect on the tape width after it is already at its maximum. At sub-melt temperatures, the spreading is restricted by the limited polymer (resin) chain movement also. Therefore, increasing the pressure will allow more chain movement and hence more fibre spreading.

# Chapter 4

# Methodology

This chapter describes the methodology that was planned to be used to conduct the experimental work and to achieve the research objective set out for this study. A flow chart showing the methodology for answering the research questions formulated is presented in Figure 4.1.

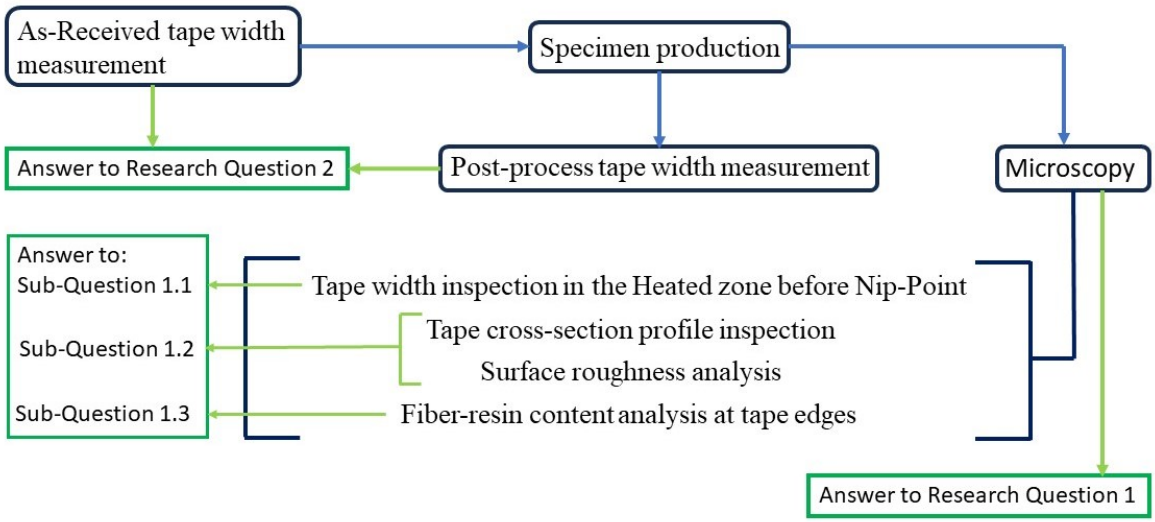


**Figure 4.1:** Methodology flow chart for answering the research questions.

The approach can be divided into two major tasks i.e., tape width measurement and microscopy. For the width measurement, it was initially planned to extract the width data of the tape in-situ i.e., by continuously measuring the width before and after placement to be able to trace the width deformation to the exact as-received tape width at a given point. This was planned to also account for the high width variations in the as-received tape as suggested in literature. However, this method was dropped due to lack of enough space on the AFP head for mounting two measuring devices (one pointed towards the incoming tape and the other one towards the placed tape after the roller) and negligible tape width variation of the

as-received tape i.e., $\pm 0.005$"($0.127mm$) for 0.25"($6.35mm$) tapes as given in the material data provided by the manufacturer. This was also confirmed experimentally. Therefore, an ex-situ method was adopted i.e., measuring the tape width after the processing and comparing with the as-received tape width data. A full factorial parametric study on the width data was performed by having different settings for the heated tape length, processing temperature and compaction pressure to check the influence of these processing parameters on the tape width deformation individually as well as any interaction effects between them to answer all the sub-questions for Research question 2.

For Research question 1, each sub-question had a specific post-processing step planned in order to answer them. This includes: Sub-question 1.1: Inspection of the tape width in the heating zone before the tape reaches the nip-point to check if there is any width deformation in this phase of the process; Sub-question 1.2: Inspection of the tape cross-section profile and analysis of the surface roughness and comparing them with the as-received tapes to understand the geometrical changes taking place during the processing; Sub-question 1.3: Comparing the fiber and resin content at the tape edges after processing with those at the tape middle and with the as-received tapes to check if the width deformation is because of only transverse resin percolation flow at the edges or a uniform flow of the fiber-resin mixture.

# Chapter 5

# Experimental set-up

This chapter describes all the experimental work performed in detail including the material and equipment used, specimen manufacturing and post-processing i.e., width measurement and microscopy.

## 5.1 Material

LM-PAEK (Low-Melt Poly Aryl Ether Ketone) thermoplastic material is a relatively newer material that has caught the interest of the aerospace industry compared to the traditionally used thermoplastic materials such as PEEK (Poly Ether Ether Ketone), PEKK (Poly Ether Ketone Ketone) and PPS (Poly Phenylene Sulphide) because of its excellent processability due to a low melt viscosity and much lower processing temperature (upto 60 °C lower) while maintaining comparable mechanical properties to others. Additionally, it has a lot of potential for in-situ AFP processing as the low melt-viscosity helps to form a good bond without requiring an additional step of consolidation in the autoclave and to reach higher processing speeds as the time required for bond formation is reduced. This was also observed by L. Raps et al. [60] in their experimental study where they found that the layup speeds investigated (1.0, 3.75, 7.5 and 15 m/min) did not have a significant impact on the bonding strength and crystallinity.

Therefore, Toray Cetex® TC1225 was used for this study in the form of 0.25" (6.35 mm) wide carbon UD prepreg tapes. The material properties are listed in Table 5.1

## 5.2 Equipment

The detailed specifications of the used equipment are listed below.

1. AFP Head: An AFP head, mounted on a Kuka KR500 robot as shown in Figure 5.1, capable of processing quarter-inch prepreg tapes and laying 16 tapes simultaneously

**Table 5.1:** As-received material properties for Toray Cetex® TC1225.

| Property | Description/ Value |
|---|---|
| Fiber | T700G Carbon UD |
| Resin | Semi-crystalline LM-PAEK |
| Fiber areal weight ($g/m^2$) | 194 |
| Resin content (wt%) | 34 |
| $T_g$ (°C) | 147 |
| $T_m$ (°C) | 305 |
| Typical $T_p$ (°C) | 340-385 |
| Tape width (inch, mm) | 0.25, 6.35 |
| Nominal consolidated ply thickness (mm) | 0.185 |

was used to manufacture the specimens in a controlled and repeatable way. Here, only one tape was laid at a time to avoid any interaction effects between the tapes.

2. Compaction Roller: An 85 mm diameter silicone roller with a hardness of 60 shore was used along with a 165 $\mu m$ thin Teflon protective foil on it to avoid burning of the roller during the manufacturing.

3. Heating device: A 130 mm wide broadband ($\lambda \simeq 200\ nm - 1050\ nm$) Xenon flashlamp system humm3® from Heraeus Noblelight Ltd. Cambridge was used. The maximum input power for the flashlamp was 14 kW with an estimated input to output power efficiency of 0.5. A triangular-end shaped light guide as shown in Figure 5.2 was used. The two edges have different lengths and angles which can be seen in the figure.

4. Tool: A heated layup tool mounted vertically with respect to the robot and covered with a thin polyimide Upilex® film for easy release was used. Vacuum was applied to create a smooth surface without any wrinkles.

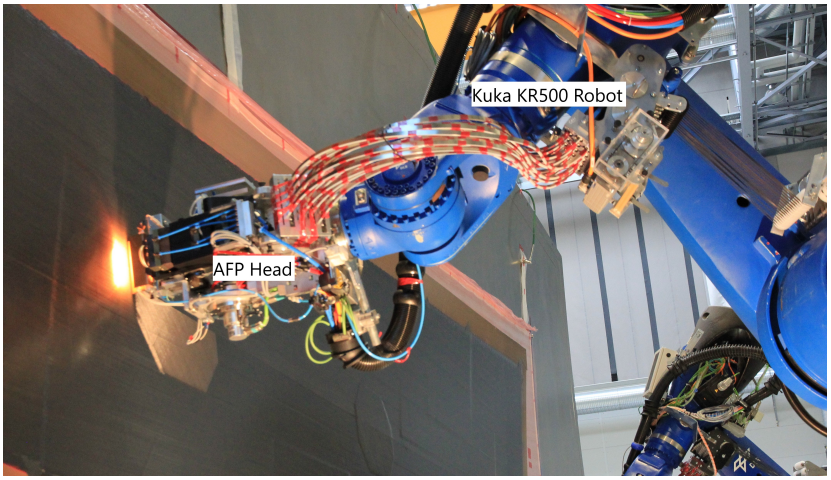


**Figure 5.1:** AFP head mounted on a Kuka KR500 robot.

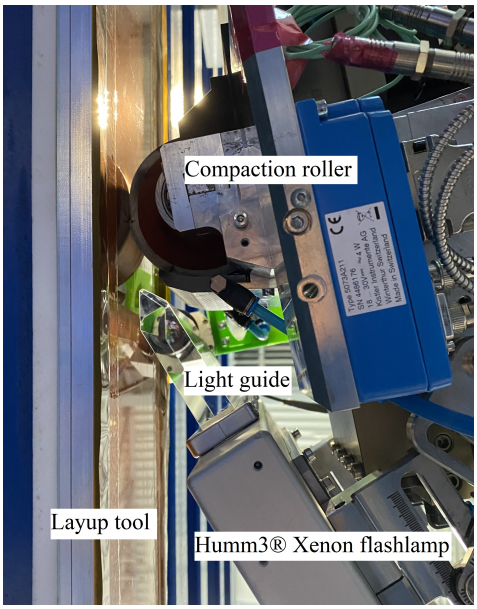


**Figure 5.2:** Equipment used to manufacture the specimens.

## 5.3 Specimen manufacturing

### 5.3.1 Process parameters

**Table 5.2:** Process parameters used in the experimental study.

| Heated length | Compaction force (N) | Nip-point temperature (°C) |
|---|---|---|
| Short (35-40 mm) | 300 | 370 |
| Long (45-50 mm) | 900 | 420 |
| | | 250* |
| | | 300* |

The processing parameters for the experiments were determined based on relevance to in-situ AFP manufacturing. The only limitation in the used set-up was the power limitation of the humm3® flashlamp which would directly pose a limitation on the highest nip-point temperature achievable during the process. Therefore, a constant placement speed of 850 mm/min was used for all the specimens which was slow enough to reach the desired highest temperature of 420°C at the nip-point. Three variables i.e., nip-point temperature, compaction force and heated length were selected for a full factorial Design of Experiments (DoE) with two data points for each. For compaction force and heated length, high and low settings were used to get clear effects and for temperature, two temperatures were selected based on the typical processing temperature range and suggested nip-point temperature range for in-situ AFP processing by the material manufacturer. Additionally, two extra temperature data points (marked with a * in Table 5.2) were added to check the effects when the material is below the $T_m$ but above the $T_g$ and just around the $T_m$. These data points are given in Table 5.2. Three samples of length 580 mm for each configuration of process parameters were manufactured. Other process parameters that were kept constant throughout the experimental work are Tool

temperature = 80°C and AFP head pitch angle = 80° (angled 10° away from the flashlamp).

### 5.3.2 Compaction pressure settings

The compaction pressure for in-situ consolidation of the tape was varied by changing the force applied by the AFP head. Two data points i.e, 300 N and 900 N were used for the experimental study. To estimate the compaction pressure, ink imprints from the roller (as shown in Figure 5.3) were used to measure the contact area under a range of forces applied by the AFP head statically as the effect of roller rotation on the normal pressure is negligible and therefore the dynamic pressure applied during the process can be simplified to a static one [61]. Finally, the applied force was divided by the measured contact area to calculate the average compaction pressure. This method however, is only an approximation as it is assumed that the pressure distribution remains uniform for the entire contact area, whereas in reality, the pressure would be higher at the center of the roller in the tangential direction. Moreover, the tape will experience a higher pressure than the rest of the contact area because of the difference in height. Figure 5.4 shows the applied force and pressure relation. It can be seen that the relation is non-linear. This is because the roller is conformable and therefore the contact area also increase with increasing force, thereby reducing the average pressure applied.

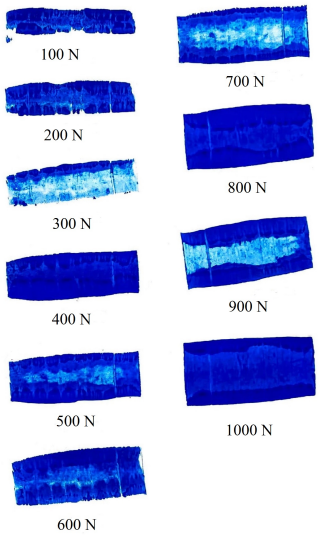


**Figure 5.3:** Ink imprints from the roller.

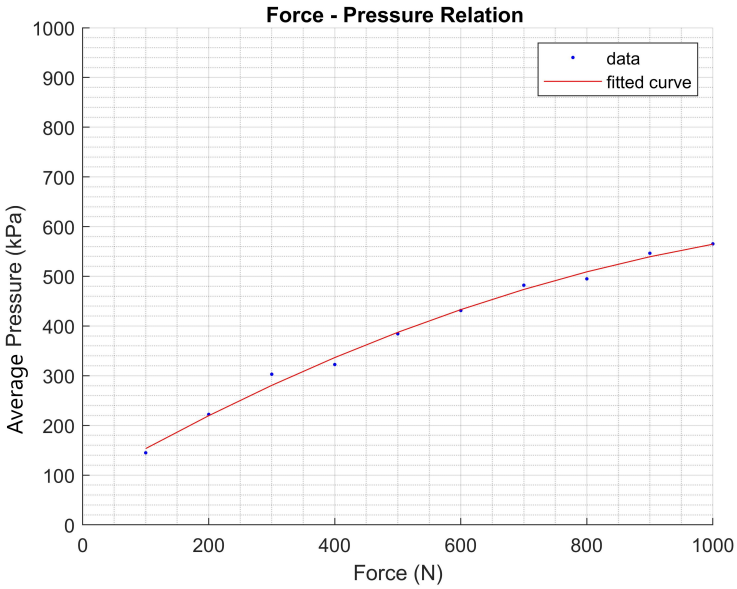


**Figure 5.4:** Relation between applied compaction force and average pressure.

Validation of the pressure applied during the manufacturing was done by measuring the force values from the AFP machine for three dry runs before the actual specimen manufacturing. This is because it was not possible to monitor the force values in-situ during actual specimen manufacturing. Figure 5.5a shows the force variation curve obtained along the programmed course length (corresponding to the location on the specimen). The measurements were made at several points along the course length between 185 mm and 435 mm (from which the

specimens for further analyses were extracted) and a cubic spline interpolation was performed to get the curve. The corresponding pressure values for the curve was then calculated and plotted in Figure 5.5b based on the force vs pressure relation shown in Figure 5.4. The average pressure values achieved for this study were therefore 298 kPa for the 300 N specimens and 543 kPa for the 900 N specimens with (260, 325) and (515, 561) kPa as the minimum and maximum values recorded respectively. The reason for the force and thereby pressure variations along the course length is believed to be because of the roller not being completely balanced with respect to the axle and the layup tool not being completely flat.

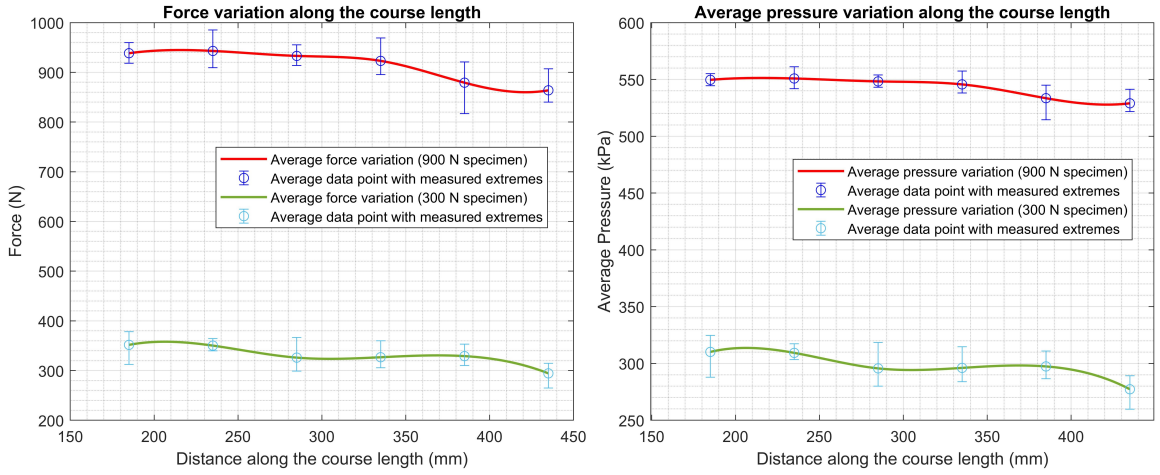


**(a)** Applied force variation

**(b)** Average pressure variation

**Figure 5.5:** Variations in applied force and corresponding average pressure along the course length.

### 5.3.3 Temperature settings

The nip-point temperature was varied by changing the pulse energy (voltage) and thereby the power (kW) of the broadband radiation from the humm3® xenon flashlamp. These are given in Table 5.3. The other two programmable parameters of the flashlamp i.e., pulse duration and frequency were fixed at 2.5 ms and 90 Hz respectively (highest setting) for all the specimens. Additionally, the mounting angle and distance of the flashlamp with respect to the incoming tape was adjusted to focus the light emitted more towards the nip-point.

The temperature was monitored and measured in-situ during the specimen manufacturing using an Optris PI640 thermal camera mounted using a custom 3D printed mount on the AFP head as shown in Figure 5.6. Because of lack of space around the incoming tape, the thermal camera was angled such that the best possible view of the incoming tape could be captured and used for temperature measurements as close to the nip-point as possible. This is shown Figure 5.7. The thermal camera emissivity value for this experimental set-up was measured to be 0.875. Appendix A describes the calibration process for measuring and compensating for the emissivity value in detail.

Figure 5.8 shows the thermal camera images captured while manufacturing the specimens. Several rectangular measuring bars that recorded the maximum temperature in it were placed

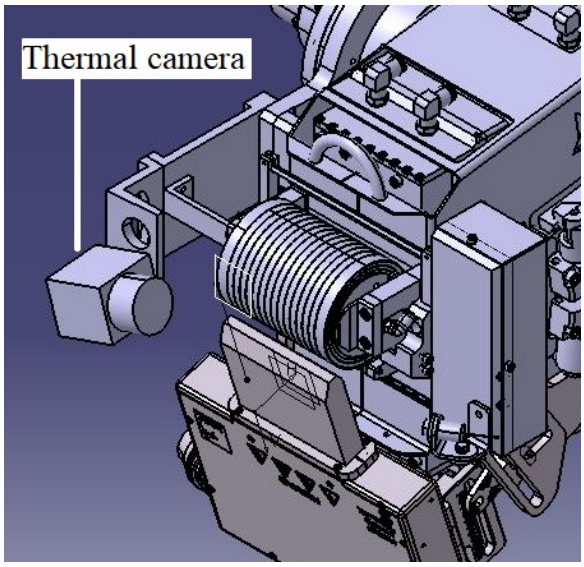


**Figure 5.6:** CAD model of thermal camera positioning.

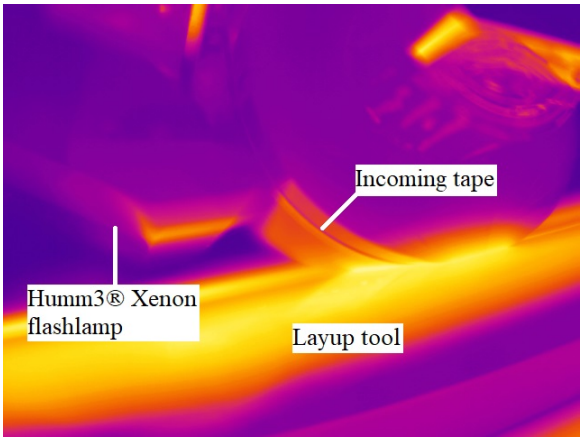


**Figure 5.7:** Thermal camera view.

at an approximate interval of 5 mm from each other with the closest one (S1) being approximately 25 mm away from the "actual" nip-point which is the first point of contact between the roller and the incoming tape. However, this point (S1) was considered to be the "visible" nip-point and used for the reference nip-point temperature for the experimental study as it was observed that the temperature started to drop after this point due to the radiation being blocked by the geometry of the roller. Additionally, it was not reliable to measure the temperature closer to the nip-point than this point due to a large viewing angle between the tape and the view of the thermal camera and reflections from the layup tool.

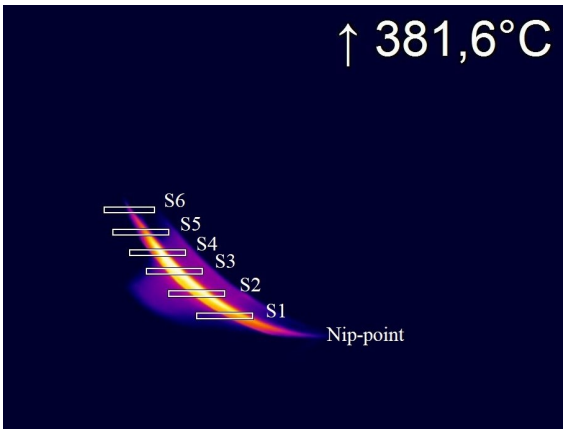


**(a)** Long HL specimens

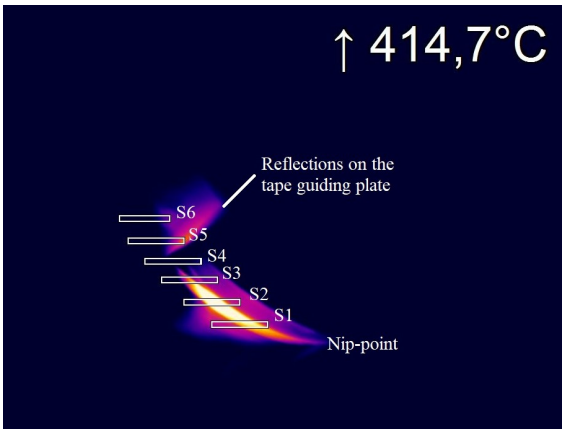


**(b)** Short HL specimens

**Figure 5.8:** Thermal camera image captured during manufacturing.

Another point to be noted is that the temperature distribution along the heated length of the incoming tape was not uniform, which can also be seen clearly in Figure 5.8a and Figure 5.8b where points S3 and S2 are at higher temperatures respectively. This is because the light

guide edge was the closest to these points on the incoming tape (light guide edge tangential to the roller) (see Figure 5.10) and therefore was heated more and reached higher temperatures. The temperature distribution trend along the heated length is shown in Figure 5.9. These trend lines were plotted by averaging all the temperature data from all the specimens and performing a cubic spline interpolation through it. The standard deviations of the data are also indicated by the error bars in the figure.

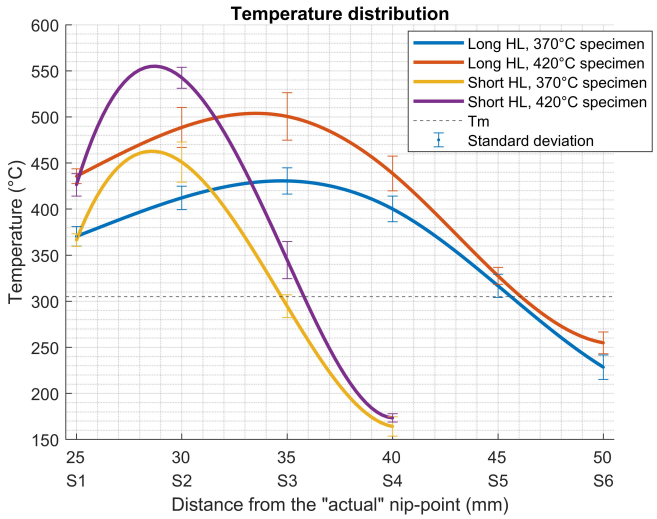


**Figure 5.9:** Temperature distribution along the heated length of the tape.

It was observed that upto 600 °C was reached for some of the short Heated Length (HL), 420 °C specimens for a very short time around point S2 (< 0.7 seconds) which is very high compared to the suggested processing temperature of upto 470 °C for in-situ AFP processing by the manufacturer. Therefore, the surface roughness data (given in subsection 6.1.2) and the cross-section view of the specimens under the microscope were checked for any abnormalities as it was expected that the surface roughness would increase sharply for a burnt resin specimen due to increased voids and bare fibers on the surface. However, the data did not show any abnormalities and the specimens was deemed viable for the experimental study.

### 5.3.4 Heated length settings

The Heated Length (HL) in this study is defined to be the length of the incoming tape that is heated above the $T_g$ during the manufacturing in addition to the shadow zone as opposed to [32] where only the length above the $T_m$ is defined to be the HL. The short and long settings for the HL was achieved by making changes to the experimental set-up. For the long HL, the longer edge of the light guide was used to expose a longer tape length to the broadband radiation while for the short HL, the shorter edge of the light guide was used along with a metallic tape guiding plate that blocked some length of the incoming tape from being irradiated by the flashlamp. These are shown in Figure 5.10. Since the shorter edge was used, the energy density emitted towards the incoming tape was reduced and therefore higher flashlamp power had to be used for the short HL specimens to reach the same temperature as for the long HL specimens.

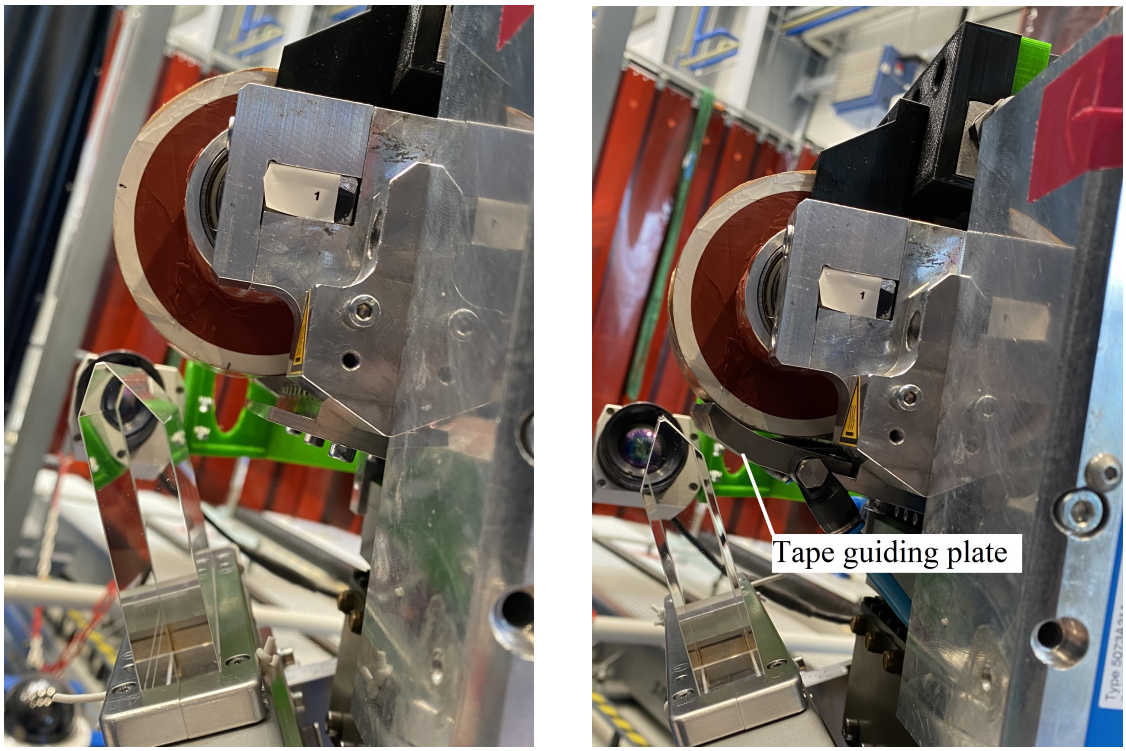


**(a)** Long HL setting **(b)** Short HL setting

**Figure 5.10:** Set-up used for long and short Heated Length (HL) specimens.

The heated length was monitored during the specimen manufacturing by the temperature measuring bars (as shown in Figure 5.8a and Figure 5.8b) which were placed at known approximate distance from each other. Additionally, the exact heated length was measured after the processing with a measuring scale as the heated part of the tape above the $T_g$ was visually distinguishable from the non-heated part due to the heated part taking the shape of the roller. This is shown in Figure 5.11. The measured HL values are given in Table 5.3.

It was observed that the HL changed by 5 mm for 300 N and 900 N specimens because of the change in contact area under the roller. Since the contact area increased with increasing force (see Figure 5.3), the length of the tape under the roller increased as well, thereby, reducing the heated length before the nip-point for higher applied force. Additionally, the heated length for the 250 °C specimens reduced further as the temperature dropped below the $T_g$ faster.

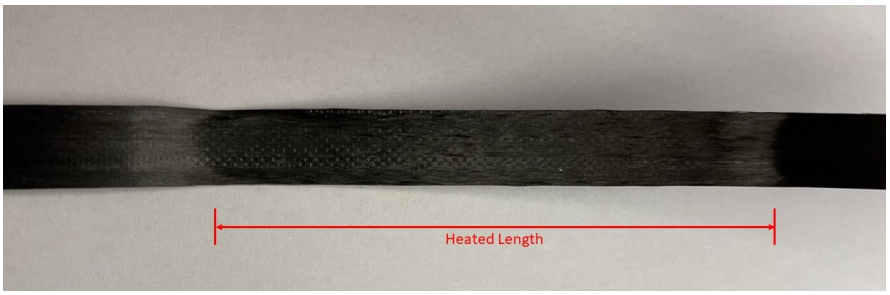


**Figure 5.11:** Visually distinguishable Heated length

**Table 5.3:** Summary of all the specimens with different configuration of process parameter settings used in the experimental study: Target and actually achieved values averaged over 3 samples manufactured for each configuration.

| Name | Target values | | | Flashlamp power (kW) | Achieved values (average) | | |
|---|---|---|---|---|---|---|---|
| | Heated length | Compaction force (N) | Nip-point temperature (°C) | | "Visible" nip-point temperature (°C)[SD] | Heated length (mm) | Compaction pressure (kPa) |
| S/300/370 | Short | 300 | 370 | 10.28 | 364.4 [12.1] | 40 | 298 |
| S/300/420 | | | 420 | 12.99 | 436.4 [11.2] | | |
| S/900/370 | | 900 | 370 | 10.81 | 368.9 [13.4] | 35 | 543 |
| S/900/420 | | | 420 | 12.81 | 420.3 [16.5] | | |
| L/300/370 | Long | 300 | 370 | 9.87 | 381.7 [11.6] | 50 | 298 |
| L/300/420 | | | 420 | 11.30 | 435.4 [14.6] | | |
| L/900/370 | | 900 | 370 | 9.87 | 363.8 [12.7] | 45 | 543 |
| L/900/420 | | | 420 | 11.64 | 434.8 [13.4] | | |
| S/300/250 | Short | 300 | 250 | 5.45 | 230.3 [8.4] | 30 | 298 |
| S/900/250 | Short | 900 | 250 | 5.45 | 232.5 [11.1] | 30 | 543 |
| S/900/300 | Short | 900 | 300 | 7.14 | 292.9 [11.4] | 35 | 543 |

## 5.4 Tape width measurement

Three approaches were explored for measuring the tape width. These are discussed below.

1. **Laser scanner**: In this approach, Leica T-Scan 5 laser scanner along with Leica absolute tracker AT960 from Hexagon was used to scan a length of the as-received tape at a frequency of 160 scanning lines/second and the data was imported as a point cloud into CAD to get the 3D profile of the complete tape as shown in Figure 5.12. To determine the width, a cross-section profile as shown in Figure 5.13 was extracted and rough measurements were done using the CAD software. This was then compared with measurements done by a caliper for validation. It can be seen that the tape edges captured by the laser scanner were not sharp with a large transition length and therefore no threshold can be applied for marking the tape edges accurately and obtaining the accurate width measurement. Another problem was that the scanner missed a lot of data points potentially because of surrounding reflections and therefore certain areas had to be scanned multiple times to get the data. The laser scanner's measuring point density and therefore its resolution for width measurement is also limited to 0.075 mm. Because of these limitations and drawbacks, this approach was rejected.

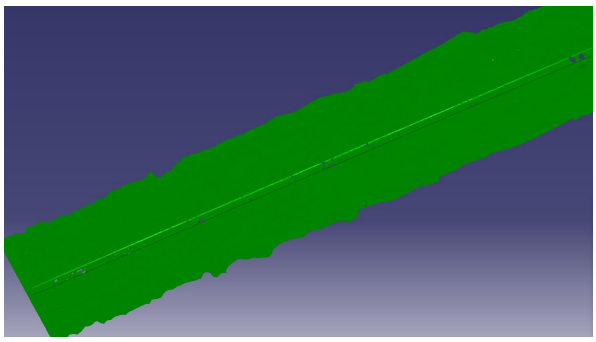

**Figure 5.12:** 3D profile of the tape scanned by a laser scanner.

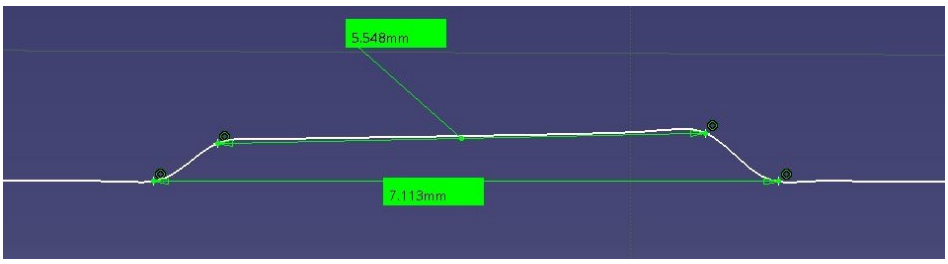


**Figure 5.13:** Cross-section profile view with measurements at top and bottom surface of the tape.

2. **Microscope**: This approach utilized a Keyence VHX-5000 Digital microscope to capture an image of the tape's surface and width measurement was done using the in-built 2D measurement tool of the microscope software. Figure 5.14 shows an example of a measurement done at a point on the as-received tape. The drawbacks of this approach are that the measurement points had to be placed manually at the tape edges which can

introduce some errors and the measurements could be performed only at limited number of points on the tape which would lead to the loss of a lot of data points, especially when the width is not uniformly deformed. Therefore, this approach was also rejected.

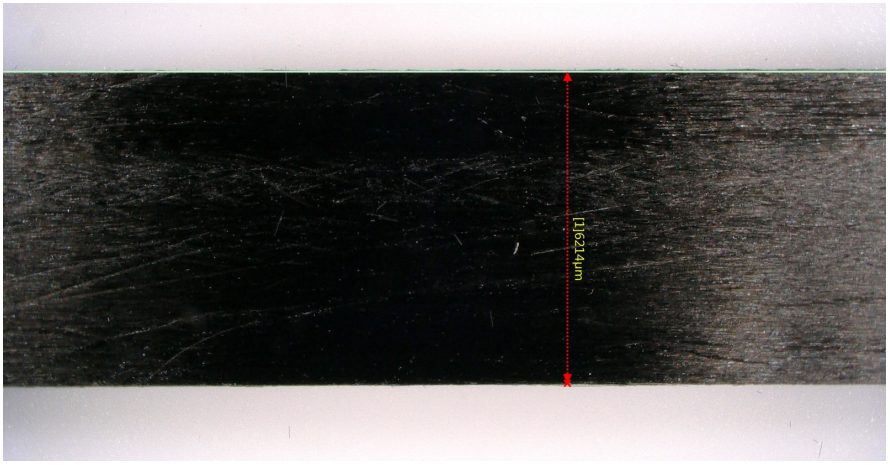


**Figure 5.14:** Width measurement at a point using the in-built 2D measurement tool on a microscope.

3. **Image processing**: In this approach, an image of certain length of the tape surface was captured using the microscope camera and was then processed in MATLAB to obtain the width measurement data. The image processing involved the following steps and is illustrated in Figure 5.15 and Figure 5.17:

   *(i) RGB image to grayscale:* The image was captured in RGB color format on the microscope. Therefore, it was first converted to a grayscale image using the in-built function in MATLAB that utilizes the weighted sum of the R, G, and B components to return grayscale values.

   *(ii) Setting a threshold:* The threshold to differentiate between the background and the tape was set by plotting a histogram of the grayscale values of the image and then taking the grayscale value that occured the least number of times in the image. This was considered to be a very good approximation to detect the tape edges as there was a clear drop in the histogram (see Figure 5.15) indicating the separation between the tape and the background.

   *(iii) Grayscale image to binary image:* The threshold grayscale value was then used to convert the image into a binary image i.e., 1 (white) for all pixel values below the threshold and 0 (black) for all pixel values above the threshold. Therefore, a black and white image is obtained with white representing the tape.

   *(iv) Digital tape:* Based on the binary image, the first and last pixel in the width direction representing the tape i.e., 1 (white), were selected and a digital tape in the form of two lines representing the tape edges was achieved.

   *(v) Width measurement:* Finally, the width measurement data was extracted by counting the number of pixels between the tape edges and multiplying by the size of the pixel. This was done for each pixel in the tape length direction to obtain the width measurement data at each pixel and therefore the entire tape length was scanned, down to the

pixel level resolution i.e., around 11 $\mu m$. Since this approach calculated the width at each pixel in the tape length direction by counting the number of pixels within the tape edges in the width direction, it was made sure that the tape was horizontally parallel to the image captured by the microscope by using reference lines on the microscope software.

The measurement was validated by rough measurements from a caliper and therefore, this approach was selected for the tape width measurement because of the high resolution, accuracy, simplicity and larger data acquisition.

### 5.4.1 As-received tape width measurement

For the as-received tape width measurement, 10 images of size 1400 (width) X 1200 (height) pixels were taken approximately at every 1 m of the as-received tape spool which was then used to manufacture all the specimens. A Keyence VHX-5000 Digital microscope was used to capture the images at 20X magnification which resulted in a pixel size of 11.031 $\mu m$ and the image processing was conducted as explained before to get the width measurement data. An example of the as-received tape image processing is shown in Figure 5.15.

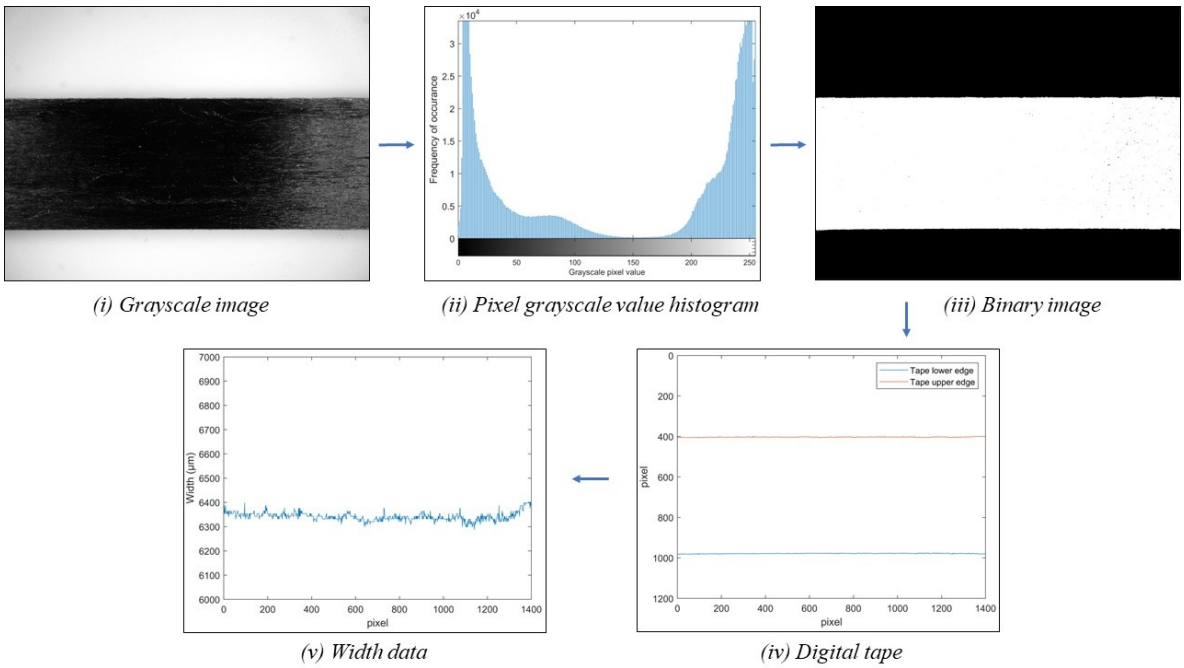


**Figure 5.15:** Image processing steps to extract width data: As-received tape.

### 5.4.2 Post-process tape width measurement

For the post-process tape width measurement, two images of size 5934 (width) X 770 (height) pixels were taken at the locations shown in Figure 5.16 (highlighted in green) for each specimen. These locations were taken for evaluation as it was expected that the process would be unstable around the start and end of the course length and therefore, approximately 150

mm of the tape at the start and end was rejected. A Keyence VR-5000 Wide-Area 3D measurement microscope was used to capture the images at 25X magnification using the in-built image stitching feature to capture a longer image in the width direction. This resulted in a pixel size of 11.793 $\mu m$. For the image processing, the images were captured in grayscale using the monochrome setting and therefore the first step of converting the images from RGB to grayscale could be skipped. An example of the image processing for the post-processed tape is shown in Figure 5.17.

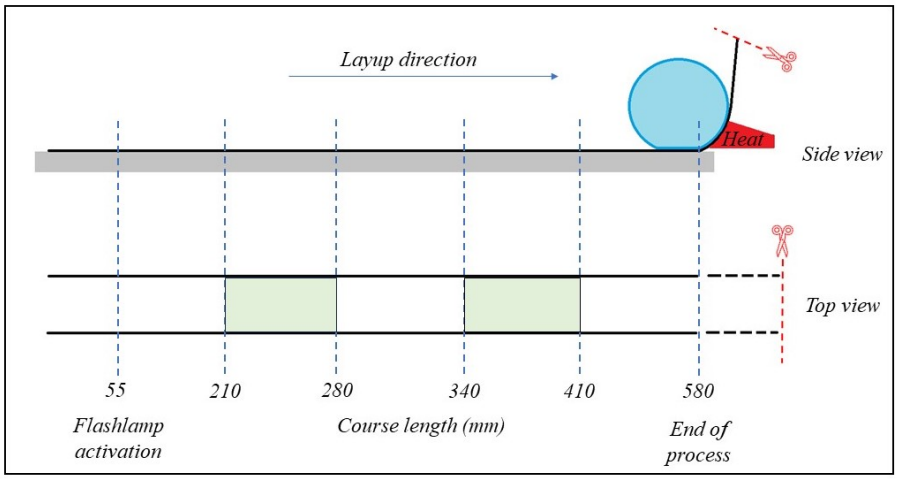


**Figure 5.16:** Specimen course length and scanned areas (in green) for width data extraction.

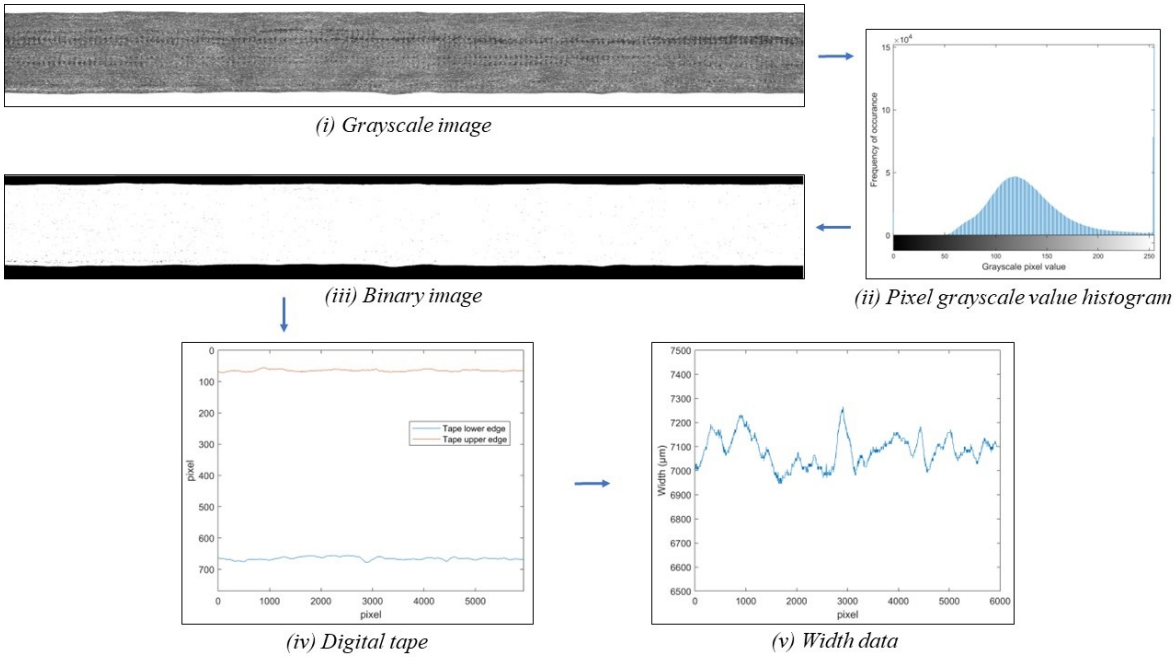


**Figure 5.17:** Image processing steps to extract width data: Post-processed tape.

## 5.5 Microscopy

The methodology to answer all the sub-questions for research question 1 followed some microscopic analyses and inspection of the tape. These are divided into two categories i.e., surface and cross-section microscopy.

### 5.5.1 Surface microscopy

#### 1. Width inspection in Heated zone

To check the width of the tape in the heated zone i.e., the heating phase of the process, the tape surface image was taken at the location highlighted in green in Figure 5.18 and processed similarly to the image processing used for the post-processed tape width measurement (subsection 5.4.2). Figure 5.18 schematically illustrates the tape after the end of the process as shown in Figure 5.16. The length of the tape marked as the heated length very well represents the heating phase during the process as it was still heated after the end of the process without being consolidated by the roller. This allowed the inspection of the tape before compaction with all the other boundary conditions of the process such as roller compaction pressure on one side and tape under tension from the other side. The tape tension was maintained as the tape was not cut immediately at the end of the process but after some time to allow for the tape to cool down. However, this resulted in the tape taking the shape of the roller and being curved after the last compaction point (end of process point at 580 mm course length). Therefore, a microscope glass object was placed on the tape and weights were used to flatten the tape as shown in Figure 5.19.

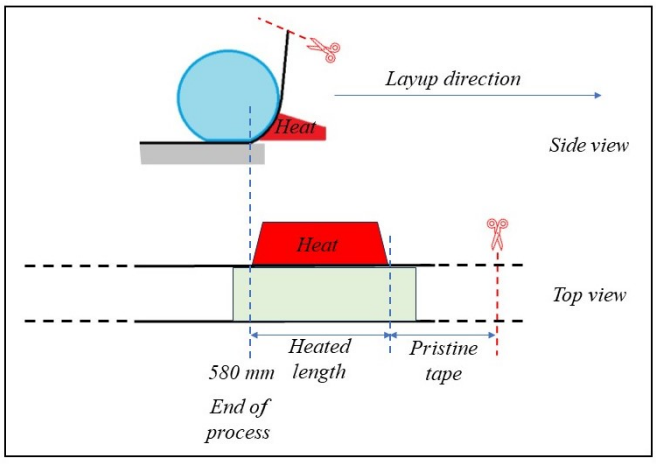


**Figure 5.18:** Tape after end of process and scanned area (in green) for width data extraction in the heated zone.

#### 2. Roughness analysis

The surface roughness analysis was performed according to ISO-4287 standard on a Keyence VK-X1000 Laser Scanning Confocal Microscope (LSCM) using the multi-line roughness fea-

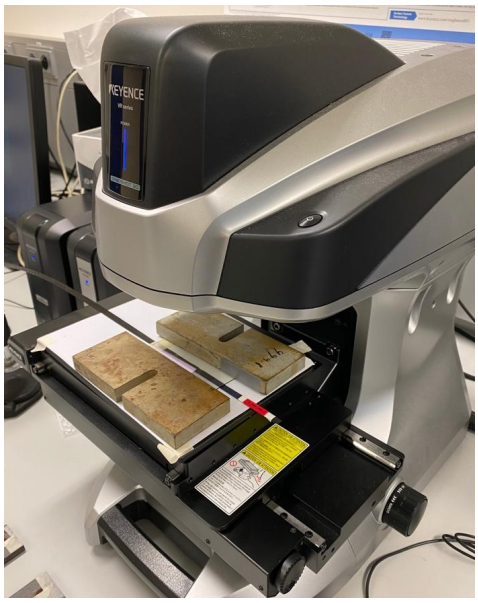


**Figure 5.19:** Setup used to take the tape surface image at the heated zone after the end of process location.

ture at 20X magnification. 9 images were stitched in the width direction of the tape at a random location near the middle of each manufactured specimen to obtain an image size of approximately 717 $\mu m$ (along the tape length) X 4431 $\mu m$ (along the tape width). This allowed for at least 5 sampling lengths for roughness evaluation according to the standard guidelines. However, according to the standard, a sampling length (cut-off) of 2.5 mm is recommended for distinguishing the roughness and the waviness for $2 < R_a \leq 10$ $\mu m$ ($R_a$ = Arithmetical mean roughness). This was not possible here as using a sampling length of 2.5 mm would mean that only 2 sampling lengths could be evaluated due to the limited width i.e., 6.35 mm (as-received) of the tape. Therefore, the sampling length recommended for $0.1 < R_a \leq 2$ $\mu m$ i.e., 0.8 mm was used.

The roughness analysis steps included correcting any tilt in the image by using the automatic tilt correction mode as shown in Figure 5.20a. Then, 11 analysis lines were placed approximately 56.5 $\mu m$ apart along the length of the tape as shown in Figure 5.20b to extract 11 profiles with a sampling length of 0.8 mm as mentioned above to obtain 5 sampling lengths along each of the 11 profiles as shown in Figure 5.20c. Finally, the averaged $R_a$ (Arithmetical mean roughness) and $R_q$ (Root mean square roughness) over the 11 profiles were extracted for each specimen from the software.

### 5.5.2 Cross-section microscopy

Cross-section microscopy was performed after all the other analyses, measurement and inspection as the specimens had to be cut and embedded into a resin block in order to analyse its cross-section. Small samples were cut out at a random location around the middle of each of the manufactured specimen. These samples were then secured in a clip that could hold a total of 5 samples and each clip was placed in a mould for resin embedding as shown in Figure 5.21a. Epofix resin system was used for the embedding as it had a slow cure cycle of 12

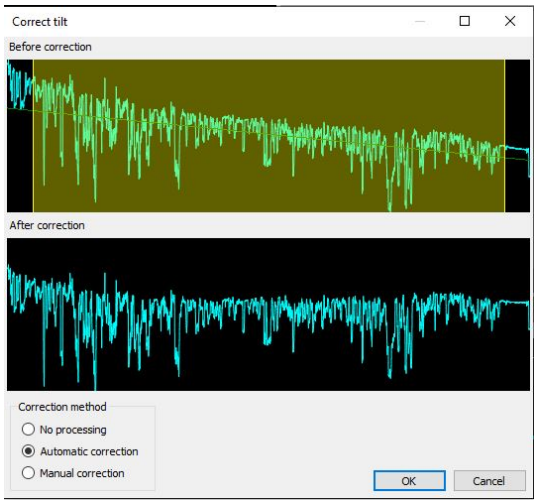


**(a)** Automatic tilt correction

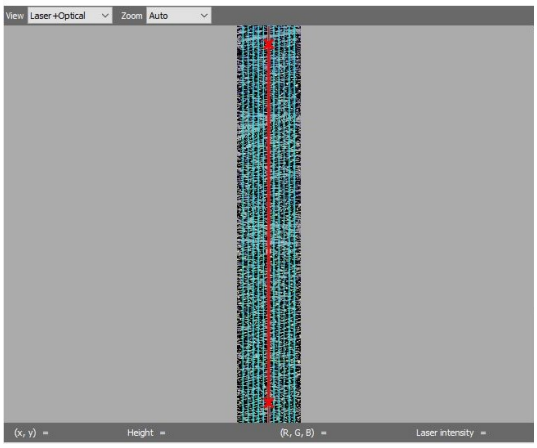


**(b)** 11 analysis profiles placed along the tape length

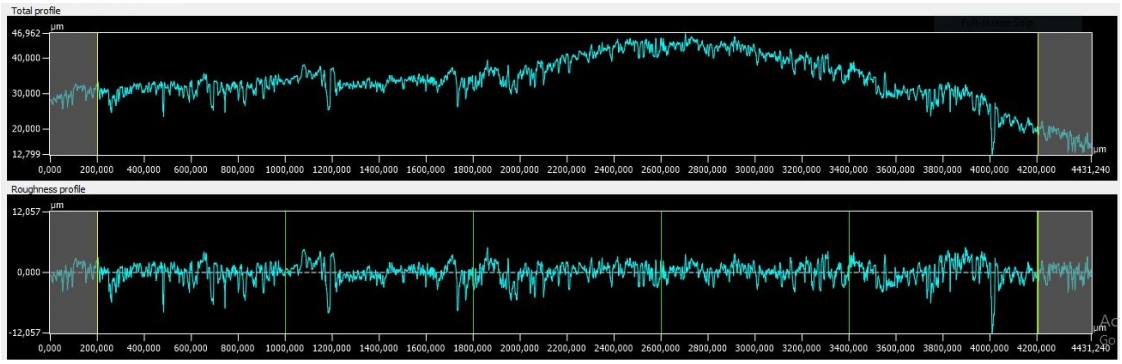


**(c)** 5 sampling lengths for each ananlysis profile

**Figure 5.20:** Surface roughness analysis steps.

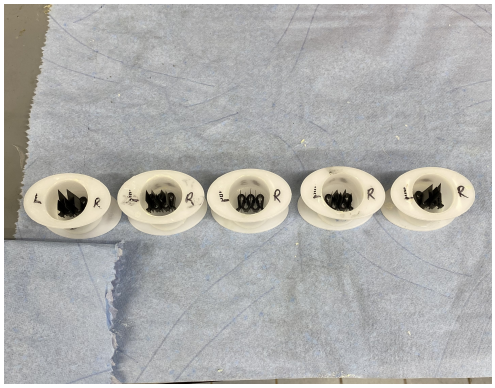

**(a)** Samples placed in moulds for resin embedding

**(b)** Struers Tegramin grinding and polishing machine

**Figure 5.21:** Resin embedding for cross-section microscopy

hours and therefore minimal heat generation during curing to avoid any change in the sample characteristics while embedding. After curing, the resin block was ground and polished in

different steps from high roughness to low roughness using the Struers Tegramin Automatic Preparation Machine as shown in Figure 5.21b to finally achieve a surface roughness as low as 0.25 $\mu m$ that could be used for analysis.

The cross-section microscopy involved two analyses i.e., overall tape cross-section profile inspection and fiber-resin content analysis. The methodology for each is described below.

#### 1. Tape cross-section profile inspection

The overall tape cross-section profile was inspected using the Keyence VK-X1000 LSCM at 2.5X magnification. The focus variation mode was used to stitch 2 images and capture the entire cross-section of the tape by automatically focusing at the surface. Figure 5.22 shows an example of the image captured using this method for the as-received tape.

**Figure 5.22:** Tape cross-section profile for as-received tape.

#### 2. Fiber-resin content analysis

Images were captured using the Keyence VK-X1000 LSCM at 20X magnification utilizing the focus variation mode and image stitching was avoided to obtain high resolution and quality images from the microscope for analysis. The size of the image captured using this setup was 1024 X 768 in pixels which equals to 724.16 X 543.12 $\mu m$. The fiber-resin content analysis was then performed on ImageJ software using the void content measurement plugin which automatically converts the pixel values of the selected evaluation area in the image into an interactive grayscale histogram that can be used to manually select the regions of interest in the image.

The first step i.e., selecting the evaluation area (tape cross-section area) in the image was performed by using the "Wand (tracing) tool". A white pixel in a carbon fiber was selected and using the "legacy" mode, the threshold was increased till it selected the entire tape cross-section area. Then, the background was cleared using the "Clear Outside" option from the edit menu. These are shown in Figure 5.23.

The second step was to select the areas in the histogram corresponding to the fibers, resin and voids. The histogram had clear peaks for the resin and fiber selection, however the void selection was done by visually looking at the image and making sure that all the black areas (representing voids) were selected. The content of the selected area was calculated by the software as a percentage value of the total evaluation area and therefore the fiber, resin and void content was extracted from the images. An example of the fiber, resin and void areas selected using the histogram is shown in Figure 5.24.

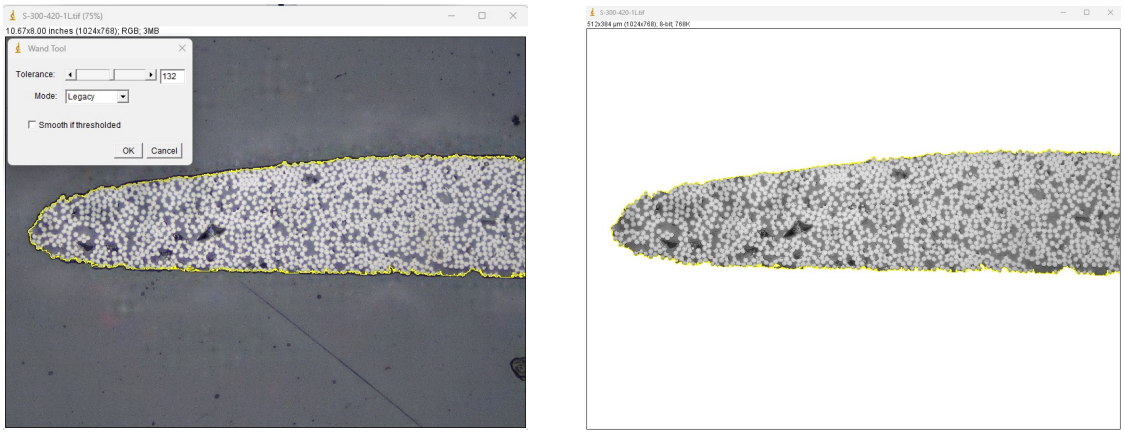


**(a)** Evaluation area selection **(b)** Background cleared for evaluation

**Figure 5.23:** Step 1 of fiber-resin content analysis using ImageJ: Evaluation area selection and background removal.

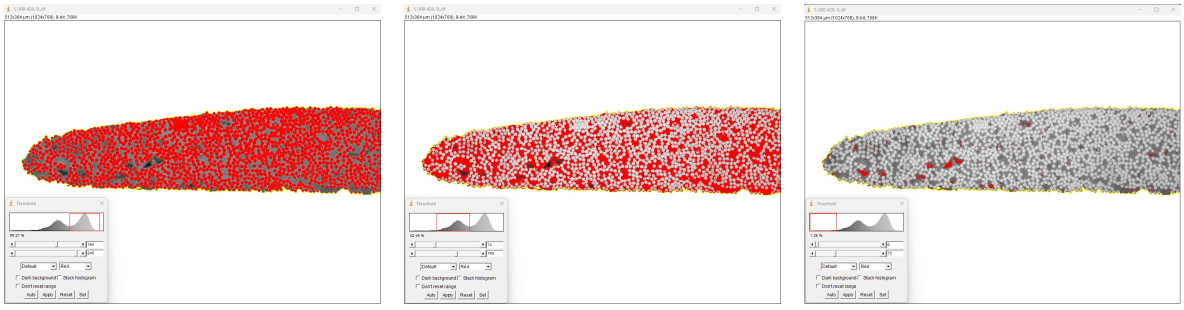

**(a)** Fibers **(b)** Resin **(c)** Voids

**Figure 5.24:** Step 2 of fiber-resin content analysis using ImageJ: Selection based on grayscale histogram.

# Chapter 6

# Results and Discussion

This chapter presents, analyses and discusses the results of all the experiments and investigations carried out in this work to answer the research questions and therefore achieve the research objective. The chapter follows in the same order as that of the research questions formulated. First, the characterization and investigation results for the tape width deformation mechanism is discussed to understand the governing mechanism behind it. Then, the results for the influence of the processing parameters on the tape width deformation is presented and analyzed based on the understanding of the governing mechanism.

## 6.1 Characterization and investigation of tape width deformation mechanism

The characterization and investigation of the tape width deformation mechanism was done in the post-processing microscopy stage of the work using the methodology and set-up as described in section 5.5 for each of the following subsections.

### 6.1.1 Tape width inspection in the heating zone

Figure 6.1 shows a typical post-processed tape inspection in the heating zone as described in Figure 5.18. It is clearly seen from the digital tape in Figure 6.1b that the tape width deforms in the entire heating zone i.e., the heating phase of the process as hypothesized and illustrated in Figure 3.1. However, further looking at the width data in Figure 6.1c, it was seen that the deformation follows a unique pattern. This has been illustrated in Figure 6.2 where $L_h, L_c, W_i, W_f$ are the heated length, contact length under roller, initial tape width and final tape width respectively. To further analyse this, the width data graphs were divided into 5 different zones manually and a linear curve was fitted through each of the zones. Note that the data had some outliers in the form of sudden spikes because of detection of some loose fibers or particles in the image processing. This, however, did not affect the curve fitting and therefore was not deleted.

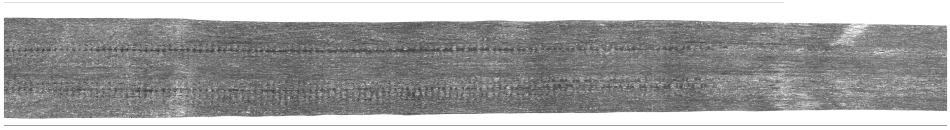

**(a)** Grayscale image of tape in Heated zone

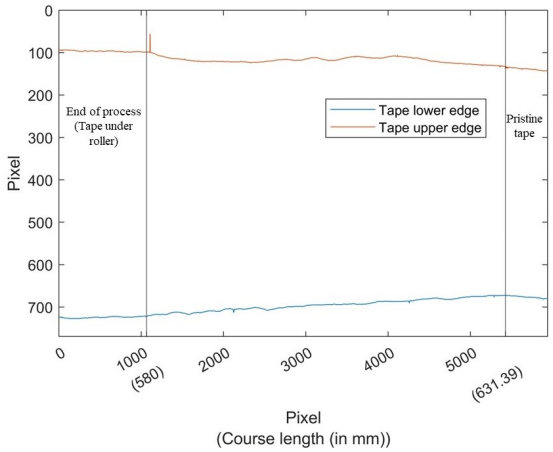


**(b)** Digital tape

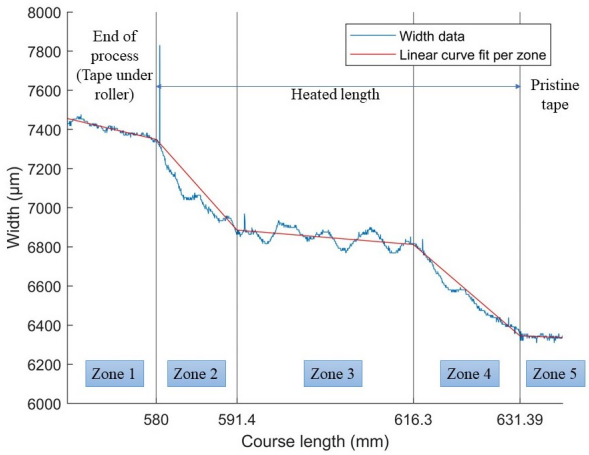


**(c)** Width data with zone divisions and linear curve fit per zone

**Figure 6.1:** Tape profile inspection in Heated zone

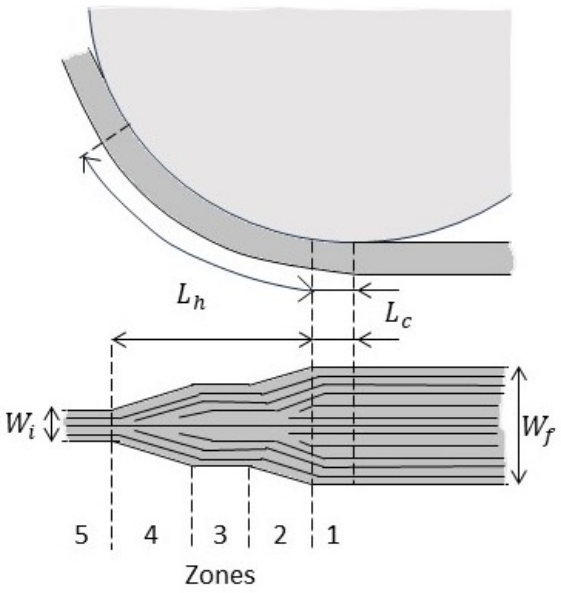


**Figure 6.2:** Tape width deformation as observed from results.

Zones 1 represent the end of process i.e., the last part of the tape length that was heated and consolidated under the roller and zone 5 represent the pristine tape i.e., the tape that was

not heated during the process (refer Figure 5.18). Therefore, zones 2, 3 and 4 represent the heated length during the process. It can be seen that zones 2 and 4 have a clear slope in the width deformation data whereas, zone 3 shows a flat plateau-like region. The slope in zone 2 suggests that there is width deformation due to the roller compaction in zone 1 and therefore the tape further widens before the nip-point in zone 2.

Referring to the temperature distribution curves along the heated length of the tape as shown in Figure 5.9, it is clear that not the entire heated length is heated above the $T_m$. Therefore, using this information, the slope in zone 4 is explained to be an indication of the tape below the $T_m$ as the tape is not in the melt state completely and is therefore restricted in the width deformation due to the restricted movement of the polymer (resin) chains below the $T_m$. And, the plateau in zone 3 is an indication of the tape that is completely in the melt state and therefore, can deform without any restrictions.

Furthermore, the horizontal length and slope data of zones 2 and 4 for all the 3 samples manufactured per specimen configuration was extracted from the curve fits and analysed. Figure 6.3 shows the data for the horizontal length of the slope in zone 2. Some observations that can be made from this plot are:

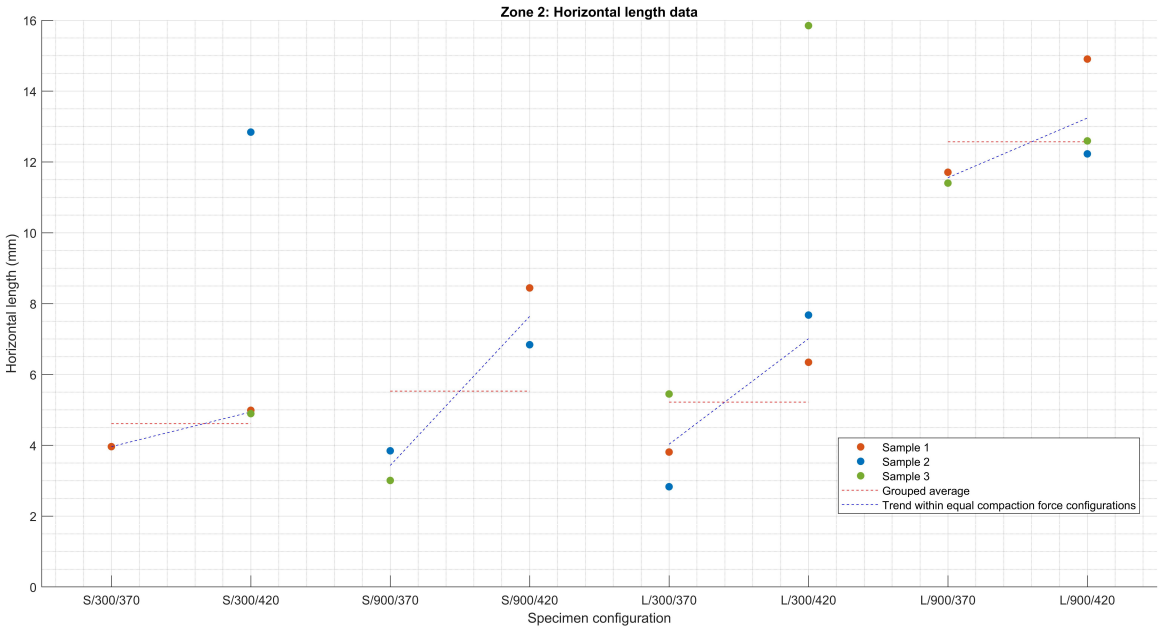


**Figure 6.3:** Zone 2 horizontal length data of all specimens.

1. The sample data for some specimen configurations are missing. This is because these samples did not show distinct zones in the width deformation data but rather had a consistent slope throughout. An example is shown in Figure 6.4.

2. For the long heated length configurations, a clear difference in the average horizontal length is observed for the 300 N and 900 N configurations (5.22 mm for L/300 (excluding the outlier for L/300/420) and 12.57 mm for L/900 configurations). This increase in the horizontal length at zone 2 with increasing compaction force further confirms the additional width deformation due to the roller compaction force.

3. For the short heated length configurations, there is less difference in the average horizontal length between the 300 N and 900 N configurations i.e., 4.61 mm (excluding the outlier for S/300/420) and 5.53 mm respectively .

4. For the S/300/370 specimen, there is no clear slope in zone 2 for 2 out of 3 samples indicating no additional width deformation due to the compaction force. An example sample is shown in Figure 6.4

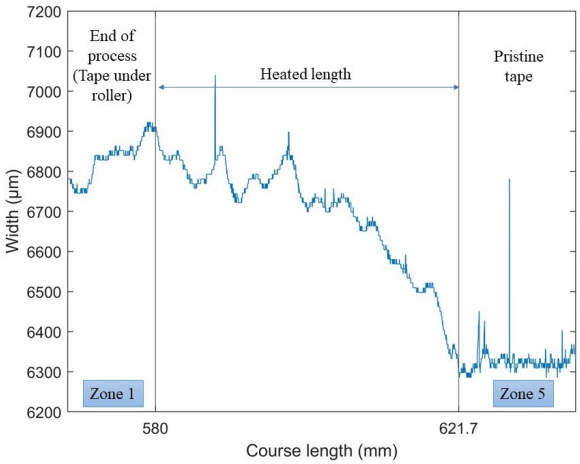


**Figure 6.4:** S/300/370 sample 2 with no distinct zone 2.

5. Furthermore, it can be seen that the the average horizontal length also increases with increase in temperature for all the configurations as shown by the trend lines in blue. This shows that the width deformation takes place over a larger length due to the compaction force as the temperature is increased.

### Discussion:

The temperature dependence of the average horizontal length in zone 2 indicates that for the 370 °C configuration specimens, there is still some restricted movement of the polymer chains. Referring again to the temperature distribution curves along the heated length of the tape in Figure 5.9, it can be seen that the temperature was measured approximately 25 mm away from the "actual" nip-point and therefore it is highly likely that the tape temperature for the 370 °C configuration specimens dropped below the $T_m$ because of the apparent shadow zone. For the 420 °C specimens, it is more likely that the tape remained above the $T_m$ and therefore less restricted movement of the polymer chains resulting in larger length of the tape deforming at the same compaction pressure.

This also explains the exception of the lowest setting i.e., S/300/370 specimen with no clear indication of width deformation due to the compaction force as the low temperature combined with the low compaction force results in negligible width deformation under the roller. This however, is not true for the L/300/370 specimen since the long heated length is associated with more heating time which is assumed to promote better heat propagation through the thickness of the tape and therefore comparatively less restrictions on the polymer chain movements.

It is hypothesized that for the short HL configuration specimens, unlike the long HL configuration specimens, the effect of the increasing compaction force does not have a significant difference in the average horizontal length due to part of the tape in the melt state i.e., zone 3 being closer to zone 2 because of the shorter heated length. This would therefore lead to an overlap of width deformation in zones 2 and 3 and making it impossible to clearly see the effects of just the compaction force. This hypothesis also explains why more short HL samples in general has missing data points in Figure 6.3 i.e., having a consistent slope throughout instead of having distinct zones and more scatter in slope value data for zone 2 as shown in Figure 6.5.

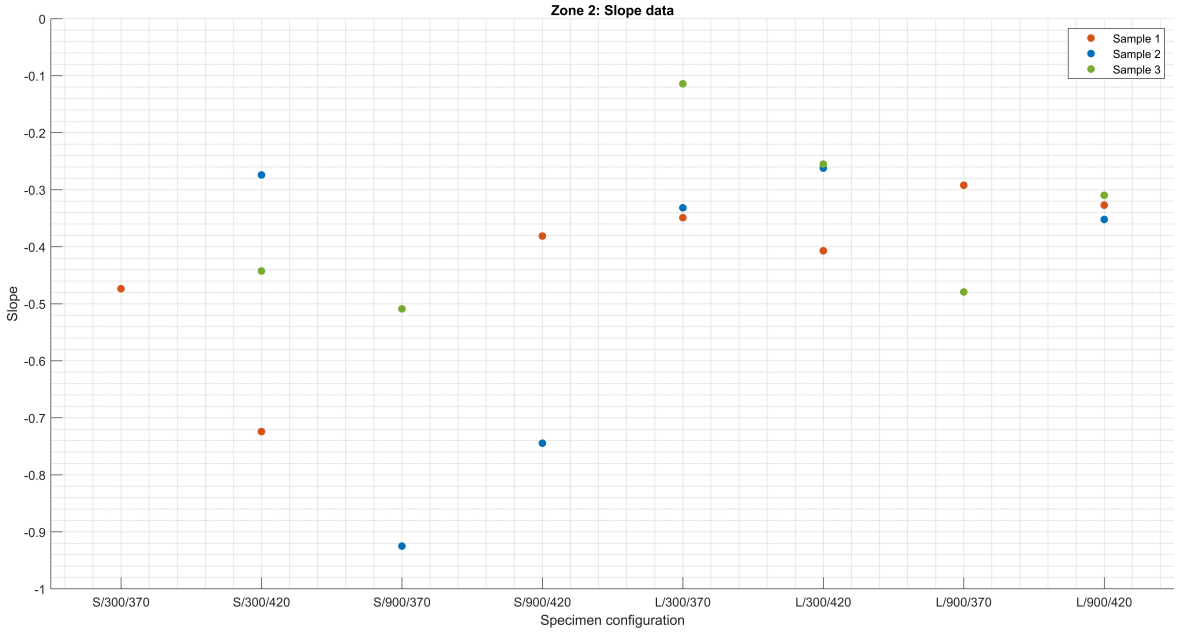


**Figure 6.5:** Zone 2 slope data of all specimens.

Additionally, for the long HL configuration specimens, the larger horizontal length in zone 2 can be directly related to greater width deformation as the slope remains roughly the same, as shown in Figure 6.5. For short HL, this cannot be confirmed because of the large scatter in slope value.

The horizontal length and slope data for zone 4 did not show any distinct trends or observations and is given in Appendix B.

### 6.1.2 Surface roughness analysis

The surface roughness of all the samples after processing (taken from a random location around the middle of the manufactured tape length) were analysed on the heated side of the tape and the *Rq* (Root mean square roughness) data is presented here in the form of bar charts for further analysis and comparison. The same data has been plotted over all the three different processing parameters i.e., heated length, nip-point temperature and compaction force in the x-axis separately in order to observe their influence individually. The average

and measured extreme $Rq$ values for the as-received and the deconsolidated tape are also indicated in the charts for clear reference.

### Effect of heated length

Figure 6.6a and Figure 6.6b show the $Rq$ data over the heated length for the 300 N and 900 N compaction force specimens respectively. Comparing the $Rq$ values at the same nip-point temperature, it is observed that the roughness clearly decreases, approaching as-received surface roughness, with increase in heated length for the 370 °C nip-point temperature specimens and remains the same for the 420 °C specimens.

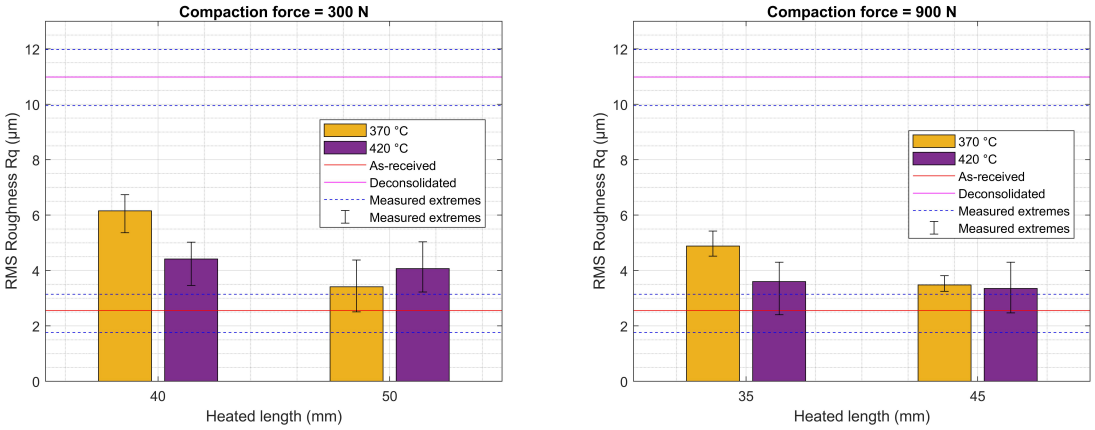


**(a)** $Rq$ with measured extreme values plotted over heated length for 300 N compaction force.

**(b)** $Rq$ with measured extreme values plotted over heated length for 900 N compaction force.

**Figure 6.6:** RMS Roughness $Rq$ values over heated length.

### Effect of processing temperature

Figure 6.7a and Figure 6.7b show the $Rq$ data over the nip-point temperature for the short and long HL specimens respectively. It can be seen from these plots that the roughness clearly decreases with increasing processing temperature, but only for the short HL specimens. For the long HL specimens, the results indicate an increase in roughness for the 300 N specimens, however, due to the high scatter, this cannot be said with full confidence. For the long HL, 900 N specimens, the roughness change is statistically indifferent because of the complete overlap in the measured extreme values. Figure 6.7c shows the decrease in roughness with increase in processing temperature for short HL and 900 N compaction force specimens, including the extra temperature data point specimen at 300 °C. A linear decrease in the average $Rq$ value is clearly observed from the plot.

### Effect of compaction pressure

Figure 6.8a and Figure 6.8b show the $Rq$ data over the compaction force for the short and long heated length (HL) specimens respectively. It can be seen that the roughness clearly

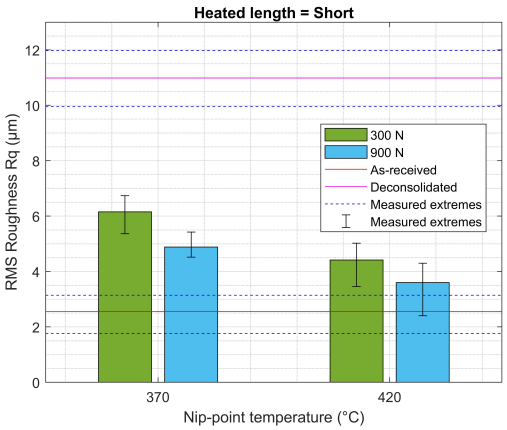


**(a)** $Rq$ with measured extreme values plotted over nip-point temperature for short HL.

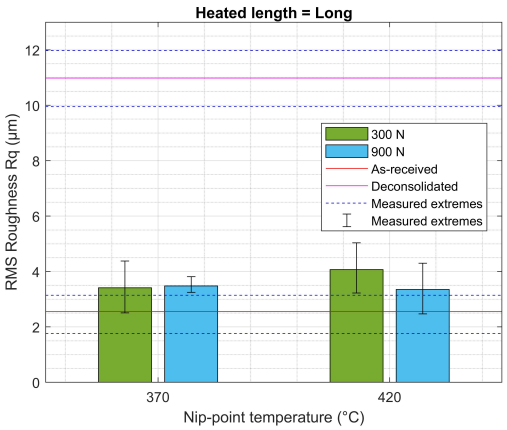


**(b)** $Rq$ with measured extreme values plotted over nip-point temperature for long HL.

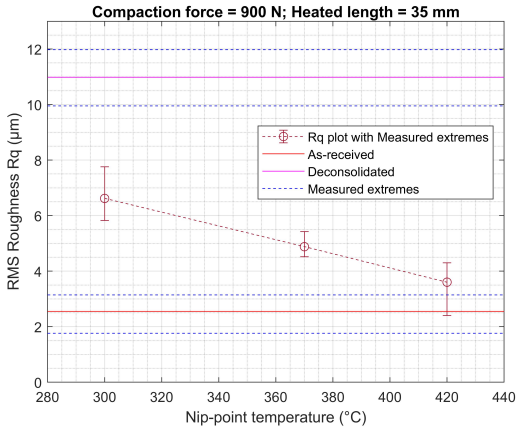


**(c)** $Rq$ with measured extreme values plotted over nip-point temperature for 900 N compaction force and short HL.

**Figure 6.7:** RMS Roughness $Rq$ values over nip-point temperature.

decreases only for the short HL, 370 °C specimens with increase in compaction force. For all the other specimens, the roughness either remains the same or reduces, however, again this cannot be said with full confidence due to high scatter in data and overlap in the measured extreme values.

### Discussion:

Based on the results and observations, it is clear that the roughness stays independent of the processing parameters for all the long HL and 420 °C configuration specimens. This indicates that the temperature distribution might have an influence on the roughness value as the material would be able to consolidate more uniformly and result in lower roughness when the tape is more uniformly heated with larger part of the tape in the melt state thereby, promoting the flow of the polymer resin. Therefore, the longer heated length and higher temperature is assumed to promote better heat propagation through the thickness of the

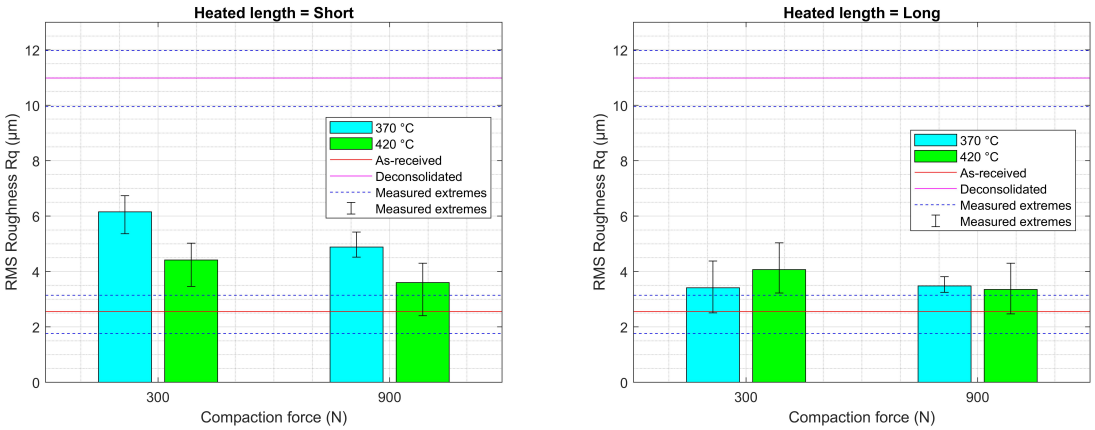


**(a)** $Rq$ with measured extreme values plotted over compaction force for short HL.

**(b)** $Rq$ with measured extreme values plotted over compaction force for long HL.

**Figure 6.8:** RMS Roughness $Rq$ values over compaction force.

tape as well as more length of the tape being above the $T_m$ during consolidation and would overshadow the effects of other processing parameters. Based on this, the clearly observed trends in the plots can be explained i.e., roughness change only for the 370 °C specimens with heated length in Figure 6.6, roughness change only for the short HL specimens with processing temperature in Figure 6.7 and roughness change only for the short HL and 370 °C specimens with compaction force in Figure 6.8.

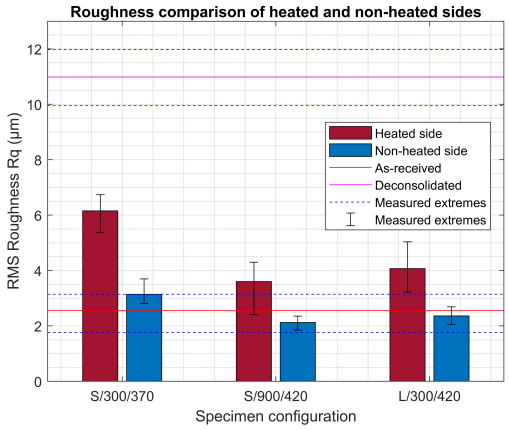


**Figure 6.9:** RMS Roughness $Rq$ comparison of heated vs non-heated side for three randomly selected specimens.

Additionally, the $Rq$ values of three random specimens were checked on the non-heated side of the tape and compared with that on the heated side. Figure 6.9 shows the obtained result for this. It is clear that the heated side in general has more roughness compared to the non-heated side. This, however, contradicts the results presented before which shows that the roughness value is lower for higher temperatures (Figure 6.7c). One of the possible reasons for this could be because of the difference in the surface roughness of the tool and the roller itself which would affect the roughness of the tape as it comes in contact with them during

consolidation. However, here this does not hold true as the thin Teflon foil used on the roller had a small pattern on it which would actually result in higher roughness of the tape on the roller (non-heated) side.

Therefore, to investigate this anomaly, the tape cross-section profile was checked at the heating phase i.e., before it was consolidated by the roller as given in Figure 6.10a and it was found that the top surface which is the heated side has more roughness compared to the other side even during the deconsolidation phase. Therefore, the anomaly can be explained by this information that the tape had lower roughness on the non-heated side to begin with and therefore resulted in lower roughness values after consolidation. The reason for having lower roughness on the non-heated side during deconsolidation is believed to be because the temperature on the non-heated side most probably does not reach $T_m$ because of the very short heating time and even if it reaches the $T_m$, the non-heated side is pressed against the roller due to the tape pre-tension which would restrict large out-of-plane deconsolidation.

### 6.1.3 Tape cross-section profile inspection

The tape cross-section profile was inspected under the microscope for all the samples including the as-received tape and deconsolidated tape as given in Figure 5.22 and Figure 6.10a respectively. Looking at all the samples, it was found that the tape deformed in a specific shape as shown in Figure 6.10b i.e., having a thickness slope at the edges of the tape, compared to the rectangular edges for the as-received or deconsolidated tapes, for all configurations except the S/300/370 specimen. For the S/300/370 specimen, the edge profile looked more like the as-received tape i.e., mostly rectangular edges as shown in Figure 6.10c.

**(a)** A typical deconsolidated tape

**(b)** A typical tape after consolidation for all configurations except S/300/370

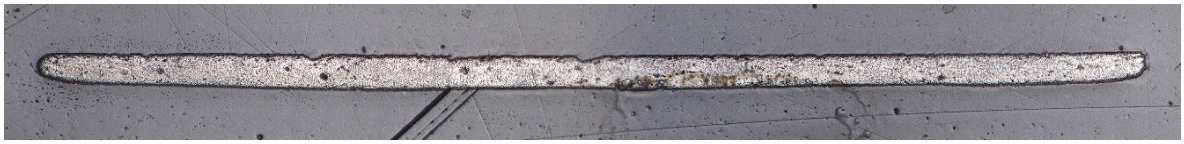

**(c)** A typical S/300/370 configuration tape

**Figure 6.10:** Tape cross-section profile inspection under the microscope with top surface being the heated and bottom surface being the non-heated side of the tape.

The thickness slope at the tape edges was measured as shown in Figure 6.11 using the built-in 2D measurement tool on the microscope software to analyse the edge deformation profiles further and quantify them. A uniform procedure was followed to extract the length of the sloped edges by drawing two parallel lines first (taking the heated side as the reference and

drawing a parallel line to it at a rough average thickness in the middle flat part of the tape) and then measuring the edges of the tape from the point where it starts to drop with respect to the parallel line till the tape end point. The edge length data for all the samples is presented in Figure 6.12 and the rough thickness measurement is presented in Figure 6.13.

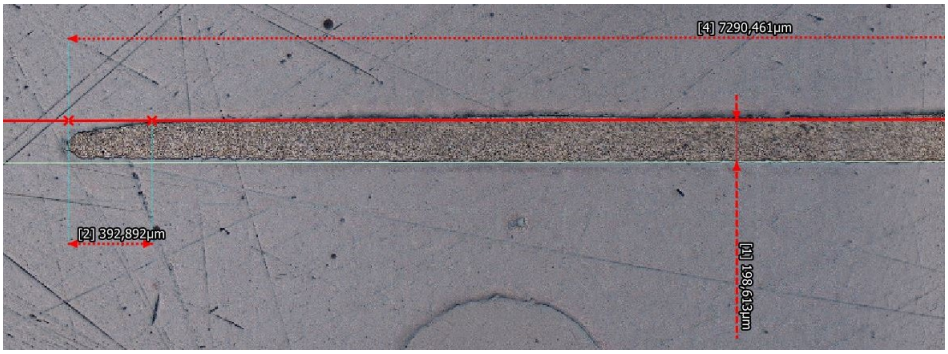


**Figure 6.11:** Tape edge measurement using the microscope 2D measurement tool.

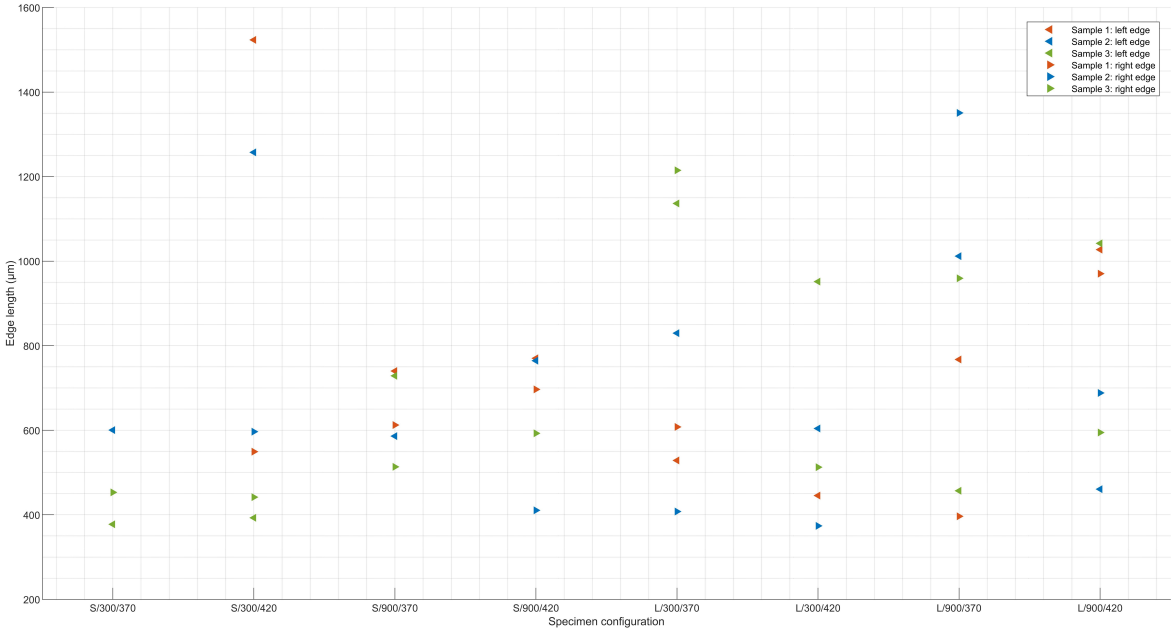


**Figure 6.12:** Tape edge length data of all samples.

From the edge length data in Figure 6.12, no unique trend is observed for different specimen configurations and the data seems to be more concentrated between 400 and 1000 $\mu m$. The missing data for some samples again represent that there was no apparent edge slope observed but rather a rectangular edge shape. For the thickness data in Figure 6.13, it is observed that the tape thickness after processing remains mostly similar or less than that of the as-received tape with few exceptions where the thickness seems to be higher. These exceptions are explained to be because of the rough thickness measurement taken and can be confirmed by looking at the edge length data in Figure 6.12. Comparing the two graphs, it can be seen that generally the samples having higher thickness than the as-received tape also has a longer

edge length, meaning that the average parallel line drawn at the rough average thickness was not accurate and was taken too far apart which also led to the edge length data to be much higher than other samples.

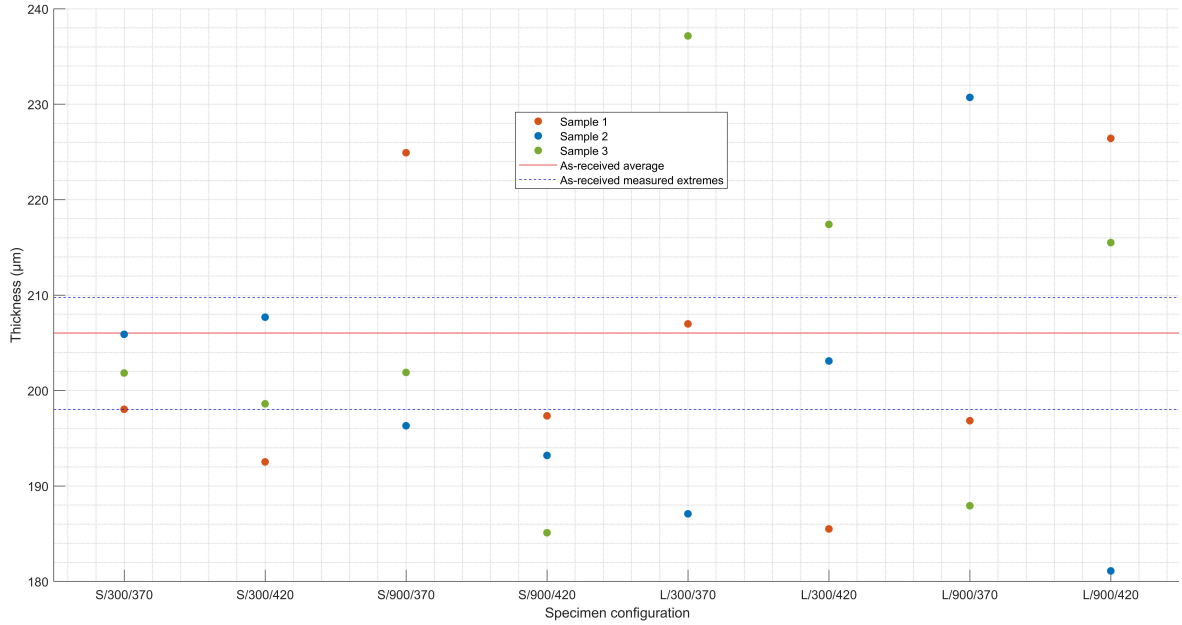


**Figure 6.13:** Tape thickness data of all specimens including as-received thickness and measured extreme values.

**Discussion:**

The observed gradual reduction in the thickness around the tape edges is believed to be because of the compaction under the roller i.e., in the consolidation phase of the process as the as-received and the deconsolidated tapes do no show this edge shape. Additionally, the edge slope decreases towards one side of the tape for all samples i.e., towards the heated side (see top surface in Figure 6.10b and Figure 6.10c) with the heated side being almost flat. This again confirms that the observed edge deformation shape forms as the conformable roller on the non-heated side applies a compaction force on the tape with the heated side being on the flat tool. The tape under the roller therefore takes the shape of the transitioning shape of the conformable roller at the edges as the tape is in the melt phase and can easily deform. Furthermore, the exception observed here for the S/300/370 configuration specimen agrees with the exception of the S/300/370 specimen showing no indication of width deformation due to the compaction force in the results presented in subsection 6.1.1.

### 6.1.4 Fiber-resin content analysis

The fiber, resin and void content data was extracted for one random sample for each specimen configuration along with that for the as-received tape for reference. The obtained data has been presented in Figure 6.14 in the form of bar charts. For each tape analysed, the fiber, resin

and void content were measured at the left edge, somewhere near the middle of the tape width and at the right edge. The edge length determined in the previous section (subsection 6.1.3) was used as the analysis length for the edges when smaller than the length of the image i.e., 724.16 $\mu m$. Figure 5.23 shows an example of a typical tape edge after processing and the presence of both fibers and resin along with some voids can be clearly seen.

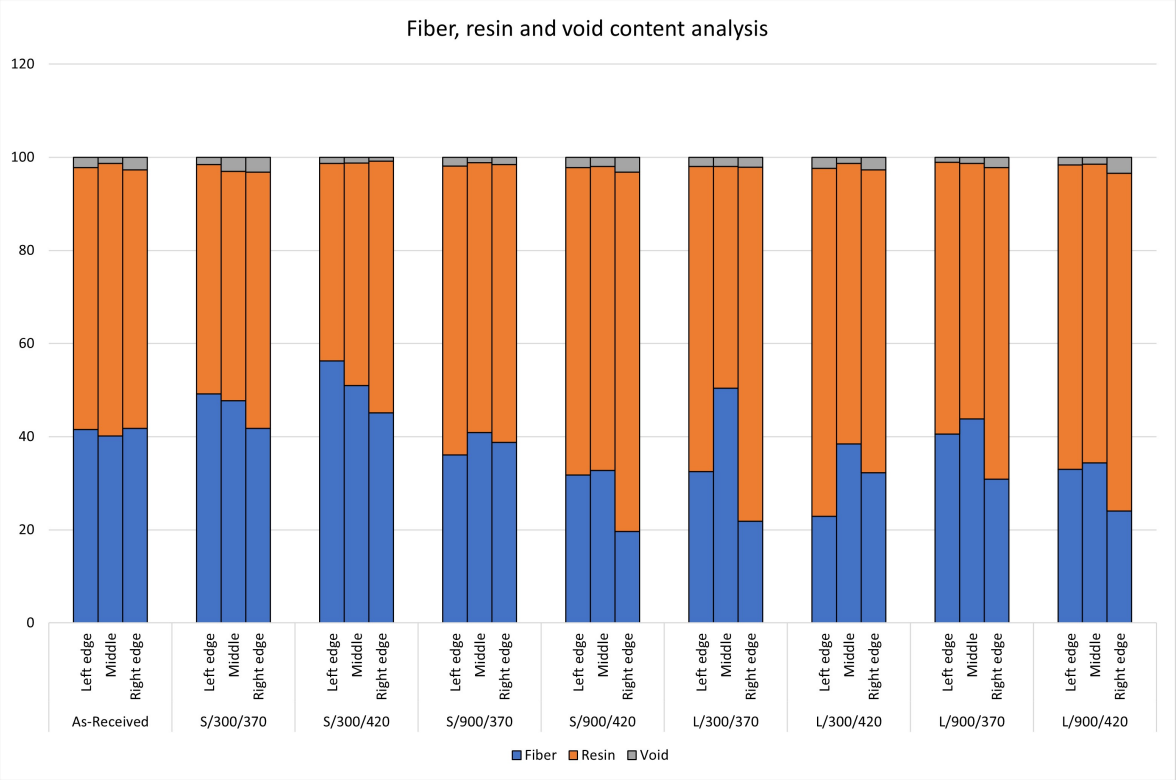


**Figure 6.14:** Fiber, resin and void content analysis at the left edge, middle and right edge of a random sample per specimen configuration along with that of the as-received tape.

### Discussion:

The results show the presence of both fibers (19 - 56 %) and resin (42 - 77 %) at the tape edges. Therefore, this indicates that the width deformation involves spreading of the fiber-resin mixture.

From the obtained data, it is observed that the specimens with long HL and S/900/420 generally had a reduction in the fiber content at the tape edges when compared to the as-received tape. However, the data does not explicitly show this trend to be true as the fiber content in the middle part of the tape is also not uniform and the difference in the fiber content between the two edges seems to have a huge difference. These factors add towards the uncertainty and hence no conclusions can be drawn regarding comparison of the fiber vs resin content. Therefore, more data would be required to remove the uncertainty.

Moreover, the void data also does not show any increasing or decreasing trends for the tape edges and ranges between 0.8 - 3.5 %.

## 6.2 Influence of processing parameters on the tape width

Several specimens were manufactured with different settings for the heated length, processing temperature and compaction pressure as explained in subsection 5.3.1 to understand its influence on the tape width deformation and the width data was extracted using the image processing approach as given in section 5.4. The following subsections present the results obtained in the form of bar charts representing the average tape width after processing in $\mu m$ along with the as-received tape width for comparison. For the as-received width data, ten images with a total length of 154.4 mm corresponding to 14,000 data points were averaged to get the mean and the standard deviation of the data. And, for the post-processed tape width data, two images (at locations shown in Figure 5.16) with a total length of 139.9 mm corresponding to 11,868 data points per sample were combined for all three samples per specimen configuration i.e., a grand total of 419.7 mm (35,604 data points) to get the mean and standard deviation of the width data for each specimen configuration.

### 6.2.1 Effect of heated length

Figure 6.15a and Figure 6.15b show the width data over the heated length for the 300 N and 900 N compaction force specimens respectively and the two nip-point temperatures of 370 °C and 420 °C are plotted in each graph. Comparing the widths at the same nip-point temperature, there is a clear increase in the width as the heated length increases for the specimens at 370 °C nip-point temperature and 300 N compaction force. For all the other configurations, the width change is either similar or have a slight increase with increase in heated length, however with an overlap in the standard deviation (shown as the error bars on the bar chart). This indicates that the width generally increases with increase in heated length, however, this can only be said with full confidence for the 300 N, 370 °C specimens.

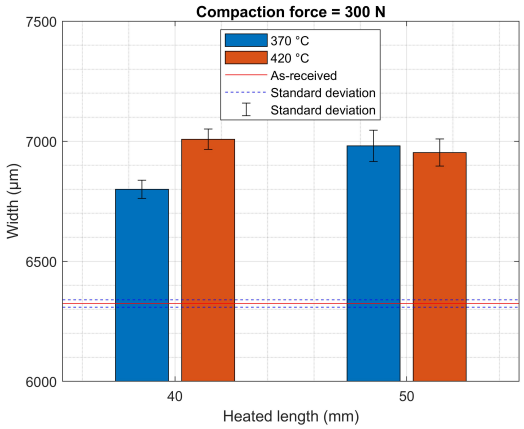


**(a)** Average widths with their standard deviation plotted over heated length for 300 N compaction force.

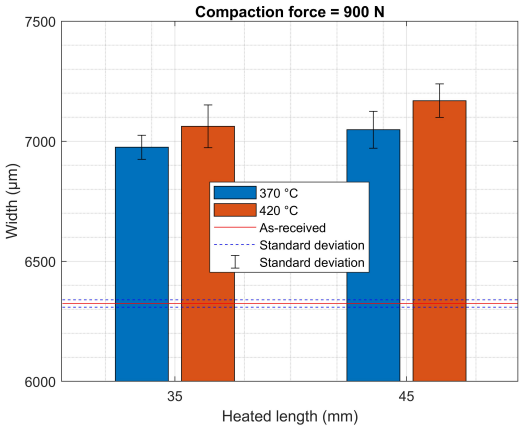


**(b)** Average widths with their standard deviation plotted over heated length for 900 N compaction force.

**Figure 6.15:** Tape width values over heated length.

**Discussion:**

The influence of longer heated length is directly associated with two factors, i.e., larger length of the tape being in the melt phase and more heating time. These factors are assumed to promote better heat distribution in the length and thickness direction of the tape and thereby promote the spreading of the fiber-resin mixture due to less restricted movement of the polymer chains in zones 2, 3 and 4 i.e., the heated length of the tape as described in subsection 6.1.1. However, this can only be seen clearly in the results for the specimens at 370 °C nip-point temperature and 300 N compaction force.

For the 420 °C configuration specimens, it is assumed that the higher temperature will itself promote better heat propagation through the thickness of the tape and therefore overshadow the effect of the longer heated length. Similarly, for the specimens at 370 °C and 900 N, additional width deformation due to the higher compaction force is believed to overshadow the effect of the longer heated length.

### 6.2.2 Effect of processing temperature

Figure 6.16a and Figure 6.16b show the width data over the nip-point temperature for short and long HL configuration respectively and the two compaction forces of 300 N and 900 N are plotted in each graph. For the short heated length, width data for the specimens below the $T_m$ i.e., at 250 °C is also plotted and it can be seen that the width deformation already takes place below the $T_m$. An average increase of upto 6.87% for the 900 N compaction force specimen is observed.

For the short HL configuration specimens in Figure 6.16a, a clear increase in width can be seen as the temperature increases for the 300 N compaction force specimens with no overlap of standard deviations. For the 900 N specimens, there is a clear increase in width when the $T_m$ is hit i.e., between the two temperatures below (250 and 300 °C) and above (370 and 420 °C) the $T_m$, however, the width remains the same for the two temperatures below and above the $T_m$ as the standard deviation data almost completely overlap. This is shown in Figure 6.16c.

For the long HL configuration specimens in Figure 6.16b, no clear trends can be drawn for the 300 N specimens because of the complete overlap in the standard deviations. For the 900 N specimens, the data indicates an increase in width with temperature, however, it cannot be said with full confidence because of the overlapping scatter in data.

**Discussion:**

The effect of processing temperature is directly related to the melt viscosity and polymer chain movement. As the temperature increases, the melt viscosity of the resin decreases along with less restrictions in the movement of the polymer chains which would thereby promote the spreading of the fiber-resin mixture. This can be seen clearly from the results of the short HL configuration specimens where the width increases with increase in temperature. Again, additional width deformation due to the higher compaction force is believed to be the reason for the overlap in data for the two temperatures below and above the $T_m$, thereby adding to the uncertainty. And, better heat distribution resulting in lower restrictions on the polymer

chain movement due to the long HL is believed to be the reason for the overlap of data in the results of the long HL configuration specimens.

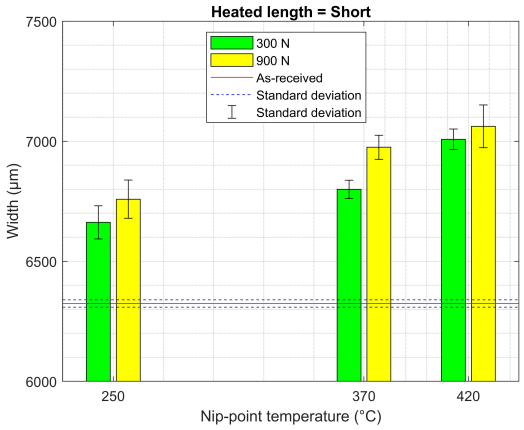


**(a)** Average widths with their standard deviation plotted over nip-point temperature for short HL.

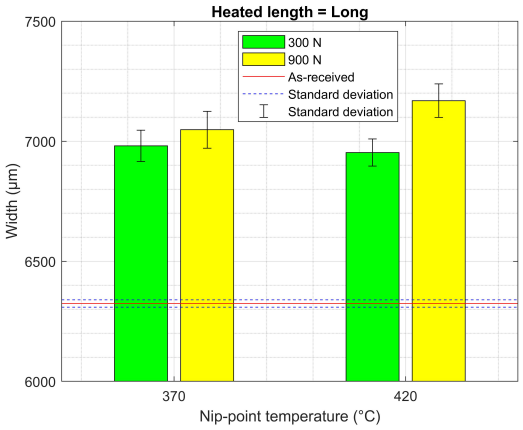


**(b)** Average widths with their standard deviation plotted over nip-point temperature for long HL.

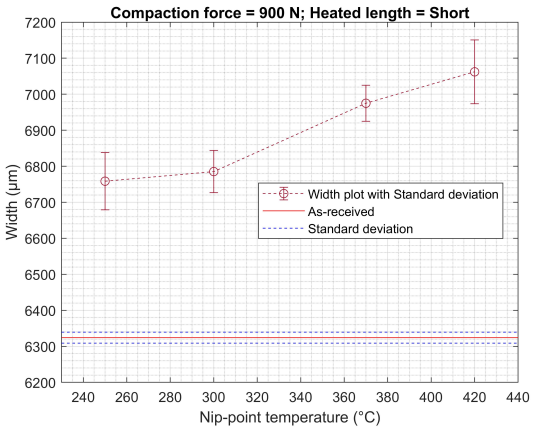


**(c)** Average widths with their standard deviation plotted over nip-point temperature for 900 N compaction force and short HL.

**Figure 6.16:** Tape width values over nip-point temperature.

### 6.2.3 Effect of compaction pressure

Figure 6.17a and Figure 6.17b show the width data over the compaction force for the short and long HL respectively and the different nip-point temperatures are plotted in each graph. For short HL configuration specimens in Figure 6.17a, there is a clear width increase with the compaction force for the 370 °C specimens with no overlap of the standard variations. The width increase is also seen in the 250 °C specimens, however with an overlap in the standard deviations. For the 420 °C specimens, there is no statistical difference between the two compaction forces as the width data completely overlaps.

For long HL configuration specimens in Figure 6.17b, the width increase is clear for the 420

°C specimens with no overlap in data. Again, the data for the 370 °C specimens indicates a slight increase, however, it cannot be said with full confidence because the data almost fully overlap.

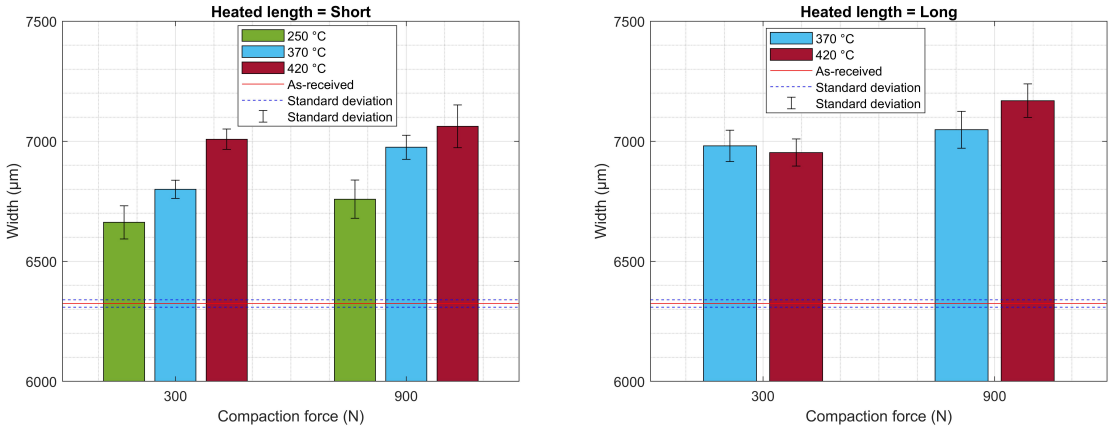


**(a)** Average widths with their standard deviation plotted over compaction force for short HL.

**(b)** Average widths with their standard deviation plotted over compaction force for long HL.

**Figure 6.17:** Tape width values over compaction force.

### Discussion:

Previous results show that the width deformation takes place due to the spreading of the fiber-resin mixture. Therefore, the effect of the compaction pressure is directly dependant on the melt viscosity of the resin and the strain of the fibers. For the short HL configuration, the specimens at 370 °C shows an increase in width with compaction force which means that there is some restricted movement of the polymer chains at this temperature and therefore, increasing the compaction force helps in the flow of the polymer chains and thereby increases the width. For the specimens at 420 °C, either a very low melt viscosity or the maximum strain of the fibers is achieved and therefore the spreading remains the same with increase in compaction force.

A contrasting result is observed for the long HL configuration, where the width of the specimens at 370 °C remains the same and that for the 420 °C specimens increase with compaction force. For the 370 °C specimens, again, a better heat distribution with longer HL is believed to be the reason for no clear change in the width as it overshadows the effect of the higher compaction force in helping with the flow of the restricted polymer chains. For the 420 °C specimens, an increase in the width indicates that further spreading of the fibers was possible due to the longer heated length before reaching the maximum strain as in the case of short HL, 420 °C specimens. Therefore, the flow of polymer chains seems to be the controlling factor for the 370 °C specimens and the fiber straining factor for the 420 °C specimens.

## 6.3 General Discussion

### Tape width fluctuation

From the width data and results, it can be observed that the standard deviation in the data increases for the post-processed tape when compared to the as-received tape from an overall average of 15.25 $\mu m$ to 63.11 $\mu m$. This indicates that the width fluctuations in the post-processed tape increased after processing. The possible reasons for this are the fluctuations in the processing temperature and compaction force during the process. Therefore, the temperature data from the thermal camera was analysed to see if the variations in the temperature had a direct impact on the variations in the tape width. Figure 6.18 shows an example for this analysis where the temperature data from the measurement point "S1" on the tape is plotted against the course length on x-axis. Since the temperature influences the width deformation taking place before the nip-point i.e., in the heating phase of the process, the temperature data analysed and compared with the width data locations (as given in Figure 5.16 and marked with green lines in Figure 6.18) was shifted 25 mm back and 20 mm was added on either sides as the width data measurement locations were not completely accurate. These analysed temperature locations are highlighted in red in the figure.

However, after analysing the data for all the specimens (data included in Appendix C), no direct correlation was found between the standard deviation in the temperature and the width data. Therefore, a combination of the fluctuation in the compaction pressure as given in Figure 5.5b and processing temperature might have led to the fluctuation in the tape width.

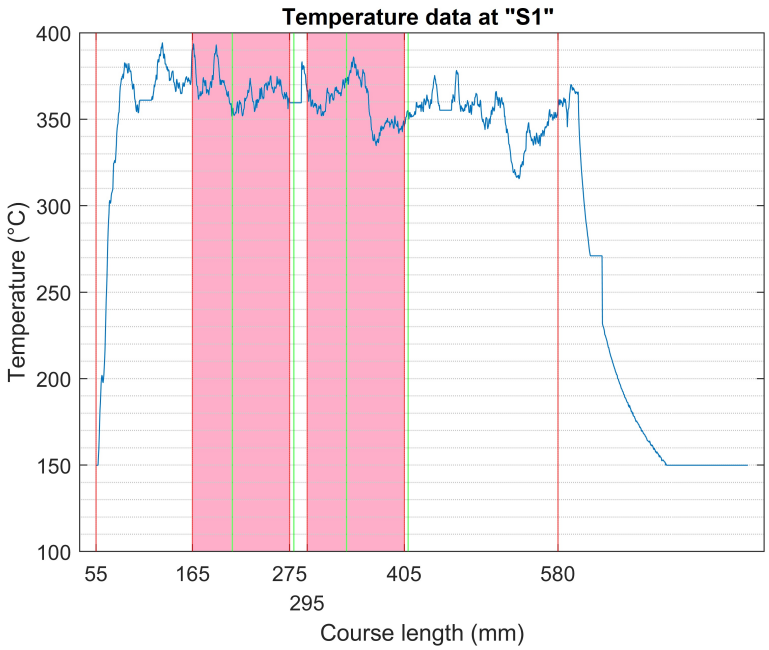


**Figure 6.18:** Temperature data from the thermal camera at measurement point "S1" on the tape over specimen course length. Temperature data highlighted in red compared to the width data locations marked with green lines.

### Effect of the shadow zone

For the specimen manufacturing, the temperature measurement was done at the "visible" nip-point which was approximately 25 mm away from the "actual" nip-point where the roller has the first contact with the tape. Therefore, this introduces some uncertainty in the data as the temperature tends to drop in the shadow zone as shown in Figure 2.4 for Laser AFP. This is also true for the humm3® flashlamp as the radiation gets blocked by the geometry of the roller.

Additionally, the length of the shadow zone for the different compaction force configurations also change by approximately 5 mm because of the change in the contact area under the roller (due to roller deformation). Therefore, it might well be possible that the temperature at the "actual" nip-point remains higher for the 900 N configuration specimens due to a shorter shadow zone length. Furthermore, it is also possible that the temperature at the "actual" nip-point remains higher for the long HL configuration than the short HL configuration due to a better temperature distribution. These factors have been considered as experimental uncertainty here.

The temperature drop in the shadow zone has been taken into account in explaining some of the results which clearly indicate the same, especially for the 370 °C configuration specimens which tends to drop below the material $T_m$ of 305 °C.

### Temperature distribution trend

Some of the results indicate a common trend of dependence on the temperature distribution in the tape wherein a better temperature distribution in the length and thickness direction for the long HL and 420°C configuration specimens has been suggested as a hypothesis for explanation.

The long heated length is associated with larger length of the tape being above the $T_m$ and a longer heating time. Therefore, it is assumed that it would promote better heat distribution in the length and thickness direction of the tape respectively as the heat has more time to propagate in both the direction, thereby achieving a lower gradient i.e., more uniform temperature. This was also studied by C. Ivanyi [62] where it was found that the temperature gradient between the heated and non-heated side for laser heating was higher for samples at higher laser power for shorter heating time. However, the results cannot be extended here for the humm3® flashlamp as the heating mechanism is different for the two heating devices.

For the higher temperature, it is assumed that the heat distribution in the thickness direction is better as the higher temperature will promote the propagation of heat in the thickness direction of the tape in order to achieve temperature equilibrium between the heated and the colder non-heated side of the tape.

### Effect of compaction force on heated length

As mentioned in subsection 5.3.4, the compaction force setting had an effect on the heated length due to an increase in the roller contact area with higher force. This was measured to be approximately 5 mm. Therefore, the two processing parameters are coupled and it is

possible that the effect of the change in compaction force might have included any secondary effects of the change in the heated length. Therefore, this was considered as a limitation of the experimental setup.

# Chapter 7

# Conclusion

The research objective for this project was to investigate the tape width deformation mechanism for in-situ AFP processing of thermoplastic prepreg tapes using humm3® as the heating device and understand the influence of process parameters on the width deformation. Several experiments were performed in order to gain insight into the process and therefore get answers for the research questions formulated. A summary of the research findings are discussed in this chapter with respect to each sub-question and compared with the initially proposed hypotheses in order to draw conclusions. Finally, the relevance of this thesis to the in-situ AFP manufacturing is discussed.

## 7.1 Answers to research questions

***RQ1. What is the governing mechanism behind tape width deformation during in-situ AFP processing of thermoplastic prepregs?***

***SQ1.1 In which phase of the process does the width deformation take place?***

To answer this question, the tape surface profile was analysed to extract the tape width data in the heating phase of the process before reaching the nip-point. The results indicate widening of the tape in the entire heated length of the tape before nip-point. This confirms that the tape width deformation takes place in the heating phase of the process. Additionally, on analysing the width data further, it was found that the samples show a common trend of having a slope right after the nip-point followed by a relatively flat plateau-like region and again a steep slope in the heated length of the tape with a few exceptions which showed a more uniform slope throughout the heated length. Based on the slope right after the nip-point, it was concluded that there is additional width deformation due to the compaction pressure of the roller i.e., in the consolidation phase of the process. This was also confirmed by the average horizontal length data of this slope region wherein higher compaction force led to a longer sloped region indicating more width deformation for long HL specimens as the slope value remained roughly the same. Additionally, the average horizontal length of the slope

also increased for the higher temperature specimens due to relatively lower melt viscosity and ease of flow of the resin resulting in larger length of the tape deforming at the same compaction pressure. The flat plateau-like region and the second slope region are believed to be because of the temperature distribution along the heated length not being uniform and therefore representing the regions above and below the $T_m$ respectively.

Therefore, the initially proposed hypothesis is not completely true as the width deformation takes place both in the heating and consolidation phase of the process and can be represented as shown in Figure 6.2.

***SQ1.2 What are the geometrical changes on the tape after the process?***

To assess the geometrical changes, the surface roughness and the tape cross-section shape were analysed and compared with the as-received tape.

The surface roughness results show that the roughness remains almost the same as the as-received tape for the long HL and higher temperature configuration specimens, indicating that the temperature distribution might have an influence on the roughness value as the material would be able to flow more easily and consolidate more uniformly when the tape is uniformly heated with better temperature distribution. This would therefore result in lower roughness. Additionally, the surface roughness on the heated side and the non-heated side were compared and it was found that the heated side has a higher roughness value. This contradicts the explanation above of having a lower roughness value with increasing temperature as the heated side is at a higher temperature. The reason for this contradiction was concluded to be because of the lower deconsolidation on the non-heated side during the heating phase as the non-heated side most probably did not reach the $T_m$ and was pressed against the roller due to the tape pre-tension that would restrict large out-of-plane deconsolidation on that side.

The tape cross-section shape in general showed a smooth and gradual reduction in the thickness in the form of a slope at the edges of the tape except the lowest setting specimen i.e., short HL, 300 N and 370 °C. This was compared with the as-received and deconsolidated tape cross-section shape which had a rectangular shape at the edges. Therefore, it was concluded that the resulting shape in the post-processed tape was because of the roller compaction as the tape edges under the roller takes the shape of the transitioning shape of the conformable roller, since the tape is in the melt phase and can easily flow and deform. Furthermore, the exception of the S/300/370 specimen was related to the temperature and compaction pressure being too low to have a proper deformation under the roller.

***SQ1.3 How does the tape deform in the micro scale?***

The fiber, resin and void content was analysed for the post processed specimens (one sample per configuration) and compared to the as-received tape to understand the tape deformation in the micro scale. The result shows the presence of both fibers and resin at the tape edges meaning that the tape width deformation involves the spreading of both fibers and resin or the fiber-resin mixture. Therefore, the initially proposed hypothesis is true. Additionally, the data for long HL and S/900/420 specimens show that the resin content in the tape edges is higher than the as-received tape, indicating resin percolation flow or squeeze out in the width direction. However, no conclusions can be made regarding this as the resin content in the middle part of the tape also changes and the two edges have large variations in resin

content. Therefore, the second part of the hypothesis about the resin percolation flow cannot be confirmed and more data would be required to reach a conclusion without any uncertainty.

***RQ2. How does the process parameters influence the width deformation?***

***SQ2.1 How does the heated tape length influence the tape width deformation?***

The results show a clear increase in the width with the heated length but only for the specimens at 370 °C and 300 N compaction force. For all the other configurations, no distinct difference is observed between the two heated length settings because of the scatter in data. According to the initially proposed hypothesis, longer heated length should promote more width deformation due to two reasons i.e., reduced transverse straining of the fibers as the fibers can start spreading at a larger length and better heat distribution in the thickness direction of the tape as the heating time increases. From the results obtained, the first reasoning of the hypothesis seems to be false for the two heated length settings used as the reduced transverse straining of the fibers should be independent of the temperature. The second reasoning seems to be more relevant as the role of the temperature distribution was also indicated by the roughness results. However, the temperature distribution effect resulting from the higher temperature is believed to have influenced the effect from the 10 mm longer heated length used for this study as no clear difference is observed for the higher temperature specimens. Similarly, the effect of higher compaction force influences the effect of the longer heated length. Therefore, it can be concluded that the difference in heated length settings used does not have a significant influence on the tape width deformation except for one specimen configuration i.e., 300 N, 370 °C.

***SQ2.2 How does the processing temperature influence the tape width deformation?***

The results show an increase in the width with increasing temperature for the short HL configuration specimens and no clear trend for the long HL specimens. According to the initially proposed hypothesis, the temperature should only play a role in the width deformation until the material $T_m$ is reached i.e., once the material is in a very low melt viscosity for promoting fiber-resin mixture spreading. The change in melt viscosity above the $T_m$ is negligible and therefore no effect of temperature was expected after that. From the results obtained, the first part of the hypothesis (role until $T_m$) seems to be true as the nip-point temperature setting of 370 °C was considered to drop below the material $T_m$ in the shadow zone between the "actual" and the "visible" nip-point. Again, it is believed that the temperature distribution effect from the longer HL might have influenced the effect of the increasing temperature as no clear trend was observed for the long HL specimens. Since only one temperature setting in the DoE i.e., 420 °C was considered to be above the material $T_m$ at the "actual" nip-point, it is not possible to check the hypothesis for the case when the temperature is further increased above the $T_m$.

Additionally, the width deformation even at temperatures significantly lower than the material $T_m$ (checked at 250 °C) confirms that the fiber-resin spreading is still possible at sub-melt temperatures due to the movement of the polymer (resin) chains.

***SQ2.3 How does the compaction pressure influence the tape width deformation?***

The results show an increase in width with increase in compaction pressure for the short HL, 370 °C specimens and stabilizes for the 420 °C specimens. For the long HL specimens, the width difference between the two compaction pressures is not clear at 370 °C but clearly increases for the specimens at 420 °C. According to the initially proposed hypothesis, it was expected that the pressure will not have an effect after the fibers are already at their maximum transverse strain. This was hypothesized based on the fiber straining in the entire heated length. However, from the results of the effect of heated length, it is concluded that the role of the overall fiber straining is negligible for the two heated length settings used in this study. But, the results do show that the width increases for the 420 °C specimens when the heated length is increased, indicating that the maximum spreading (restricted by strain at break of fibers) was reached for short HL. Therefore, fiber straining at only a part of the heated length which had a spreading effect (observed width slope right after the nip-point) due to the compaction force width deformation seems to be the influencing factor here. Therefore, the hypothesis can be considered to be partially true as the reasoning applies for fiber straining only in a part of the heated length instead of the whole. The second part of the hypothesis i.e., influence of the compaction pressure on the polymer chain movement at sub-melt temperatures is also true as the width generally increases with compaction pressure for specimens below the $T_m$ except for the long HL case, wherein the better temperature distribution is believed to have influenced the effect of increasing compaction pressure.

## 7.2 Relevance for in-situ AFP manufacturing

The results obtained in this study provide a better understanding of the tape width deformation of thermoplastic prepreg tapes processed by in-situ AFP using the humm3® xenon flashlamp as the heating device. The width deformation mechanism i.e., fiber-resin spreading in the heating as well as the consolidation phase of the process instead of the conventionally considered resin squeeze out as the main mechanism can be used to accurately model and predict the final width deformation during AFP processing. This will help in having a predictive model with close resemblance to the actual manufactured structure and can be used to identify and mitigate the problem of gaps and overlaps. Ultimately, the whole AFP process should be modelled accurately to have a virtual part before the physical part is manufactured. By doing so, possible defective parts can be found and corrective measures can be taken before the part is manufactured, leading to significant cost and time savings by having no scrapped parts, and on the way to a first-time-right manufacturing process.

Moreover, the knowledge of the resulting tape edge shape i.e., a gradually decreasing edge thickness, can be used to strategically define the distance between two tapes. A small overlap in the post-process tape width can be programmed to have a more uniform thickness of the manufactured part instead of regular thickness undulations.

Finally, the processing parameters can be optimized to aim for a uniform heat distribution in the tape. The results indicate that the width deformation in general stabilizes when the process parameter settings promote a better temperature distribution in both the length and thickness direction of the tape.

Also, it should be noted that the results are indicative only for a single tape placement on a

mold, mimicking the first ply because of the experimental setup used. Therefore, the effects caused by neighboring tows in a multi-tow deposition and a substrate must be investigated separately and included with the results of this study.

# Chapter 8

# Recommendations

This study provides some useful insights into the mechanism at play for width deformation of thermoplastic prepreg tapes for in-situ AFP manufacturing and the influence of the processing parameters. However, some of the results obtained in this study were explained using hypotheses which should be confirmed. Additionally, some questions still remain unanswered. This chapter provides some recommendations for future work that will help to further understand this topic of research.

1. **Temperature distribution effect:**

   A lot of the results showed exceptions and therefore no direct trends could be drawn. However, all the exceptions pointed towards one mechanism i.e., the role of temperature distribution in the tape. It was hypothesized that higher temperature and longer heated length led to a better heat distribution in the length and thickness direction of the tape; and was used to draw conclusions from the results. Therefore, this hypothesis should be checked. Proposed methodology would be to measure the temperature on both sides of the tape to check the temperature gradient in the thickness direction of the tape. Additionally, to check the temperature distribution in the length direction a static, stand-alone set-up can be used to have a high resolution heat map of the tape through a thermal camera.

2. **Influence of nip-point temperature above $T_m$:**

   The initially proposed hypothesis for the influence of the nip-point temperature once it is already above the material $T_m$ could not be checked in this study due to a drop in temperature in the shadow zone. This most likely led the 370 °C specimens to drop below the material $T_m$ at the "actual" nip-point during the process. Therefore, a higher temperature should be used to check the influence and compare the two specimens when above the $T_m$.

3. **Mid-setting for all parameters:**

   The Design of Experiments for this study was set as high and low for all the process parameters studied to get an overall insight about their influence. However, the results

indicated overshadowing of one parameter due to a change in another one because of the high setting. Therefore, it is recommended to also include a mid-setting for the process parameters in order to avoid this problem and also get insights into the possible trends and the nature of influence i.e., linear, exponential, etc.

4. **Fiber-resin content ratio:**

   The obtained results roughly indicated higher resin content for some samples at the tape edges. However, no conclusions could be drawn due to lack of enough sample data to exclude the uncertainty. Therefore, a thorough study is recommended to check the fiber-resin ratio at the tape edges after processing to check if the resin content is indeed higher, meaning that resin squeeze out also plays a role in the width deformation of the tape.

5. **Tape width fluctuation:**

   In addition to the overall width change during the process, it was observed that the tape width fluctuation also increases when compared to the as-received tape. This would eventually still lead to the formation of very small gaps and overlaps in the final manufactured structure. In this study, the reason for having these width fluctuations was related to the experimental set-up i.e., fluctuations in the compaction force and processing temperature during manufacturing. Therefore, it is recommended to investigate further into this topic to find out if the increase in the width fluctuations is because of the external factors or the material properties itself like thickness variations in the as-received tape that could influence the tape spreading.

6. **Influence of placement speed:**

   The influence of the heated length is directly associated with two factors i.e., length of the tape that is heated and heating time. Therefore, the results for the influence of heated length in this study includes both the factors. In order to understand the individual effects of these two factors, it is recommended to also study the influence of the placement speed as its effect is only associated with heating time. Since it is impossible to decouple the heating time factor from the heated length setting, the results from the influence of placement speed can be used to compare with that of the heated length to determine the main factor playing a role for the heated length.

7. **Influence of roller hardness**

   It was observed that the tape edges had a gradual reduction in the thickness and it was concluded that this was because of the roller compaction as the tape edges under the roller takes the shape of the transitioning shape of the conformable roller on the tool, since the tape is in the melt phase and can easily flow and deform. Therefore, based on this, it is possible that the roller hardness also has an influence on the tape edge deformation profile and overall width deformation in the consolidation phase. Depending on the roller hardness, a different edge deformation profile is expected. An ideally hard roller would result in a constant gap between the roller and the tool and would not block the expansion of the material. On the other hand, a soft roller, which would contact the tool more quickly, could inhibit the expansion of the material. This should be investigated in future work.

8. **Other boundary conditions:**

   This study majorly focused on the tape width deformation mechanism and influence of the processing parameters for a single tape placed on a heated tool at a material level. However, in order to see the interaction effects for the actual manufacturing, it is recommended to also include the other boundary conditions into the setup, for example, placing multiple tapes in one go and placing the tapes on a substrate. When multiple tapes are placed, it is expected that the tape width deformation in the heating phase might be restricted due to the adjacent tape. And, when the tapes are placed on a substrate, it is expected that the width deformation in the consolidation phase might be restricted due to the fiber-resin mixture flow interactions with the substrate.

# References


[1] P.K. Mallick. *Processing of Polymer Matrix Composites*. 1st ed. CRC Press, 2017. DOI: https://doi-org.tudelft.idm.oclc.org/10.1201/9781315157252.

[2] *AERO - Boeing 787 from the Ground Up*. URL: https://www.boeing.com/commercial/aeromagazine/articles/qtr_4_06/article_04_2.html.

[3] *Boeing: Commercial Market Outlook*. URL: https://www.boeing.com/commercial/market/commercial-market-outlook/index.page.

[4] *Global Market Forecast | Airbus*. URL: https://www.airbus.com/en/products-services/commercial-aircraft/market/global-market-forecast.

[5] *The Paris Agreement | UNFCCC*. URL: https://unfccc.int/process-and-meetings/the-paris-agreement/the-paris-agreement.

[6] *I want to say two words to you: "Thermoplastic tapes" | CompositesWorld*. URL: https://www.compositesworld.com/articles/i-want-to-say-two-words-to-you-thermoplastic-tapes.

[7] Gearóid Clancy et al. "A study of the influence of processing parameters on steering of carbon Fibre/PEEK tapes using laser-assisted tape placement". In: *Composites Part B: Engineering* 163 (2019), pp. 243–251. ISSN: 1359-8368. DOI: https://doi.org/10.1016/j.compositesb.2018.11.033. URL: https://www.sciencedirect.com/science/article/pii/S135983681832300X.

[8] Falk Heinecke and Christian Willberg. "Manufacturing-Induced Imperfections in Composite Parts Manufactured via Automated Fiber Placement". In: *Journal of Composites Science* 3.2 (2019). ISSN: 2504-477X. DOI: 10.3390/jcs3020056. URL: https://www.mdpi.com/2504-477X/3/2/56.

[9] Ramy Harik et al. "Automated fiber placement defect identity cards: cause, anticipation, existence, significance, and progression". In: Jan. 2018.

[10] Alex Brasington et al. "Automated fiber placement: A review of history, current technologies, and future paths forward". In: *Composites Part C: Open Access* 6 (2021), p. 100182. ISSN: 2666-6820. DOI: https://doi.org/10.1016/j.jcomc.2021.100182. URL: https://www.sciencedirect.com/science/article/pii/S2666682021000773.

[11] Steven L. Miracle Daniel B. Donaldson. *ASM Handbook, Volume 21 - Composites - 60.1 Applications. (pp. 477).* ASM International, 2001. URL: https://app.knovel.com/hotlink/pdf/id:kt007PSCM2/asm-handbook-volume-21/fiber-plac-applications.

[12] Ajay Kumar Kadiyala et al. "Mechanical evaluation and failure analysis of composite laminates manufactured using automated dry fibre tape placement followed by liquid resin infusion". In: *Composites Science and Technology* 201 (2021), p. 108512. ISSN: 0266-3538. DOI: https://doi.org/10.1016/j.compscitech.2020.108512. URL: https://www.sciencedirect.com/science/article/pii/S0266353820323022.

[13] J.S.U. Schell et al. "Computational and experimental analysis of fusion bonding in thermoplastic composites: Influence of process parameters". In: *Journal of Materials Processing Technology* 209.11 (2009), pp. 5211–5219. ISSN: 0924-0136. DOI: https://doi.org/10.1016/j.jmatprotec.2009.03.008. URL: https://www.sciencedirect.com/science/article/pii/S0924013609000983.

[14] Khaled Yassin and Mehdi Hojjati. "Processing of thermoplastic matrix composites through automated fiber placement and tape laying methods: A review". In: *Journal of Thermoplastic Composite Materials* 31.12 (2018), pp. 1676–1725. DOI: 10.1177/0892705717738305. eprint: https://doi.org/10.1177/0892705717738305. URL: https://doi.org/10.1177/0892705717738305.

[15] Thomas Weiler. "Thermal skin effect in laser-assisted tape placement of thermoplastic composites; 1. Auflage". Dissertation. Aachen: RWTH Aachen University, 2019, 1 Online–Ressource (X, 203 Seiten) : Illustrationen, Diagramme. ISBN: 978-3-86359-739-9. DOI: 10.18154/RWTH-2019-06638. URL: https://publications.rwth-aachen.de/record/764139.

[16] Matthew J. Donough et al. "Process modelling of In-situ consolidated thermoplastic composite by automated fibre placement – A review". In: *Composites Part A: Applied Science and Manufacturing* 163 (2022), p. 107179. ISSN: 1359-835X. DOI: https://doi.org/10.1016/j.compositesa.2022.107179. URL: https://www.sciencedirect.com/science/article/pii/S1359835X22003608.

[17] Ozan Çelik et al. "Deconsolidation of thermoplastic prepreg tapes during rapid laser heating". In: *Composites Part A: Applied Science and Manufacturing* 149 (2021), p. 106575. ISSN: 1359-835X. DOI: https://doi.org/10.1016/j.compositesa.2021.106575. URL: https://www.sciencedirect.com/science/article/pii/S1359835X21002967.

[18] Omid Aghababaei Tafreshi et al. "Determination of convective heat transfer coefficient for automated fiber placement (AFP) for thermoplastic composites using hot gas torch". In: *Advanced Manufacturing: Polymer & Composites Science* 6.2 (2020), pp. 86–100. DOI: 10.1080/20550340.2020.1764236. eprint: https://doi.org/10.1080/20550340.2020.1764236. URL: https://doi.org/10.1080/20550340.2020.1764236.

[19] Anastasios Danezis et al. "Heat transfer modelling of flashlamp heating for automated tape placement of thermoplastic composites". In: *Composites Part A: Applied Science and Manufacturing* 145 (2021), p. 106381. ISSN: 1359-835X. DOI: https://doi.org/10.1016/j.compositesa.2021.106381. URL: https://www.sciencedirect.com/science/article/pii/S1359835X21001056.

[20] *Humm3®*. URL: https://www.heraeus.com/en/hng/products_and_solutions/arc_and_flash_lamps/humm3/humm3.html.

[21] *humm3 ®-Journey to industrialisation e-book [e-book] humm3 ® systems Journey to industrialisation*. URL: https://www.heraeus.com/media/media/hng/doc_hng/products_and_solutions_1/arc_and_flash_lamps_1/e-book_JUL_2021_Journey_to_Industrialisation.pdf.

[22] Sebastian Meister, Andreas Kolbe, and Roger M. Groves. "Reflectivity and emissivity analysis of thermoplastic CFRP for optimising Xenon heating and thermographic measurements". In: *Composites Part A: Applied Science and Manufacturing* 158 (2022), p. 106972. ISSN: 1359-835X. DOI: https://doi.org/10.1016/j.compositesa.2022.106972. URL: https://www.sciencedirect.com/science/article/pii/S1359835X22001610.

[23] *A flash of inspiration! - Aerospace Manufacturing*. URL: https://www.aero-mag.com/heraeus-noblelight-xenon-flash-lamp-composite-manufacturing.

[24] Pavel Simacek et al. "Role of resin percolation in gap filling mechanisms during the thin ply thermosetting automated tape placement process". In: *Composites Part A: Applied Science and Manufacturing* 152 (2022), p. 106677. ISSN: 1359-835X. DOI: https://doi.org/10.1016/j.compositesa.2021.106677. URL: https://www.sciencedirect.com/science/article/pii/S1359835X21003948.

[25] Ozan Çelik et al. "Intimate contact development during laser assisted fiber placement: Microstructure and effect of process parameters". In: *Composites Part A: Applied Science and Manufacturing* 134 (2020), p. 105888. ISSN: 1359-835X. DOI: https://doi.org/10.1016/j.compositesa.2020.105888. URL: https://www.sciencedirect.com/science/article/pii/S1359835X20301263.

[26] C.M. Stokes-Griffin and P. Compston. "Investigation of sub-melt temperature bonding of carbon-fibre/PEEK in an automated laser tape placement process". In: *Composites Part A: Applied Science and Manufacturing* 84 (2016), pp. 17–25. ISSN: 1359-835X. DOI: https://doi.org/10.1016/j.compositesa.2015.12.019. URL: https://www.sciencedirect.com/science/article/pii/S1359835X16000038.

[27] Ozan Çelik et al. "The effect of Laser-Induced deconsolidation on the compaction behavior of thermoplastic composite tapes". In: *Composites Part A: Applied Science and Manufacturing* 151 (2021), p. 106670. ISSN: 1359-835X. DOI: https://doi.org/10.1016/j.compositesa.2021.106670. URL: https://www.sciencedirect.com/science/article/pii/S1359835X21003870.

[28] S. M.Amin Hosseini et al. "On the temperature evolution during continuous laser-assisted tape winding of multiple C/PEEK layers: The effect of roller deformation". In: *International Journal of Material Forming* 14 (2 Mar. 2021), pp. 203–221. ISSN: 19606214. DOI: 10.1007/S12289-020-01568-7/FIGURES/19. URL: https://link-springer-com.tudelft.idm.oclc.org/article/10.1007/s12289-020-01568-7.

[29] C.M. Stokes-Griffin and P. Compston. "The effect of processing temperature and placement rate on the short beam strength of carbon fibre–PEEK manufactured using a laser tape placement process". In: *Composites Part A: Applied Science and Manufacturing* 78 (2015), pp. 274–283. ISSN: 1359-835X. DOI: https://doi.org/10.1016/

j.compositesa.2015.08.008. URL: https://www.sciencedirect.com/science/article/pii/S1359835X15002791.

[30] David Maass. "Progress in automated ply inspection of AFP layups". In: *Reinforced Plastics* 59.5 (2015), pp. 242–245. ISSN: 0034-3617. DOI: https://doi.org/10.1016/j.repl.2015.05.002. URL: https://www.sciencedirect.com/science/article/pii/S0034361715004002.

[31] Jonathan P.-H. Belnoue et al. "Understanding and predicting defect formation in automated fibre placement pre-preg laminates". In: *Composites Part A: Applied Science and Manufacturing* 102 (2017), pp. 196–206. ISSN: 1359-835X. DOI: https://doi.org/10.1016/j.compositesa.2017.08.008. URL: https://www.sciencedirect.com/science/article/pii/S1359835X17303081.

[32] Thijs Kok. "On the consolidation quality in laser assisted fiber placement: The role of the heating phase". PhD thesis. Netherlands: University of Twente, 2018. ISBN: 978-90-365-4606-5. DOI: 10.3990/1.9789036546065.

[33] Jos van Kollenburg. *The effects of local fibre steering: Reducing gaps and overlaps by compensating for tow width fluctuation in automated fibre placement*. Netherlands: Delft University of Technology, 2021. URL: http://resolver.tudelft.nl/uuid:ddfe7c0e-46d7-4a2f-95d2-72850c39a073.

[34] Neha Yadav and Ralf Schledjewski. "Inline tape width control for thermoplastic automated tape layup". In: *Composites Part A: Applied Science and Manufacturing* 163 (2022), p. 107267. ISSN: 1359-835X. DOI: https://doi.org/10.1016/j.compositesa.2022.107267. URL: https://www.sciencedirect.com/science/article/pii/S1359835X22004481.

[35] Muhammad Amir Khan. "Experimental and Simulative Description of the Thermoplastic Tape Placement Process with Online Consolidation". PhD thesis. Technische Universität Kaiserslautern, 2017. URL: http://nbn-resolving.de/urn:nbn:de:hbz:386-kluedo-47293.

[36] Mohammad Rakhshbahar and Michael Sinapius. "A Novel Approach: Combination of Automated Fiber Placement (AFP) and Additive Layer Manufacturing (ALM)". In: *Journal of Composites Science* 2.3 (2018). ISSN: 2504-477X. DOI: 10.3390/jcs2030042. URL: https://www.mdpi.com/2504-477X/2/3/42.

[37] Gearóid J. Clancy et al. "Steering of Carbon Fiber/Thermoplastic Pre-preg Tapes using Laser-Assisted Tape Placement". In: *2018 AIAA/ASCE/AHS/ASC Structures, Structural Dynamics, and Materials Conference*. DOI: 10.2514/6.2018-0478. eprint: https://arc.aiaa.org/doi/pdf/10.2514/6.2018-0478. URL: https://arc.aiaa.org/doi/abs/10.2514/6.2018-0478.

[38] A. J. Sawicki and P. J. Minguet. "Effect of intraply overlaps and gaps upon the compression strength of composite laminates". In: *Collection of Technical Papers - AIAA/ASME/ASCE/AHS/ASC Structures, Structural Dynamics and Materials Conference* 1 (1998), pp. 744–754. ISSN: 02734508. DOI: 10.2514/6.1998-1786. URL: https://arc-aiaa-org.tudelft.idm.oclc.org/doi/10.2514/6.1998-1786.

[39] Minh Hoang Nguyen et al. “Effect of automated fiber placement (AFP) manufacturing signature on mechanical performance of composite structures”. In: *Composite Structures* 228 (2019), p. 111335. ISSN: 0263-8223. DOI: https://doi.org/10.1016/j.compstruct.2019.111335. URL: https://www.sciencedirect.com/science/article/pii/S0263822319317672.

[40] A. Marouene et al. “Effects of gaps and overlaps on the buckling behavior of an optimally designed variable-stiffness composite laminates – A numerical and experimental study”. In: *Composite Structures* 140 (2016), pp. 556–566. ISSN: 0263-8223. DOI: https://doi.org/10.1016/j.compstruct.2016.01.012. URL: https://www.sciencedirect.com/science/article/pii/S0263822316000258.

[41] Mohammadhossein Ghayour, Mehdi Hojjati, and Rajamohan Ganesan. “Effect of tow gaps on impact strength of thin composite laminates made by Automated Fiber Placement: Experimental and semi-analytical approaches”. In: *Composite Structures* 248 (2020), p. 112536. ISSN: 0263-8223. DOI: https://doi.org/10.1016/j.compstruct.2020.112536. URL: https://www.sciencedirect.com/science/article/pii/S0263822320312174.

[42] William E. Guin, Justin R. Jackson, and Cameron M. Bosley. “Effects of tow-to-tow gaps in composite laminates fabricated via automated fiber placement”. In: *Composites Part A: Applied Science and Manufacturing* 115 (2018), pp. 66–75. ISSN: 1359-835X. DOI: https://doi.org/10.1016/j.compositesa.2018.09.014. URL: https://www.sciencedirect.com/science/article/pii/S1359835X18303646.

[43] Brian F. Tatting and Zafer Gürdal. *Design and Manufacture of Elastically Tailored Tow Placed Plates*. National Aeronautics and Space Administration, Hampton, Virginia, 2002. URL: https://ntrs.nasa.gov/search.jsp?R=20020073162.

[44] Luke Everett Turoski. “Effects of Manufacturing Defects on the Strength of Toughened Carbon/Epoxy Prepreg Composites”. PhD thesis. Montana State University, 2000. URL: https://scholarworks.montana.edu/xmlui/handle/1/8007.

[45] Mohammad Rakhshbahar and Michael Sinapius. “A Novel Approach: Combination of Automated Fiber Placement (AFP) and Additive Layer Manufacturing (ALM)”. In: *Journal of Composites Science* 2.3 (2018). ISSN: 2504-477X. DOI: 10.3390/jcs2030042. URL: https://www.mdpi.com/2504-477X/2/3/42.

[46] Byung Chul Kim, Kevin Potter, and Paul M. Weaver. “Continuous tow shearing for manufacturing variable angle tow composites”. In: *Composites Part A: Applied Science and Manufacturing* 43.8 (2012), pp. 1347–1356. ISSN: 1359-835X. DOI: https://doi.org/10.1016/j.compositesa.2012.02.024. URL: https://www.sciencedirect.com/science/article/pii/S1359835X12000929.

[47] E.L. Wang and T.G. Gutowski. “Laps and gaps in thermoplastic composites processing”. In: *Composites Manufacturing* 2.2 (1991), pp. 69–78. ISSN: 0956-7143. DOI: https://doi.org/10.1016/0956-7143(91)90182-G. URL: https://www.sciencedirect.com/science/article/pii/095671439190182G.

[48] Gearóid Clancy et al. “In-line variable spreading of carbon fibre/thermoplastic pre-preg tapes for application in automatic tape placement”. In: *Materials  Design* 194 (2020), p. 108967. ISSN: 0264-1275. DOI: https://doi.org/10.1016/j.matdes.2020.108967. URL: https://www.sciencedirect.com/science/article/pii/S0264127520305013.

[49] S.D.R. Wilson. "Lateral spreading of fibre tows". In: *Journal of Engineering Mathematics* 32 (1997), pp. 19–26. DOI: https://doi.org/10.1023/A:1004253531061.

[50] M. S. Irfan et al. "Lateral spreading of a fiber bundle via mechanical means". In: *Journal of Composite Materials* 46.3 (2012), pp. 311–330. DOI: 10.1177/0021998311424624. eprint: https://doi.org/10.1177/0021998311424624. URL: https://doi.org/10.1177/0021998311424624.

[51] J.A. Goshawk, V.P. Navez, and R.S. Jones. "Squeezing flow of continuous fibre-reinforced composites". In: *Journal of Non-Newtonian Fluid Mechanics* 73.3 (1997), pp. 327–342. ISSN: 0377-0257. DOI: https://doi.org/10.1016/S0377-0257(97)00049-9. URL: https://www.sciencedirect.com/science/article/pii/S0377025797000499.

[52] S.F Shuler and S.G Advani. "Transverse squeeze flow of concentrated aligned fibers in viscous fluids". In: *Journal of Non-Newtonian Fluid Mechanics* 65.1 (1996), pp. 47–74. ISSN: 0377-0257. DOI: https://doi.org/10.1016/0377-0257(96)01440-1. URL: https://www.sciencedirect.com/science/article/pii/0377025796014401.

[53] J.A. Barnes and F.N. Cogswell. "Transverse flow processes in continuous fibre-reinforced thermoplastic composites". In: *Composites* 20.1 (1989). Flow Processes in Composite Materials, pp. 38–42. ISSN: 0010-4361. DOI: https://doi.org/10.1016/0010-4361(89)90680-0. URL: https://www.sciencedirect.com/science/article/pii/0010436189906800.

[54] Xavier Won Brulotte. *Aspects of in-situ consolidation of thermoplastic laminates manufactured by automated tape placement: A material deformation study*. McGill University, Montreal, Quebec, 2013.

[55] Ebrahim Oromiehie, Asit Kumar Gain, and B. Gangadhara Prusty. "Processing parameter optimisation for automated fibre placement (AFP) manufactured thermoplastic composites". In: *Composite Structures* 272 (2021), p. 114223. ISSN: 0263-8223. DOI: https://doi.org/10.1016/j.compstruct.2021.114223. URL: https://www.sciencedirect.com/science/article/pii/S0263822321006851.

[56] Yannick M. Blommert. *Deconsolidation of thermoplastic prepreg tapes during the heating phase of LAFP: An experimental investigation into the effect of a resin-rich surface and tape pre-tension*. Netherlands: Delft University of Technology, 2022. URL: http://resolver.tudelft.nl/uuid:7c2c3346-121f-4aa1-8038-ef5658077ef9.

[57] Mario Adrian Valverde et al. "The Effect of Process Parameters on First Ply Deposition in Automated Fibre Placement". In: Sept. 2022. DOI: 10.12783/asc37/36424.

[58] R. Pitchumani et al. "Analysis of transport phenomena governing interfacial bonding and void dynamics during thermoplastic tow-placement". In: *International Journal of Heat and Mass Transfer* 39.9 (1996), pp. 1883–1897. ISSN: 0017-9310. DOI: https://doi.org/10.1016/0017-9310(95)00271-5. URL: https://www.sciencedirect.com/science/article/pii/0017931095002715.

[59] Sridhar Ranganathan, Suresh G. Advani, and Mark A. Lamontia. "A Non-Isothermal Process Model for Consolidation and Void Reduction during In-Situ Tow Placement of Thermoplastic Composites". In: *Journal of Composite Materials* 29.8 (1995), pp. 1040–1062. DOI: 10.1177/002199839502900803. eprint: https://doi.org/10.1177/002199839502900803. URL: https://doi.org/10.1177/002199839502900803.

[60] L. Raps et al. “CF/LM-PAEK: Characterisation and sensitivity to critical process parameters for automated fibre placement”. In: *Composite Structures* 284 (2022), p. 115087. ISSN: 0263-8223. DOI: https://doi.org/10.1016/j.compstruct.2021.115087. URL: https://www.sciencedirect.com/science/article/pii/S0263822321015026.

[61] Junxia Jiang, Yuxiao He, and Yinglin Ke. “Pressure distribution for automated fiber placement and design optimization of compaction rollers”. In: *Journal of Reinforced Plastics and Composites* 38.18 (2019), pp. 860–870. DOI: 10.1177/0731684419850896. eprint: https://doi.org/10.1177/0731684419850896. URL: https://doi.org/10.1177/0731684419850896.

[62] Charlotte M. Iványi. *Crystallization of thermoplastic composites during the heating phase of Laser-Assisted Fiber Placement: An experimental investigation into the development of degree of crystallinity in CF/PPS tapes during the heating phase of LAFP*. Netherlands: Delft University of Technology, 2023. URL: http://resolver.tudelft.nl/uuid:a8f477de-a2f0-4bcf-b956-4cf035aacc79.

[63] *ASTM E1933-14(2022) Standard Practice for Measuring and Compensating for Emissivity Using Infrared Imaging Radiometers*. URL: https://www.astm.org/e1933-14r22.html.

[64] Xiangning Li and William Strieder. “Emissivity of High-Temperature Fiber Composites”. In: *Industrial & Engineering Chemistry Research* 48.4 (2009), pp. 2236–2244. DOI: 10.1021/ie8008583. eprint: https://doi.org/10.1021/ie8008583. URL: https://doi.org/10.1021/ie8008583.

# Appendix A

# Thermal camera calibration

The calibration of the Optris PI640 thermal camera used in this study was based on ASTM E1933 standard [63] for measuring and compensating for the emissivity value. A static setup which represented the dynamic conditions during actual specimen manufacturing was used, wherein the AFP head was positioned on the layup tool with some length of the incoming tape already fed to the process. The heat from the humm3® was then applied till the temperature reached the desired value.

First, the ambient temperature near the tape was measured since it was in close proximity to the layup tool that was heated to 80 °C. It was found to be approximately 60 °C and was set in the thermal camera recording software used i.e., Optris PIX Connect. Figure A.1 shows the set-up used for the calibration process. A K-type thermocouple of size 0.13 mm was used as the contact thermometer and the objective was to match the temperature reading on the thermal camera with that on the thermocouple. The thermocouple was stuck to the tape with Kapton tape and the tip of the thermocouple (where the temperature is measured) was embedded on the surface with a hot iron. The temperature was recorded using OMEGA USB data acquisition system with the highest possible scan rate of 250 Hz. i.e. 250 measurements per second. For the thermal camera reading, a 2X2 pixel spot as shown in Figure A.2 was placed close to where the tip of the thermocouple was stuck and the average temperature in the spot area was recorded with a scan rate of 20 Hz.

Several trials were performed to match the thermal camera reading with the thermocouple reading by tuning the emissivity value on the Optris software and the final value for the emissivity was obtained as $\epsilon = 0.875$. This was confirmed by repeating the calibration process 3 times with the emissivity value set at 0.875. The calibration curves obtained are given in Figure A.3.

The maximum temperature used for the calibration process was just below the $T_m$ i.e., around 270°C. This is because at higher temperatures i.e., near and above the $T_m$ (=305°C), the thermocouple detached from the surface of the tape and therefore the temperature readings were not reliable. At 270°C, the thermocouple stayed attached to the tape surface and the calibration process was performed up to this temperature. Therefore, it was assumed that

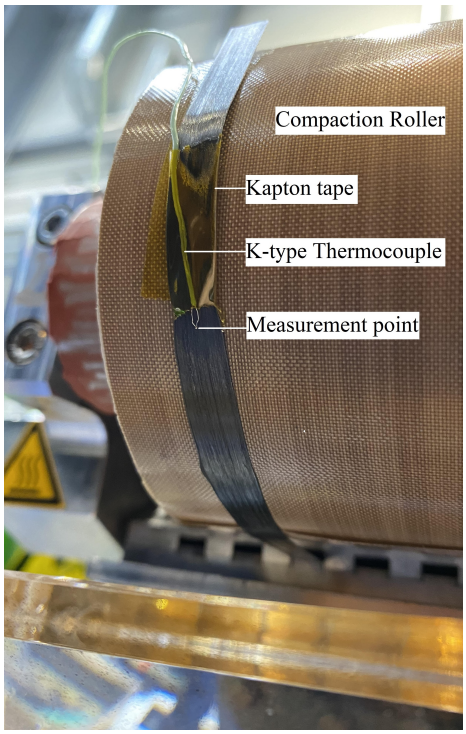


**Figure A.1:** Set-up for emissivity calibration.

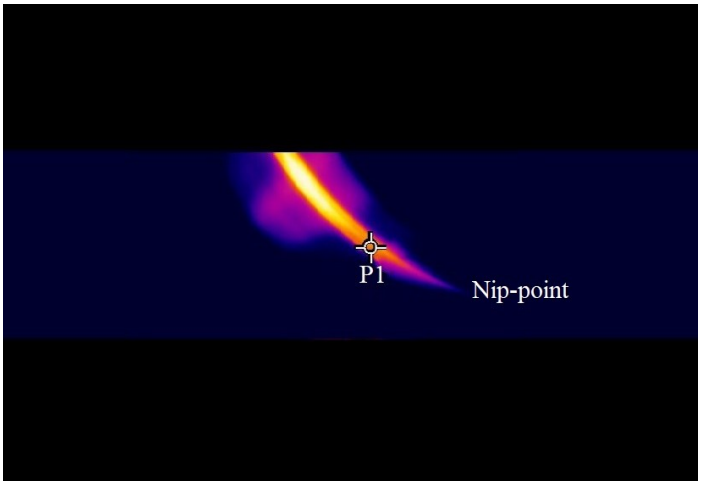


**Figure A.2:** 2X2 pixel spot on tape for average temperature reading on the thermal camera.

the emissivity value does not change significantly between 270 and 420 °C as the influence of the material's temperature on the emissivity is probably very low [64] and the obtained value of $\epsilon = 0.875$ was used for this study.

A deviation of approximately 5 °C between the thermal camera and the thermocouple data was recorded around the highest temperature achieved for calibration. This can be due to the following reasons:

1. The data recording frequency of the two equipments were not equal and therefore small deviations can occur because of the fast heating rate.
2. The reflectivity of the tape might change during heating due to out-of-plane deformations of the tape as it starts to deconsolidate.
3. The measurement from the thermocouple is at a specific point on the tape whereas, for the thermal camera, the average temperature in a bigger area of measurement is compared. Therefore, small deviations can occur as the tape might not heat uniformly.

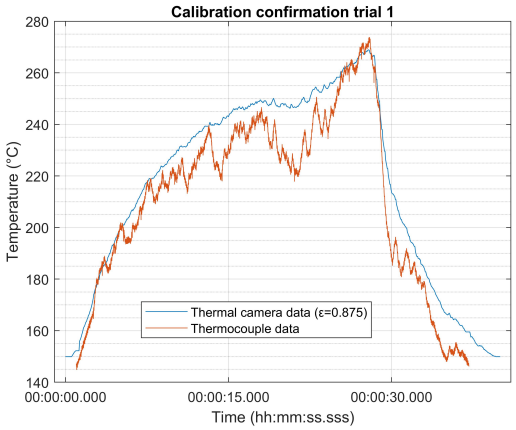


**(a)** Trial 1

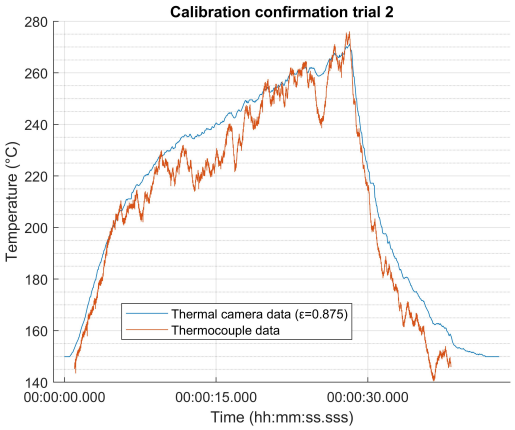


**(b)** Trial 2

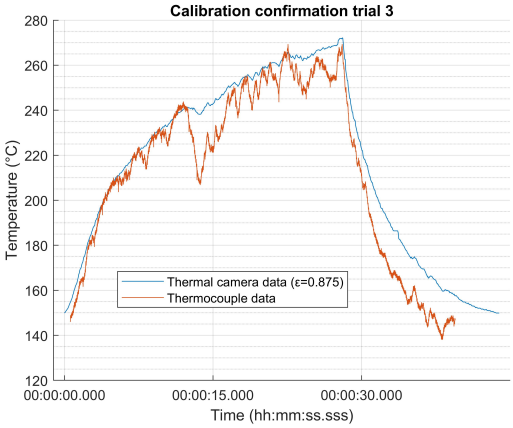


**(c)** Trial 3

**Figure A.3:** Emissivity calibration confirmation trials.

# Appendix B

# Tape width analysis in the heating zone: Zone 4 data

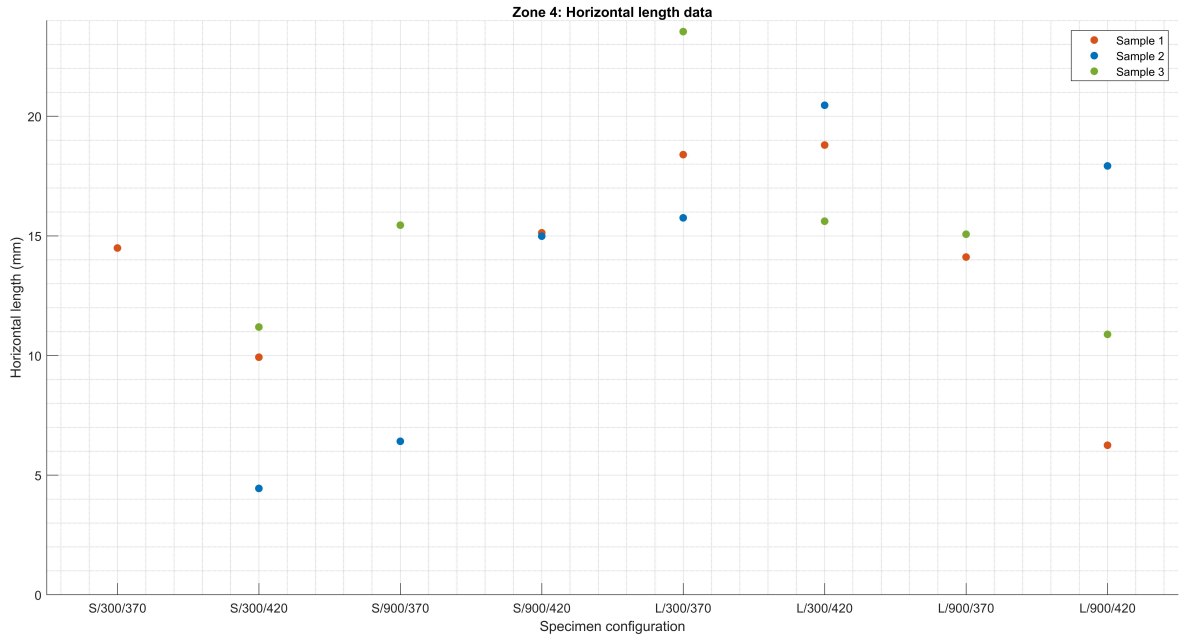


**Figure B.1:** Zone 4 horizontal length data of all specimens.

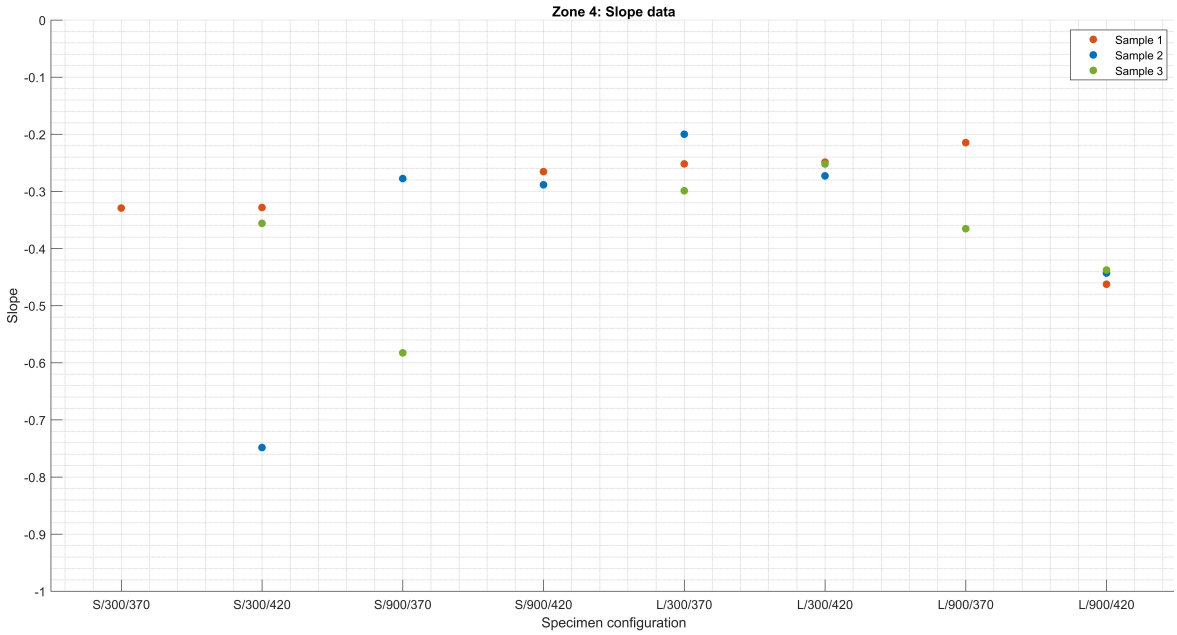


**Figure B.2:** Zone 4 slope data of all specimens.

# Appendix C

# Comparison for width and temperature data

**Table C.1:** Mean and standard deviation data for width and temperature of all samples.

| Sample | Measurement Location | Width (µm) | | Temperature (°C) | |
|---|---|---|---|---|---|
| | | Mean | SD | Mean | SD |
| S/300/250_1 | 1 | 6607.2 | 66.1 | 229.5 | 9.4 |
| | 2 | 6667.0 | 59.0 | 230.3 | 7.3 |
| S/300/250_2 | 1 | 6763.9 | 78.7 | 225.7 | 7.4 |
| | 2 | 6476.4 | 57.8 | 218.9 | 9.4 |
| S/300/250_3 | 1 | 6782.8 | 82.5 | 247.8 | 9.3 |
| | 2 | 6675.3 | 66.8 | 229.8 | 7.3 |
| | Average | 6662.1 | 69.1 | 230.3 | 8.4 |
| S/900/250_1 | 1 | 6742.0 | 96.9 | 233.9 | 10.9 |
| | 2 | 6724.6 | 77.6 | 242.3 | 12.3 |
| S/900/250_2 | 1 | 6807.9 | 73.8 | 241.6 | 8.9 |
| | 2 | 6779.6 | 95.4 | 225.3 | 11.0 |
| S/900/250_3 | 1 | 6851.9 | 54.8 | 235.5 | 10.8 |
| | 2 | 6644.7 | 71.2 | 216.4 | 12.3 |
| | Average | 6758.5 | 79.6 | 232.5 | 11.1 |
| S/300/370_1 | 1 | 6683.3 | 37.6 | 351.2 | 11.3 |
| | 2 | 6737.8 | 59.6 | 353.7 | 7.0 |

**Table C.1 continued from previous page**

| | | | | | |
|---|---|---|---|---|---|
| S/300/370_2 | 1 | 6722.5 | 29.2 | 363.1 | 13.0 |
| | 2 | 6790.6 | 30.3 | 378.4 | 17.7 |
| S/300/370_3 | 1 | 6919.8 | 33.7 | 374.7 | 8.9 |
| | 2 | 6945.4 | 26.0 | 365.2 | 12.3 |
| | Average | 6799.9 | 37.8 | 364.4 | 12.2 |
| S/900/370_1 | 1 | 6873.3 | 63.2 | 376.0 | 13.6 |
| | 2 | 6877.7 | 39.5 | 353.2 | 10.7 |
| S/900/370_2 | 1 | 6990.0 | 54.6 | 379.6 | 9.2 |
| | 2 | 7098.9 | 58.1 | 370.0 | 17.0 |
| S/900/370_3 | 1 | 7042.1 | 32.4 | 377.2 | 8.6 |
| | 2 | 6967.3 | 45.9 | 357.5 | 18.4 |
| | Average | 6974.9 | 50.1 | 368.9 | 13.5 |
| S/300/420_1 | 1 | 7057.6 | 49.8 | 446.8 | 6.2 |
| | 2 | 7091.1 | 37.6 | 420.2 | 13.8 |
| S/300/420_2 | 1 | 7067.8 | 31.1 | 449.9 | 6.8 |
| | 2 | 6991.6 | 52.4 | 446.0 | 17.4 |
| S/300/420_3 | 1 | 6824.4 | 47.4 | 436.5 | 8.6 |
| | 2 | 7017.2 | 28.9 | 418.8 | 10.3 |
| | Average | 7008.3 | 42.2 | 436.4 | 11.2 |
| S/900/420_1 | 1 | 6958.2 | 72.0 | 423.4 | 9.5 |
| | 2 | 7099.5 | 99.0 | 407.7 | 14.7 |
| S/900/420_2 | 1 | 6983.5 | 53.8 | 434.5 | 9.5 |
| | 2 | 6970.5 | 62.6 | 420.7 | 25.2 |
| S/900/420_3 | 1 | 7056.0 | 49.3 | 421.9 | 7.3 |
| | 2 | 7304.7 | 151.9 | 413.8 | 23.6 |
| | Average | 7062.1 | 88.8 | 420.3 | 16.5 |
| S/900/300_1 | 1 | 6536.0 | 48.5 | 300.4 | 6.3 |
| | 2 | 6739.7 | 56.4 | 297.1 | 9.5 |
| S/900/300_2 | 1 | 6740.8 | 61.9 | 298.6 | 13.2 |
| | 2 | 6834.7 | 67.4 | 286.7 | 10.6 |
| S/900/300_3 | 1 | 6958.4 | 59.5 | 297.8 | 16.4 |
| | 2 | 6901.3 | 56.0 | 277.0 | 10.2 |

**Table C.1 continued from previous page**

| | | | | | |
|---|---|---|---|---|---|
| | Average | 6785.2 | 58.6 | 292.9 | 11.5 |
| L/300/370_1 | 1 | 7005.8 | 60.9 | 374.8 | 4.3 |
| | 2 | 6955.5 | 46.9 | 368.1 | 11.0 |
| L/300/370_2 | 1 | 6962.2 | 34.4 | 379.7 | 6.4 |
| | 2 | 6899.2 | 74.4 | 384.6 | 13.7 |
| L/300/370_3 | 1 | 7059.7 | 65.6 | 384.8 | 8.0 |
| | 2 | 7003.2 | 93.0 | 398.0 | 19.7 |
| | Average | 6980.9 | 65.3 | 381.7 | 11.7 |
| L/900/370_1 | 1 | 7033.1 | 42.0 | 372.5 | 8.7 |
| | 2 | 6945.5 | 34.1 | 357.0 | 21.9 |
| L/900/370_2 | 1 | 6972.6 | 40.1 | 367.0 | 8.7 |
| | 2 | 7067.7 | 88.3 | 358.8 | 12.7 |
| L/900/370_3 | 1 | 7084.9 | 73.3 | 369.5 | 10.2 |
| | 2 | 7183.2 | 132.7 | 358.2 | 8.3 |
| | Average | 7047.8 | 76.7 | 363.8 | 12.7 |
| L/300/420_1 | 1 | 6930.8 | 36.6 | 438.1 | 5.0 |
| | 2 | 6979.3 | 58.7 | 430.7 | 11.3 |
| L/300/420_2 | 1 | 6689.1 | 73.6 | 452.0 | 21.6 |
| | 2 | 7083.3 | 62.7 | 430.5 | 11.2 |
| L/300/420_3 | 1 | 7029.6 | 58.1 | 439.2 | 7.7 |
| | 2 | 7005.6 | 38.1 | 422.2 | 8.5 |
| | Average | 6953.0 | 56.2 | 435.5 | 14.6 |
| L/900/420_1 | 1 | 6942.0 | 33.5 | 433.8 | 12.3 |
| | 2 | 7086.5 | 38.2 | 415.6 | 10.7 |
| L/900/420_2 | 1 | 7116.1 | 80.0 | 446.6 | 16.5 |
| | 2 | 7608.5 | 97.6 | 435.4 | 13.0 |
| L/900/420_3 | 1 | 7110.4 | 63.1 | 443.0 | 14.8 |
| | 2 | 7149.4 | 82.5 | 434.5 | 12.7 |
| | Average | 7168.8 | 69.9 | 434.8 | 13.5 |